IN A DIFFERENT LIGHT: AN EXAMINATION OF ARTIFACTS USING AFFORDABLE DIGITAL INFRARED IMAGING

A Thesis

by

SAMUEL MARSHALL CUELLAR

Submitted to the Office of Graduate and Professional Studies of
Texas A&M University
in partial fulfillment of the requirements for the degree of

MASTER OF ARTS

Chair of Committee,	C. Wayne Smith
Committee Members,	Filipe Castro
	Howard Eilers
Head of Department,	Cynthia Werner

May 2015

Major Subject: Anthropology

ABSTRACT

The objective of this thesis is to analyze the visual effectiveness of inexpensive, converted near-infrared digital cameras on a variety of artifacts. Twenty-nine artifacts ranging in condition from unconserved to having completed conservation were chosen from five main type groups; bone, ceramics, metal, paper and textile, and wood. Each artifact was imaged with both a conventional dSLR and one specifically modified to image within the near-infrared band of the electromagnetic spectrum.

Following imaging, the two types of photographs for each artifact were directly compared, analyzing visual changes between conventional and near-infrared. The changes were described and each object given a rating of "not recommended", "no change", or "recommended" in regards to infrared imaging unveiling useful data outside of that seen with normal photography. Of the twenty-nine artifacts imaged, thirteen were "recommended" as showing potentially useful information for researchers. While no definitive claims could be made due to the variety of responses across all five groups, organic artifacts, as a whole, tended to show the most potential of responding positively to near-infrared photography using modified dSLRs. Even though none of the five groups imaged consistently across all its artifacts, the ability of modified dSLRs to define patterns in staining and corrosion, differentiating inks, penetrating dirt and stained surfaces, and revealing wood grain and tree rings was well noted and showed the potential of making such cameras a useful part of an analytical toolkit for archaeologists.

DEDICATION

This thesis is lovingly dedicated to the memory of my mother, Cynthia, whose advice, support, and love allowed me the successes of today.

ACKNOWLEDGEMENTS

I would like to express my deepest gratitude to my committee chair, Dr. Wayne Smith, who without his guidance, donation of time and equipment, and constant help, this thesis would not have been possible.

I would also like to thank my committee members Dr. Filipe Castro and Mr. Howard Eilers for their enthusiasm and helpful advice in preparing this thesis.

In addition to my committee, I would like to extend a warm thank you to Helen DeWolf, Dr. Donny Hamilton, and Justin Parkoff for their assistance in helping select artifacts for this thesis, as well as allowing me to borrow them for imaging. A big thanks to Dana Casey and her family for the gracious use of her family's 19th century bible. Without you all, the contents of this work would have been much less exciting.

Finally, a thank you to all of my friends, family, and fellow colleagues who anchored my sanity in this year long journey. Without the company, jokes, and time away from my research, the writing of this manuscript would have been a lot more stressful and a lot less fun. I am indebted to all of you.

NOMENCLATURE

dSLR	Digital Single Lens Reflex Camera
NAP	Nautical Archaeology Program at Texas A&M University
ISO	International Standards Organization
DOF	Depth of Field
PEG	Polyethylene Glycol
NM or nm	Nanometers
IR	Infrared
NIR	Near-Infrared
B&W	Black and white
MP	Megapixel(s)
APS-C	Advanced Photo System type-C
CMOS	Complementary-Metal Oxide Semiconductor
AF	Autofocus
CRL	Conservation Research Lab at Texas A&M University
EM	Electromagnetic Spectrum
CCD	Charged Coupled Device
NIRR	Near-Infrared Reflectography

TABLE OF CONTENTS

LIST OF FIGURES

CHAPTER I

INTRODUCTION AND LITERATURE REVIEW

Introduction

The infrared portion of the electromagnetic (EM) spectrum has seen its use rise dramatically throughout the 20th and into the 21st centuries. First discovered by astronomer Sir Frederick William Herschel in 1800, infrared is currently used in applications including forensics, art conservation, aerial photography, medical imaging, military targeting, and astronomy (Barr, 1961; Herschel, 1800). Use of infrared imaging in archaeology, however, has been sparse and inconsistent.

The development of a myriad of affordable digital camera types has made photography more accessible to archaeologists, conservators, and conservation laboratories than at any other point in history. With this new technology, infrared imaging can now be done digitally with instant results. Rather than relying on infrared-sensitive films, the electronic sensors of digital cameras retain sensitivity into ultraviolet (UV) and infrared (IR) areas of the EM spectrum. Manufacturers limit these extended EM spectrum ranges from affecting photographs through the use of various filters in front of the camera sensor, allowing only light within the 'visible' range to pass. However, by replacing the IR and UV filters with one designed to block light in the visible spectrum, a camera capable of photographing extended ranges of the EM spectrum is created. Converting older generation digital cameras that share the same lens

ecosystem as cameras currently in use creates user-friendly and affordable IR and UV imagers.

Infrared Radiation

Human perception of the electromagnetic spectrum is limited to wavelengths between approximately 380 nm and 780 nm (Mangold, Shaw, and Vollmer, 2013).[1] This section of wavelengths is commonly referred to as 'visible light'. Other sections of the EM spectrum are broken down into similar sections. Gamma rays, X-rays, and ultraviolet rays occupy the short wavelength side of the spectrum (below visible light), while infrared waves, microwaves, and radio waves reside above visible light on the EM scale. Figure 1.1 shows the EM spectrum.

The infrared portion of the electromagnetic spectrum is further broken down into smaller entities (based on Daniels, 2007; Deutsches Institut für Normung, 1984; Verhoeven, 2008). They are:

- Near-Infrared (NIR) from 780 nm to 1400 nm (.78 µm to 1.4 µm)
- Short Wavelength Infrared (SWIR) from 1400 nm to 3000 nm (1.4 µm to 3 µm)
- Mid Wavelength Infrared (MWIR) from 3000 nm to 6000 nm (3 µm to 6 µm)
- Long Wavelength Infrared (LWIR) from 6000 nm to 15000 nm (6 µm to 15 µm)
- Far Infrared (FIR) from 15000 nm to 1000000 nm (15 µm to 1000 µm)

[1] Specific ranges vary between individuals and surrounding conditions.

Of these five subdivisions, the most important to the IR photography in this thesis is the NIR band. It contains wavelengths from the end of the visible portion of the EM spectrum, 780 nm, to approximately 1400 nm.

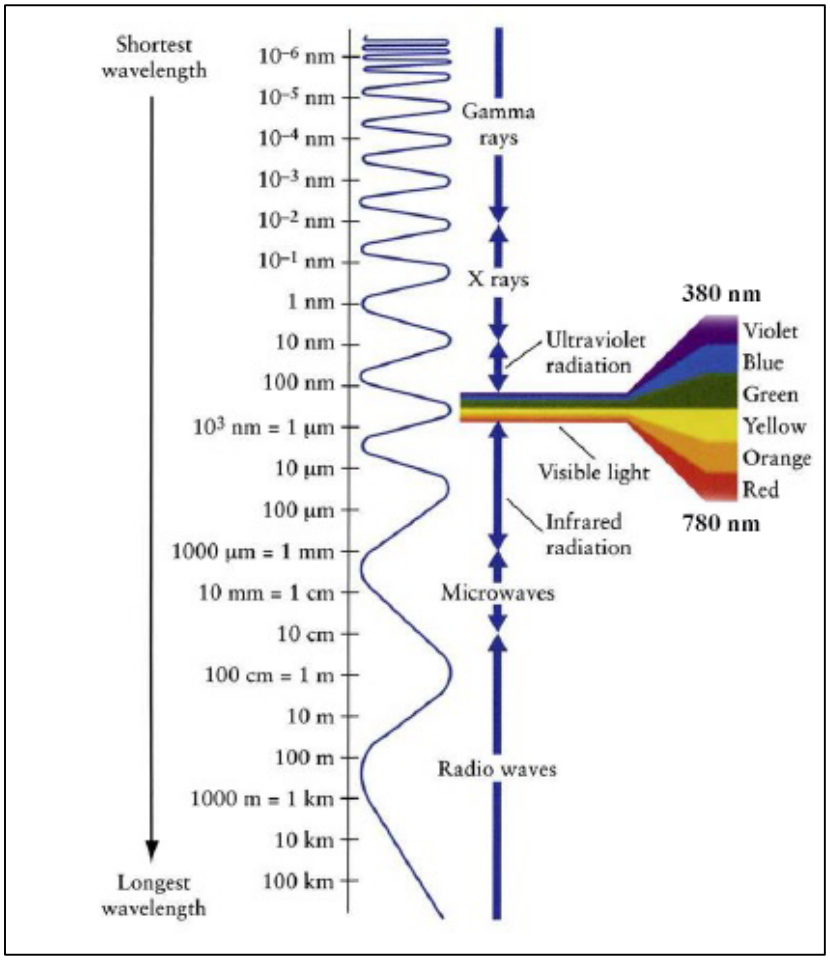

Figure 1.1: The Electromagnetic spectrum. (Adapted from Freedman and Kaufman, 2005, Figs. 5-7 and Verhoeven, 2008 Fig. 1.1).

Digital NIR Photography

Digital cameras have become a mainstay in modern society. From phones to professional dSLRs, at no point have cameras been in the hands of so many. The first

digital camera was invented in 1975 by Eastman Kodak engineer Steve Sasson. Originally weighing eight pounds, the camera recorded 0.01 megapixel black and white photographs to a cassette tape and took 23 seconds for a single image to be produced. This data was then read from the tape and displayed on a television set (Zhang 2010).

Modern iterations of digital cameras have made photography simpler, smaller, less time consuming, and more forgiving. Results are instant, allowing corrections to be made immediately rather than relying on bracketed shots and a little bit of luck as in film. In addition to these advantages digital cameras offer in capture, storage, and data manipulation, they also offer the user a relatively streamlined photographic experience. This is important in allowing NIR imaging to be more accessible than ever before.

Digital Camera Sensors

Today, silicon-based sensors dominate the digital camera world. Four broad types have been developed; Charge Coupled Device (CCD), Complementary Metal Oxide Semiconductors (CMOS), Junction Field Effect Transistors (JFET), and CMOS-Foveon™ X3 sensors. Of these, CCD and CMOS are the most common.

Silicon is a semiconductor, meaning it shares properties between conductors, such as copper, and insulators, such as glass. To improve its conductivity, a process called ‘doping’ is applied to the sensor. When a sensor is doped, the photosite is treated with an impurity, creating positive “holes” and allowing the photodiode to collect light (Rand et al, 2005; 28). Photons striking these areas of the silicon sensor have the ability to energize electrons to a higher energy state, if the energy of the photon is greater than

that of the bandgap.[2] In silicon, the approximate value of the energy needed to reach this state is 1.12 eV at room temperature (Janesick, 2001; Verhoeven, 2008). Essentially, this means that any photon with energy up to approximately 1127 nm (with energy below 1.12 eV) will pass through silicon without any interaction, as if the material is transparent (Darmont, 2009). Figure 1.2 plots the penetration depth of silicon versus wavelength superimposed with the visible light spectrum.

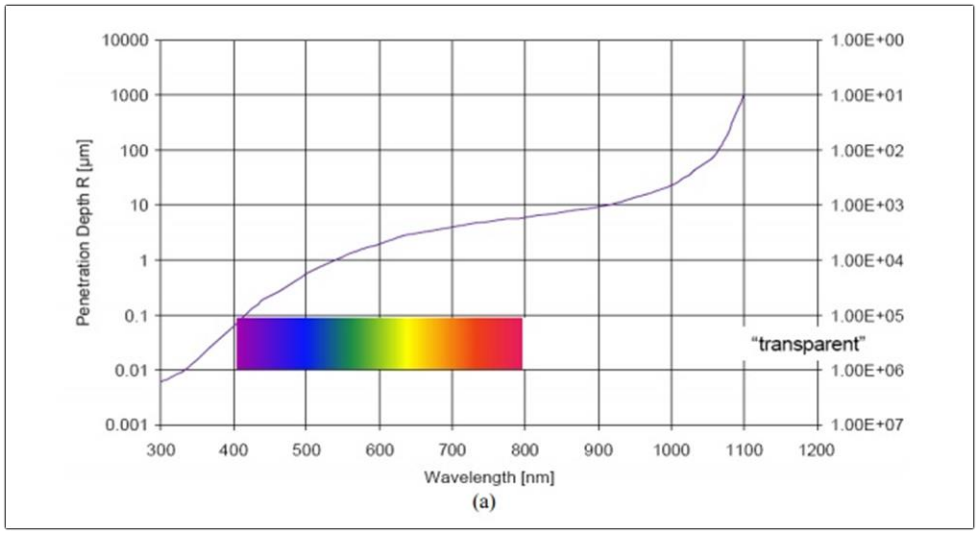

Figure 1.2: The penetration depth of silicon vs wavelength for digital camera sensors. (From Darmont 2009, Figure 1.)

Despite the varying manufacturing techniques and properties of the four broad types of sensors, the expected maximum sensitivity range of approximately 1100 nm remains the same due to the use of silicon in all four. Comparatively, most infrared films

[2] The bandgap refers to the difference between the conduction band and valence band, or the minimum amount of energy for an electron to be removed from its bound state into a condition where no electron states can exist.

had a substantial drop off in NIR sensitivity around 900-925 nm, depending on the dyes used (Verhoeven, 2008).

To keep the higher NIR sensitivity of the sensors from interfering with the images of everyday users, manufactures have added a series of filters designed to block both UV and IR wavelengths. For IR, the filters work in one of two ways. The first, and most common, makes use of an ionic colored glass to absorb unwanted IR frequencies. The other, called a hot mirror, reflects infrared light back to its source but allows visible light to pass (LifePixel 2015). These filters do not block all wavelengths of IR. However, the remaining small percentage able to penetrate these filters has no noticeable effect on conventional photographs.

Converting Digital Cameras to NIR

Most modern digital cameras are capable of imaging NIR out of the box. To do so, the addition of an opaque NIR filter is required to be attached to the front of the lens, allowing only IR waves to penetrate through the lens and to the camera sensor.[3] However, with only a small percentage of IR waves able to penetrate the filter in front of the camera sensor, exposure times are increased to many seconds to capture the required amount of IR radiation to correctly expose for an image. For photography requiring

[3] This method of capturing IR photographs was the typical method of capture for film cameras. A deep red filter placed in front of the lens allowed only a small amount of red and some NIR waves to pass, but gave the photographer a dim view through the viewfinder. In the case of pure NIR image capture with a completely opaque filter, no image is visible through the viewfinder and the lens must be pre-focused prior to the addition of a filter. This method makes pure NIR photography on film time consuming and difficult. Additional information can be found in Verhoeven, 2008.

quick composition and capture, such as aerial photography, this style of infrared capture is not suitable (Verhoeven, 2008).

The removal and replacement of the IR filters in front of the digital camera sensor alleviate the problems of requiring long exposures. By replacing the hot mirror with a 'cold mirror', or one that reflects visible light and allows only IR waves to pass, IR photographs can be taken handheld and with active use of the viewfinder. In addition to these advantages, the use of a converted dSLR allows a photographer lower ISO speeds, functional autofocus (when properly calibrated) and manual focus, metering, and does not require the use of external filters. These advantages make use of a converted dSLR less complex and more intuitive for researchers, allowing them to operate it as a normal digital camera with only minor tweaks.

It is important to note that modern digital cameras are complex. While guides can be found online to pursue converting many types of digital cameras to IR at home, it is recommended that a professional service like LifePixel, Precision Camera of Enfield, Connecticut, or some other reputable shop is used. The opening of a camera body by untrained professionals can result in the voiding of the manufacturer warranty or irreparable damage to the camera itself.

Overall, the use of modified IR digital cameras, particularly dSLRs, offer many advantages over their film IR counterparts. Besides the obvious advantages of instant capture, storage, and data manipulation, converted dSLRs provide the user with functional autofocus, metering, a higher sensitivity to IR, and a streamlined shooting experience that does not rely on external filters and attachments. These advantages make

converted dSLRs a tool worthy of examination for archaeological labs and researchers seeking an affordable, simplistic tool to add to their arsenal. The following section will examine how infrared imaging has been used in archaeology in the past.

Literature Review

The applications of infrared light in the analysis of paintings are perhaps the best known by the general public, but numerous other applications have been tested in the past decades. In this thesis, the author will focus on less popular applications related to archaeology.

Development of Infrared Film

Infrared-sensitive film was first discovered in 1873 by Hermann Wilhelm Vogel. Vogel discovered that including certain dyes in combination with the silver halides (salts) in photographic emulsions increased sensitivity at longer wavelengths (Lamore 1959; 1487). By 1909, American physicist Robert Williams Wood had taken the first known infrared and ultraviolet photographs of subjects and the Moon (Encyclopedia Britannica 2015, Wood 1910). Even with this breakthrough, commercially available infrared film only became available in the 1930s. By 1937, thirty-three types of black and white infrared film were available from five manufacturers. Seventy years later, the last commercially available 35mm infrared film by Kodak was discontinued (LifePixel 2015).

With the increasing availability of infrared sensitive films in the 1930s, researchers began to take notice of the properties of infrared photography to reveal

subtle, if not hidden details in a wide variety of circumstances. Among these included the imaging of excavation practices, landscapes for ecological studies, soils, textiles, paintings, tattooing, pottery, and use in aerial photography. The following sections briefly describe work done in all these areas using infrared sensitive films and digital photography. However, literature cited is limited to studies using handheld infrared film or digital cameras. Those using more advanced multispectral imagers and related devices were not considered.

Excavation Practices

Infrared photography has proved useful to archaeologists in studying disturbances in the stratigraphic record of a site. During excavations at the Barbeau Creek Rock Shelter in southern Illinois from 1952-53, it was found infrared sensitive film recorded midden profiles unseen in previous panchromatic photographs. The infrared photographs clearly distinguished the borders of each line of strata, sharply defined flakes of charcoal, and caused bits of limestone scattered throughout the area to stand out remarkably well (Beuttner-Janusch 1954; 85-86).

In addition to better defining stratigraphic layers, infrared imaging was deemed useful by Reichstein (1974) in uncovering hidden Bronze Age plough marks unseen by the human eye. Following this same trend, Hirsch and Hurtgen (1975) were able to determine faint red patches of floor at Gournia contained traces of paint, similar to painted floors at Tiryns. (Hirsch and Hurtgen 1975; 265).

Textiles

The non-invasive study of archaeological textiles has also been made possible through infrared imaging. Baldia and Jakes (2007) created protocols for detecting use of different colorants in textiles by using IR photography in addition to several other types. Older studies by Coremans (1938) and Dorrell (1994) highlight the use of infrared-sensitive films to examine fabrics. Coremans detected evidence of unseen tapestry restoration while Dorrell used infrared to differentiate visually similar fabrics from one another. The most recent example comes from Buti *et al* (2014), who used infrared reflectography (NIRR) for a first characterization of material used and its distribution in a pre-Hispanic Maya screenfold book, the Madrid Codex.[4]

Tattooing

Several studies have used NIR to reveal tattoos on human remains, both in forensic and archaeological settings. Smith and Zimmerman (1975) began with the analysis of a sixteen-hundred year old mummy of an Inuit woman from St. Lawrence Island, Alaska. Alvrus *et al* (2001) followed with their analysis of three tattoos found in a collection of human remains from the site Semna South in Sudanese Nublia. More recently, technical articles in forensics have emerged, notably Duncan and Kingle's 2011 technical brief on the use of infrared imaging to enhance the visibility of tattoos (Duncan and Kingle 2011).

[4] IR reflectography refers to the visualization of areas under surface pigments using shortwave IR cameras.

Pottery and Stone

Infrared has been used in the dating and classification of trace pigments and writing on ceramics and stone. Milanesi (1963), using NIR photography in conjunction with radiography, demonstrated the advantages of infrared imaging in the classification and dating of prehistoric pottery sherds (Verhoeven 2008). Later, archaeologists in Herculaneum were able to successfully use NIRR to increase the readability of a notice board containing several layers of inscription, shedding new light onto the types of messages left by historic inhabitants (Falcone 2007). Few publications examine large numbers of ceramic or stone samples with infrared photography. Instead, the most common tool used is infrared spectroscopy. This technique reveals information about the molecular makeup of the object being studied (Nielsen 1951). However, this advanced technique lies outside the scope of the research objectives for this thesis.

Aerial Photography

According to Verhoeven (2008), aerial photography has historically been one of the fields where most use NIR-based imaging has occurred in archaeology. A large body of publications covering aerial IR photography and archaeology span the previous sixty years (Agache, 1968; Aqdus, Hanson, and Drummond, 2012; Braasch, 2007; Edeine, 1956; Gumerman and Neely, 1972; Hampton, 1974; Powlesland et al., 1997; Rigaud and Bouyer, 1986; Strandberg, 1967; Verhoeven, 2007). It has proven to be a powerful tool for archaeologists, allowing them to differentiate between healthy and stressed or dead vegetation (Verhoeven, 2007) and causing crop marks and other soil features to become

better distinguished in images. In addition, archaeologists discovered the NIR region of the EM spectrum did not have the same degree of atmospheric scattering, allowing infrared images to cut through haze, providing better clarity and improved contrast of landforms below (Conlon, 1973; Rawling, 1946).

Wood and Metals

No published research of the use of NIR imaging on archaeological wood or metals was discovered in the background research for this thesis. However, a number of articles were found examining wood through infrared spectroscopy (Pizzo *et al*, 2008; Picollo, 2010; Tsuchikawa, 2013; Via, *et al.*, 2014). The research of wood and metals in this thesis attempts to characterize their visual responses to IR photography in comparison to conventional imaging.

Research Objectives

The research for this thesis seeks to answer two main objectives.

1. Can low-cost, converted, near-infrared dSLRs provide useful visual information to archaeologists and conservators in the examination of a wide selection of archaeological artifacts?
2. If so, what types of artifacts offer the most promise of revealing additional information when imaged?

To answer these two objectives, a variety of twenty nine artifacts in different states of conservation and condition have been assembled. Through imaging these

objects, it is hoped to separate artifact types that photograph well under infrared from those that do not. By understanding this difference, researchers will have a better idea of whether infrared imaging can aid in analyzing a particular type of artifact and what kind of variations may be seen when compared to visible light photography.

The goal of this study is not to explain how or why visible changes between conventional and IR photography occur in the selected artifacts. Rather, the author seeks to define expected baseline changes within artifact groups. Following visual comparisons between the two photographic types, a recommendation to the effectiveness and potential of low cost IR photography for each selected artifact will be made.

CHAPTER II

EQUIPMENT AND SOFTWARE

A variety of equipment and software is required to successfully capture infrared images in an efficient manner. The following selections were made with two particular goals in mind: affordability and ease of use.

It is understood that many archaeologists and conservators are not trained or familiar with digital photography in its current state. However, a working knowledge of the basic operations of a DSLR and photographical settings are important in being able to recreate the techniques described later in this thesis. Guides and videos to become more familiar with these settings and techniques can be found in various forms, including Youtube™ videos, online articles, published books, and a personal favorite, AdoramaTV™.[5]

The rest of this chapter is divided into sections covering camera bodies, lenses, lights, software, and accessories. Each sub-section describes the tools used during research in detail, including specifications and the reasoning behind their choosing. The equipment listed is by no means all-inclusive. Varying lab conditions, camera and lighting availability, and personal preference will present opportunities for different equipment setups with similar results.

---

[5] AdoramaTV™ can be accessed through the Adorama website, http://www.adorama.com, or directly at http://www.adorama.com/alc/category/AdoramaTV. They provide a wide variety of videos on most aspects of photography and serve as a useful tool in gaining a better understanding of the basics of photography.

Cameras

Two cameras were chosen to carry out the research presented in this thesis. One was converted to capture only infrared light while the other was left unmodified to take normal photographs within the visible light spectrum. A Canon 20D APS-C camera was chosen by Dr. Wayne Smith to be converted into the IR-only body. Originally released in 2004, the body can be found used online or in local camera stores for typically less than $150.[6] It comes outfitted with an 8.2-megapixel CMOS sensor measuring 22.5 x 15.0 millimeters, creating a field of view 1.6 times the focal length of a Canon EF lens (Canon, 2014). The ISO ranges from 100 to 1600, plus up to 3200 using the 20D's extended range. While the camera is dated, it provides an inexpensive and flexible option for modification.

A Canon 30D was used to take unmodified, visible spectrum photographs for comparison with the IR-only camera. This camera was selected because it uses an identical sensor as the 20D. By utilizing cameras with the same sensor, changes due to differences in sensitivity, resolution, field of view, and other factors would be eliminated.

Differences between the 20D and 30D are largely limited to ergonomic and visual changes, including a smaller form factor, larger LCD screen, and menu changes. A detailed list of each camera featured compared to each other can be found in a review

[6] Common selling prices were taken from a survey of Ebay™ listings on September 29 2014.

posted by Shawn Barnett and Dave Etchells through Imaging Resource (Barnett and Etchells 2006). 30D bodies can be found used for prices similar to the 20D.[7]

Precision Camera of Enfield, Connecticut performed the visible to infrared conversion for the 20D.[8] Among their options, they list several types of infrared conversion, including 590NM, 665NM, 715NM, and 830NM (Precision Camera, 2014). Each number represents the wavelength of light, in nanometers, below which will not penetrate into the camera sensor. For example, a camera modified with the 715NM conversion will only allow wavelengths of light of 715NM and above to reach the sensor. A typical, unmodified DSLR is designed to capture light in the wavelengths of 400-700NM.

For the purposes of this research, an 830NM conversion was chosen. At this wavelength, almost no visible light penetrates to the sensor of the camera, allowing for low saturation and high contrast images in black and white directly from the camera.[9] NIR photographs from the 20D can then be compared to the visible spectrum images taken by the 30D without any post-production editing to remove red cast, keeping with the intent to remain simple to use.

---

[7] Prices were taken from Ebay™ listings on September 29 2014.

[8] Precision Camera can be contacted through their website (http://www.precisioncamera.com), or by telephone (800-665-6515). To enquire specifically about infrared conversion, they request e-mailing them at ir@precisioncamera.com. Most conversions cost between $200-$300, depending on camera model and type.

[9] It is important to note all IR-converted cameras require a custom white balance setting to remove the red casting present from longer-wavelength visible light penetrating to the sensor. 830NM is the highest IR conversion level Precision Camera offers and the only one that produces black and white IR photos directly out of the camera.

Lenses

The lens selected for all photographs taken throughout this thesis was the Canon EF-S 60mm *f*/2.8 USM Macro. A recent survey of prices show this lens selling new at New York City based Adorama Camera for $469.00[10] and for approximately $300.00 used on Ebay™. Optically, this lens shows relatively little distortion across the frame, sharp border-to-border results, and low chromatic aberrations (Photozone 2005)[11]. When selecting a lens, especially for archaeological photography, it is important to choose a lens with low distortion (Fisher 2009). While modern software such as Adobe Lightroom™ and Adobe CameraRaw™ can correct lens distortions, minimal distortion lenses provide the simplest and most accurate solution.

When paired with the sensors of the 20D and 30D, the EF-S 60mm lens has an effective field of view of 96mm (60mm x 1.6 crop factor) on an APS-C 'crop' sensor. This camera set up proved useful for smaller objects, but was found limiting for larger artifacts. In cases where imaging large artifacts is needed, increasing the distance from the object can most times provide a simple solution. For artifacts too large for this method, a low distortion wide-angle lens is recommended.

Manual focus provided best results for all modern autofocus lenses. Once a camera is converted to NIR, the lens focus calibration no longer correctly locks onto a subject due to the absence of visible light striking the sensor and the different focusing

---

[10] The lens can be found listed at http://www.adorama.com/CA6028AFSU.html as of September 29th, 2014.

[11] More information about this lens can be found on Canon's USA webpage: http://www.usa.canon.com/cusa/professional/products/lenses/ef_lens_lineup/lens_macro_pro/ef_s_60mm_f_2_8_macro_usm.

points of NIR wavelengths (LifePixel 2014). More modern DSLRs with a "Live View" function have better capabilities to focus on infrared from the sensor. However, the 20D and 30D do not have that capability.

Lights

A simple, constant output, two-light setup was used to illuminate the artifacts with infrared light. The two lights, a Smith Victor A80 with a Phillips 60-watt tungsten filament incandescent light bulb and a Bowens Travelite 750 using a General Electric tungsten filament 250-watt incandescent bulb, represent typical photography lights that can be found in most labs and institutions that possess photographic capabilities. The A80 operates via an on/off switch and does not allow change to the intensity of light emitted from the bulb, casting light at a constant rate at maximum output. The Travelite 750 is a full-featured photographic light that allows changes in light output as well as flash capabilities. As used for the photographs in later chapters, however, a constant output from the 250-watt bulb was used.

Both incandescent bulbs used in the lights are readily available at most large box retailers and hardware stores. Specific photography lights are not required if they are unavailable. Instead, any lamp or light source with a directional output can be used as a replacement. However, if varied output is desired, a photographic light similar to the Travelite 750 is recommended.

Light types other than incandescent bulbs were not tested and lie outside the scope of this thesis. However, it was noticed during photographic research that the

fluorescent tube lights common in many academic and office buildings did not put out enough infrared light to interfere with the NIR images taken with the 20D. Only during exposures greater than one second at base ISO and f/2.8 would fluorescent tube lights cause issue. It is suggested that a converted NIR camera be used to test the ambient NIR emission from surrounding light sources prior to shooting. LifePixel's Infrared Camera Conversion Primer provides an informative write up of the use other lighting sources such as HID, fluorescent, and sunlight (LifePixel 2014).

Flash photography is possible using a converted NIR camera (LifePixel 2014 and Davidhazy 1993). A Canon Speedlite 380EX was tested in conjunction with the NIR 20D and emitted enough IR light to create a well exposed image. Used with other flash units, off camera flash photography presents a viable option for proper exposure of artifacts for infrared imaging. However, flash units were not used to keep initial costs low and to prove an easy to use, static system was adequate to capture quality infrared images of artifacts.

Software

Canon's EOS Utility 2.3 and ImageBrowser 6.1.0.15 were used to tether-capture directly from both the Canon 20D and 30D to a 2011 13" Macbook Pro running OSX 10.9.2.[12] This allowed complete physical separation from the camera bodies, negating the risk of accidental vibrations or other errors caused by physical interaction during the

[12] A Macbook Pro running OSX was the platform available to the author, but all listed software is available for Windows based computers.

shutter operation of the camera. It also enabled images to be immediately viewed at full size following capture. Corrections to shutter speed, ISO, or aperture can be made through the EOS Utility, while adjustments to focus must be made on camera.

Most camera manufacturers include tethered-capture software with their DSLR camera bodies, including Nikon, Olympus, Canon, among others. Common third-party software available for tethered-capture include Adobe Lightroom™ and Phase One's Capture One Pro. Not all cameras, especially older body models similar to the 20D and 30D, are compatible with tethered capture from these third-party programs. The proprietary software from each manufacturer is recommended for best results.

Other Accessories

Several other items were used throughout the photography process to assist in photography. Most important was the Vanguard Abeo Pro 283CT tripod. A tripod is important because it isolates and steadies the camera for slower shutter speeds, providing a consistent platform where distance from the photographed object can remain consistent. The same is not reliably possible taking hand held photographs.

When selecting a tripod, several considerations should be kept in mind. First is flexibility; how many different adjustment points does the tripod have? The greater the adjustability of the tripod, the more potential positions the camera body can be mounted, allowing for a variety of different photographic set ups. This proved useful switching between small artifacts that required a shorter height above the object, and larger ones needing a greater distance to capture the entire object in frame. If size differences

between imaged artifacts are limited, less emphasis can be placed on the adjustability of a tripod.

The second point to consider is the size and weight of the tripod and the environment it will be used in. For this research, a static lab set up was used, meaning a larger tripod was not a hindrance to mobility. However, the tripod was constructed of carbon fiber, making it very light. This proved to be a problem when the camera was extended horizontally away from the leg base, causing the weight of the camera body to . To counteract this problem, a lead weight was suspended from the center of the tripod to give it greater stability. If working in a small lab, in the field, or an area that requires constant movement, a small, light tripod may be most beneficial and easiest to use. Ultimately, tripod choice is predicated on personal preference, use environment, and availability. The above suggestions are based on what was useful for the author during research.

Another helpful accessory was a battery grip for use with each camera, particularly if shooting a large number of photos or unable to charge or replace batteries.. The Canon BG-E2 battery grip accepts two batteries, allowing long segments of shooting without worry of the camera dying mid-shoot. Another, cheaper alternative to a battery grip is having a supply of multiple batteries. However, this requires removing the camera from a tripod set up prior to replacing the battery.

Black poster board was used as a backdrop for each shot. The dark color allowed the higher contrasted areas of the NIR photographs taken with the 20D to be able to be

more clearly seen when compared to a white background. Color choice in a backdrop is entirely dependent on the desired outcome of the photographs and their intended use.

Closing Remarks on Equipment

The goal of the above choices in camera bodies, lenses, lights, software, and accessories were to create a NIR capture system that was both affordable for existing labs and required little additional training to produce workable images for diagnostic use. None of the selections are absolutely required to create a working photography setup, however, it is intended to provide a starting point for individuals with limited experiences in photography. Different working environments will require the addition or subtraction of equipment. To determine the equipment and software that best suit the needs of a particular lab or field site, experimentation may be needed before a suitable system can be finalized and worked into existing methods and workflow.

CHAPTER III

METHODOLOGY

The intent of this chapter is to define how the artifacts used during research were selected, imaged, and analyzed to determine the effectiveness of using converted NIR DSLRs on variety of different artifact types.

Artifact Selection

The Conservation Research Lab at Texas A&M University's Riverside Campus is a working lab; meaning archaeological materials are received from many sites and institutions around the world. Each lot of artifacts is accompanied by contracts to fund work by Texas A&M researchers and students to properly conserve the material. Through this system, many diverse types of artifacts pass through the lab space, including metals, wood, textile, and ceramics. However, not all types of artifacts are available at one. Many are returned following conservation while others sit at various stages in their stabilization processes. This reality limited the selection choices of several types of artifacts.

Other than CRL, artifacts and samples were also drawn from the teaching conservation laboratory inside the Anthropology building on Texas A&M's main campus. Rather than serving as a working lab, this space is used to teach classes on conservation and as a storage and display space for many artifacts from Port Royal,

Jamaica.[13] The acquisition of samples from this lab aided in filling gaps in artifacts available for research. However, despite best efforts, not all artifact types were able to be collected for use.

The selection of artifacts began at five parent categories: Metals, Ceramics, Wood, Bone and Textile. Each parent category consisted of sub-categories naming specific artifact types of the parent category type. For example, 'Metals' included subcategories of iron, lead, pewter, cupreous metals (brass, bronze, etc.), silver, and white metal[14]. The complete list of parent and sub-categories can be found on the artifact table in APPENDIX I.

Within each sub-category, two conditions of the artifact were sought – conserved and unconserved. The conservation processes varies between minimum and invasive, depending on the artifact's composition, making it important to include both conditions where change from pre-conservation to post-conservation is substantial. Other artifacts, such as ceramics, typically require little in the way of invasive treatments once recovered from a marine environment, meaning the importance of obtaining examples of pre-conservation and post conservation ceramics is diminished.

---

[13] More information about Texas A&M University's excavations at Port Royal Jamaica can be found on the Texas A&M Nautical Archaeology Program webpage at http://nautarch.tamu.edu/portroyal/.

[14] The Merriam-Webster Dictionary Online defines white metal as any of several light-colored alloys used especially as a base for plated silverware and ornaments and novelties. http://www.merriam-webster.com/dictionary/white%20metal.

Overall, 30 artifacts were used in this study, representing most the parent categories and sub-categories in both conserved and unconserved states. Not all artifacts could be obtained in both pre-conservation and post-conservation conditions.

Artifact Naming

A descriptive naming system was developed to give each artifact a unique identifier to keep track of it throughout the photography process. The first letter represented the conservation state of a particular artifact, C for conserved or U for unconserved. Following the first letter, the second letter delineated the parent category of the object, M for metal, W for wood, C for ceramic, T for textile, and B for bone. The third letter defined the sub-category of a sample, such as the type of metal, ceramic, or wood. For certain artifacts, a fourth letter was added to better differentiate it from its peers. For example, the ceramic white clay would be represented WC rather than W.

Following the sub-category representation, conserved artifacts reserved the last one to two letters to describe the type of treatment the sample had undergone during the conservation process. Reoccurring letter representations included P for a polyethylene glycol treatment, F or FD for freeze-drying, and SO for silicone oil. Information about the conservation processes used at Texas A&M's CRL can be found in Donny L. Hamilton's Conservation Manual (Hamilton 2010).

The end of each assigned name terminates in a number. This represented the order a particular artifact was photographed within its parent category. If an artifact was named CMPER1, it designates that the artifact was a conserved, metal, made of pewter,

treated through electrolytic reduction (ER), and the first of the metals to be photographed. Explanations of each name given to an artifact can be found in APPENDIX I.

Photographic Setup

The photographic setup designed for this study was created with two goals in mind; ease of use and accessibility. As described in Chapter II, the lighting set up consisted of two static output lights, a Bowens Travelite 750 using a General Electric tungsten filament 250-watt incandescent bulb and a Smith Victor A80 with a Phillips 60-watt tungsten filament incandescent light bulb. Each was placed at approximately 45-degrees from the artifact to be photographed, the Travelite 750 on the left and Smith Victor A80 on the right.

Between the two lights, the tripod was placed and arranged so the camera body was positioned horizontally over the artifact at a height of 60 centimeters from the ground. Suspended from the center of the tripod was a three-pound lead weight, used to give the tripod additional stability due to the horizontal configuration used.

From here, the camera was tethered via USB cable to a 2011 13" Macbook Pro running Canon's EOS Utility 2.3 and ImageBrowser 6.1.0.15, allowing image capture and review without risk of disturbing the camera during the photographing of each artifact. Camera settings were changed using the EOS Utility and each image was viewed full size through ImageBrowser immediately after capture to ensure good focus and proper lighting.

To better isolate the artifact, a backdrop of black paper was placed underneath the artifact, allowing contrast, particularly in the infrared images, to be more visible. This was complimented with a black tri-fold board placed behind the area where the artifact would be imaged on the black background. It served to help isolate the photographed object from surrounding light sources.

Reference measurements were recorded using a right-angled millimeter scale for most artifacts. The only exceptions occurred where objects proved too large to properly scale. In its place, a 3-centimeter or 12-inch scale was used depending on the artifact size. For example, a 3-centimeter scale was chosen for the wood artifact UWHAD7 due to the height of the artifact surface. The variance in height from the black background and artifact surface caused depth-of-field issues with any scale placed on the background, requiring it to be raised. Use of the small, 3-centimeter scale proved best for providing measurement reference and not obscuring the surface of the artifact. The height was not changed in these situations unless absolutely needed in an attempt to minimize variables. Artifacts CWHSO5 and CBPS1 required use of a 12-inch scale to show the length of each object.

Figure 3.1 shows the setup as it sat in the Wilder 3-D Imaging Laboratory. The floor was chosen as the ideal location because it allowed the author easy access above the artifacts, lights, and camera simultaneously. It also kept the distance from the floor at a minimum should any of the equipment or objects to be photographed be mistakenly bumped by others with lab access.

Figure 3.1: Image of the Wilder 3-D Imaging Laboratory photography setup

Two locations were used to photograph the artifacts used in this thesis. The first, the Wilder 3-D Imaging Laboratory, was primarily used for artifacts that were available from the teaching conservation lab in the Anthropology Building at Texas A&M University. These objects had been stabilized, cleaned, and in some cases, conserved a substantial amount of time prior to the research written here. This enabled the author to transport them the short distance down the hall to the Wilder Laboratory safely.

The second location was at the Conservation Research Laboratory (CRL) at Texas A&M's Riverside Campus. Here, artifacts of many kinds reside in all stages of conservation. CRL treats artifacts on a contract basis from numerous private, state, federal, and international groups. As such, transporting these artifacts from CRL to the Wilder Laboratory, a distance of sixteen miles round-trip, was deemed unwise by the author. Figures 3.2 and 3.3 show the setup created for imaging at CRL. It was recreated

to match the lighting and positioning as closely to the Wilder setup as possible. Locations were labeled on the ID card with each artifact as ‘Wilder’ or ‘Riverside’ to denote the different locations.

Figure 3.2: View 1 of the Riverside photography setup at CRL

Figure 3.3: View 2 of the Riverside photography setup at CRL

Each artifact received at minimum two photographs, one unmodified and one infrared. On average, most of the twenty nine objects had four pictures taken of them, covering each side in both 'unmodified' and infrared photographs. Additional photographs were taken if the artifact required additional coverage.

An incident light reading was taken with a handheld light meter to determine the exposure values needed for the unmodified 30D. Once measured, $1/180^{th}$ of a second at f 4.0 with an ISO of 400 was deemed to be the correct exposure. Testing with these settings confirmed the light meter's output.

Nearly all of the photographs taken with the 30D used the above settings. However, some exceptions were necessary to create images that were clear enough for visual comparison. The artifacts that required modification imaged darker due to less reflective surfaces. To compensate, shutter speed was changed from $1/180^{th}$ to $1/90^{th}$. ISO and f-stop were not changed to minimize variability.

A typical light meter designed to measure visible light did not provide settings to produce adequate infrared pictures for analysis. To solve this problem, the shutter speed was changed while the aperture was left at f 4.0 and the ISO at 400. This minimized the depth of field and noise changes that would occur in switching these settings between the 20D and 30D. After attempting numerous shutter speeds and analyzing the histogram after each shot, a shutter speed of $1/100^{th}$ was reached. The final camera settings for infrared images with the 20D were $1/100^{th}$ with a f-stop of 4.0 and an ISO of 400.

Like the visible photographs, some exceptions were made in the shutter speed of particular objects that imaged considerably darker than others. Following the method

outlined for the 30D and visible images, the shutter speed was reduced from 1/100th to 1/50th. In all cases, this produced photographs that were within the realms of correct exposure.

Analysis of Images

The viability of using modified infrared dSLRs for archaeological imaging was determined on the comparison of unmodified and infrared photographs of each artifact. Inherently, this method introduces a number of biases due to the qualitative rather than quantitative nature of analysis. However, such comparative visual examinations are part of the evaluations archaeological conservators use to describe and treat artifacts. The information, when interpreted conservatively, can prove as useful as hard data created through measurement and chemistry.

Analysis of each object took place on a large, single monitor where infrared and unmodified images of the same view and perspective were placed side by side. The author directly compared photographs, looking for changes in detail, clarity, visibility of features, and other characteristics that may have changed.

To quantify visual results into useful information for archaeologists, a system was created to give recommendations of the success of infrared photography using modified dSLRs for particular artifact types. This system consisted of three levels: Not Recommended, No Change, and Recommended. While simple, it was designed to allow archaeologists and conservators to quickly glance at the numerous artifact types and

determine whether near-infrared photography may be a useful solution for a particular object.

Each level had basic guidelines to which the differences between the unmodified and NIR photographs were compared. To be declared ‘Not Recommended’, an artifact had to show loss of detail, clarity, or photograph worse in infrared in some other significant way. ‘No Change’ was chosen when no discernable differences were able to be determined between objects photographed ‘normally’ or through infrared. For an artifact to be given a ‘Recommended’ title, the infrared image had to show details unseen in the unmodified image that have the potential to better inform a researcher of its historical or conservation state.

APPENDIX I contains the final table listing artifacts, their names, types, and final rating. Following this table, APPENDIX II holds every photograph used to reach the final conclusions highlighted in APPENDIX I.

CHAPTER IV

BONE

Two bone artifacts were available for analysis with the NIR dSLR. Details about each artifact are listed below in Figure 4.1. The first artifact examined, CBPS1, consisted of a large piece of pig skin, fat, and bone that had been treated through silicone oil, as described in Dr. Donny L. Hamilton's Methods of Conserving Archaeological Material from Underwater Sites (Hamilton 2010; 28-29). In the manual, this method is described for wood conservation. However, silicone oil has proven to be successful in treating a wide variety of organic artifacts, including wooden stocks of muskets, Columbian mammoth bones, and hair (Cox 2008, Daniel 2007, Sager 2008).

ARTIFACT ID	ARTIFACT TYPE	SPECIFIC TYPE	CONSERVATION METHOD	ID EXPLANATION	IMAGING LOCATION
BONE					
CBPS1	Bone	Pig Bone and Fat	Silicone Oil	Conserved Bone Pig Skin	Riverside
UBS2	Bone	Stained Pig Bone	Unconserved	Unconserved Bone Stained	Wilder

Figure 4.1: Table of bone artifacts analyzed in this chapter.

CBPS1

Overall, CBPS1 retained much of the original skin and fat color and texture as would be expected if viewing a similar cut of pork today. The exposed bone has darkened to an earthy brown color, however. It was unknown to the author whether this

result was a product of site processes or conservation treatment. CBPS1 was imaged on one side only due to its large size and awkward contouring on the non-imaged face. Due to the size of the artifact, the camera height was raised to 85 centimeters to obtain wider coverage.

Figures 4.2 and 4.3 show the photographs taken of CBPS1 with the unmodified Canon 30D and NIR converted Canon 20D DSLR respectively. In Figure 4.2, the differing coloration of the artifact is evident, changing from darker tones in the lower portions on the left side of the photograph to a lighter coloration approaching right. The considerably darker pieces visible at the top, bottom, and right side of the figure show the coloration of the protruding bones, mentioned earlier. Small granulations of detached skin are evident throughout the photograph, adding to the texture that can be seen in combination with coloration changes.

Figure 4.2: Unmodified photograph of CBPS1.

At first glance, the NIR photograph of CBPS1 exhibits substantially less contrast between light and dark tones than its normal counterpart. The dark spot on the left side, for example, is not as well defined, nor are the darker toned protruding bones. However, this does not mean the darker bones are indistinguishable from the surrounding skin. In fact, the bones stand out well in comparison to the less contrasted surroundings, with exception to the bone furthest to the right.

Skin tones, overall, have a more uniform, less muddled look. The grayscale image produced by the NIR photograph are less distracting to the eye. Less visible, too, are the small skin granulations mentioned previously. While still visible if sought for, they do not stand out in the same way as in Figure 4.2. This may be due to the desaturated nature of the image, however.

On the upper-right portion of CBPS1, the mottled patterning of the skin is more defined than in figure 4.2. The light and dark patterning can be more reliably traced than attempting to navigate through the range of contrasted tones in Figure 4.2. This is not true for the rest of the artifact, where greater contrast can be seen in the image from the unmodified camera.

.

Figure 4.3: NIR photograph of CBPS1.

Conclusions for CBPS1

Near-Infrared imaging, in the case of silicone oil treated pork skin, fat, and bone, provides a cleaner, more unified look to skin tone and texture when compared to a typical photograph. In some areas, light and dark contrasts are better defined in NIR, however, the majority of the skin tones of CBPS1are better realized under normal photography from the Canon 30D. If looking for a uniform, lower contrast image of silicone oil treated skin and fat with bone, NIR photography may provide the best choice. In most cases, where the identification of skin staining, bone location, and the overall look for a similar artifact is important, unmodified, visible spectrum photography provides the most advantages. In conclusion, NIR is LESS effective for overall analysis than visible spectrum photography under tested conditions.

UBS2

The second artifact, UBS2, was an untreated piece of pig bone from an unknown site. Much of the bone exhibits signs of discoloration and staining, including distinctive rust colored markings on one of its faces. In addition to the staining, UBS2 retained considerable amounts of dirt over its surface. Each end of the bone showed signs of breakage. It could not be determined by the author as to what part of the animal the bone originated. UBS2 was imaged once on each face, one side displaying predominately soil staining while the reverse exhibited significant 'rust'-colored surface patches at each end.

UBS2 was chosen to test the capabilities of the NIR camera on unconserved and stained bone without any tissue remaining. Four photographs were taken in total, one of each side with both visible and infrared photography. The images can be viewed in figures 4.4 through 4.7.

Figure 4.4: The 'initial' side of UBS2 as seen with an unmodified camera.

The initial face of UBS2 under visible light (Figure 4.4) shows a surface heavily stained by soil and presumably an iron-based substance. Soil staining grows darker from left to right, traveling from the left end up the curvature of the bone, gradually becoming more orange in color where an iron substance likely contacted the bone's surface. Many of the detail marks are easily seen on its surface, though others are obscured by the dirt and stains.

On the reverse side, seen in Figure 4.5, soil staining is less prevalent, replaced instead with heavier 'rust'-colored staining. Holes and striations in the bone are also visible, however, not all are easily followed in the photograph.

Figure 4.5: The reverse side of UBS2 as seen with an unmodified camera.

The NIR photographs of UBS2 show slightly more visual promise than CBPS, particularly with soil staining. As seen in Figure 4.6, the patterning of the darker and lighter areas of soil stained and unstained bone are better defined, particularly on the

upper end. The ‘rust’-colored staining, however, is all but invisible to NIR. A similar trend continues on the reverse side, with areas of darker soil staining more clearly defined while portions covered in red stains are all but invisible in Figures 4.6 and 4.7.

Figure 4.6: The ‘initial’ face of UBS2 in NIR.

Cracks in the bone appear to be well defined in NIR, especially on the ‘reverse’ side of UBS2 (Figure 4.7). Splits originating near the small square section of removed bone can be easily followed to the right, as can gouges above and to the right. Holes, however, lack the same clarity seen through the 30D. The differences do not appear to be similar if the unmodified image from the 30D is desaturated. The cracks continue to stand out to a greater degree than without NIR.

Figure 4.7: The ‘reverse’ face of UBS2 in NIR.

Conclusions for UBS2

The practicality of using NIR for examining stained, untreated bone rest on the characteristics to be examined. The 20D displayed darker soil staining well and with more contrast than its visible counterpart. Despite this, the red stains do not register with any substance on the same NIR images. Cracks, while visible under normal circumstances, are better defined under NIR conditions. The effectiveness of infrared photography on UBS2 is largely limited to analyzing darker stains and cracks. However, stains from iron-based sources are nearly invisible under the same conditions, limiting the overall usefulness of obtaining a better complete picture of the artifact. In conclusion, NIR is useful in limited applications for untreated stained bone, to include dark, earthy stains and cracking. Any light stains may not be properly imaged, as it is likely the infrared waves completely penetrate the surface staining.

Conclusions for Bone

Both CBPS1 and UBS2 responded well to infrared imaging. In CBPS1, the definition of the exposed bone was increased relative to the surrounding skin due to the normalization of skin color. This allowed details such as skin creases, tears, and discolorations to be more pronounced and more easily recognized by the eye.
The infrared photography of UBS2 enhanced surface cracks and soil staining present on the bone's surface, making it easier for archaeologists to treat deterioration or more thoroughly clean for display or study.

The response of both of these objects to NIR imaging is encouraging. While it is impossible to predict that infrared photography will be beneficial to all bone artifacts in the same manner, it provides qualitative evidence that attempts may be worthwhile endeavors for labs seeking to uncover hidden details in their examinations. Figure 4.8 provides a summary of final recommendations.

ARTIFACT ID	ARTIFACT TYPE	SPECIFIC TYPE	ID EXPLANATION	RATING: IR vs VISIBLE
BONE				
CBPS1	Bone	Pig Bone and Fat	Conserved Bone Pig Skin	Recommended
UBS2	Bone	Stained Pig Bone	Unconserved Bone Stained	Recommended

Figure 4.8: table of final recommendations

CHAPTER V

CERAMICS

The collection of ceramics analyzed in this study include nine separate artifacts representing nine types. Each sherd received minimal conservation treatment, limited to fresh water baths to clean and desalinate each piece. Previous research of using NIR imaging on ceramics has revealed has allowed more conclusive classification and dating (Milanesi, 1963). In addition, Verhoeven (2008), used a NIR dSLR to demonstrate the

ARTIFACT ID	ARTIFACT TYPE	SPECIFIC TYPE	CONSERVATION METHOD	ID EXPLANATION	IMAGING LOCATION
CERAMICS					
UCPW1	Ceramic	Pearlware	Unconserved/fresh water bath	Unconserved Ceramic Pearl	Wilder
UCP2	Ceramic	Porcelain	Unconserved/fresh water bath	Unconserved Ceramic	Wilder
UCWW3	Ceramic	Whiteware	Unconserved/fresh water bath	Unconserved Ceramic White	Wilder
UCCW4	Ceramic	Creamware	Unconserved/fresh water bath	Unconserved Ceramic Cream	Wilder
UCSW5	Ceramic	Slipware	Unconserved/fresh water bath	Unconserved Ceramic Slip	Wilder
UCTE6	Ceramic	Tin Enamel	Unconserved/ fresh water bath	Unconserved Ceramic Tin	Wilder
UCStW7	Ceramic	Stoneware	Unconserved/fresh water bath	Unconserved Ceramic Stone	Wilder
UCCE8	Ceramic	Coarse Earthenware	Unconserved/fresh water bath	Unconserved Ceramic Coarse Earthenware	Wilder
UCWC9	Ceramic	White Clay	Unconserved/fresh water bath	Unconserved Ceramic White Clay	Wilder

Figure 5.1: Table of ceramic artifacts analyzed in Chapter V.

ability of the technology to discern areas of increased reduction. It is expected by the author for NIR to show visible differences in its interaction with printed designs on ceramics. Figure 5.1 highlights the details of each ceramic sherd.

UCPW1

UCPW1 represents a large, intact sherd of a pearlware plate recovered during Texas A&M Nautical Archaeology Program's 1990s excavations at Port Royal, Jamaica. At first glance, the most striking feature of the artifact is the blue transfer-printed design visible on its interior surface. Developed in 1779 by Josiah Wedgwood, this style of ceramic remained popular until the 1820s (Hamilton, 2015). While UCPW1 is incomplete, a substantial part of the blue printed design remains. Even though the scene is incomplete, it appears to follow the 'blue willow' pattern in its design. The blue ink has bled somewhat into the surround white ceramic. Whether this is a product of the firing process or the deposition environment is unknown.

The underside of UCPW1 lacks any discernable markings, sporting a uniform blue tint common amongst pearlware ceramics' due to the addition of cobalt blue. Numerous nicks and chips expose the white clay of the ceramic underneath, while a sherd identification number of 3, written in black, is visible near the center of the dish of the plate.

Figure 5.2: Unmodified image of UCPW1

Figure 5.2 shows the 'blue willow' design of UCPW1 as it appears to the human eye. Overall, the piece shows good clarity and is only marred by small stains near the edge of the plate well as it approaches the rim. The printed willow remains clear in all but a few areas, where the blue pigment can be seen to bleed into the surrounding white background, both on the rim and in the design in the well, particularly around the willow tree. In large part, this does not appear to be a problem in identifying the design, however, when compared with the infrared image of UCPW1 in Figure 5.2, the difference is clear.

In the infrared image, the clarity of the printed 'blue willow' design is markedly improved. The soft edges where the blue pigments have bled into the surrounding ceramic are gone, leaving a clear, crisp image which may enable better interpretation and recording of the printed design. It appears the longer wavelengths of infrared light are

able to penetrate the thinner areas of blue pigment, essentially making them invisible to the camera sensor.

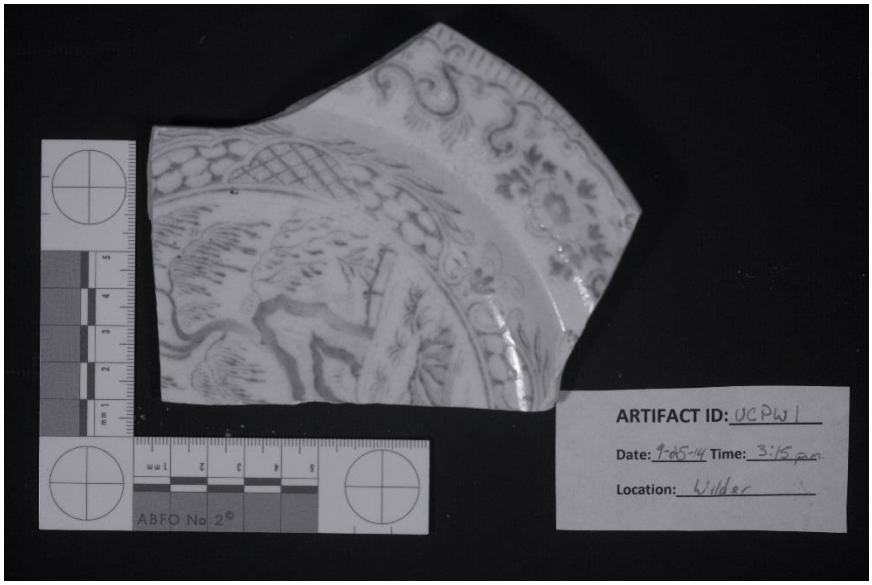

Figure 5.3: Infrared image of UCPW1

This does not come without risk, however. Thin, faint features visible to the human eye are at jeopardy of becoming obscured through infrared imaging. For example, the thin line below the willow branches and above the small plants within the plate well has been nearly completely obscured. A similar effect can be seen in the circular scroll work on the right side of Figure 5.3, just after the end of the leaves circling the well rim. The loss of detail, of which elements may be important, must be kept in mind if relying on infrared imaging to image pearlware or similarly produced ceramics.

The backside of UCPW1 shows little difference between visible spectrum imaging and infrared. In Figure 5.4, a number of small white specks are visible where the ceramic has been nicked by either use or the archaeological environment. These disappear in Figure 5.5, as the infrared camera does not record color and desaturates the image.

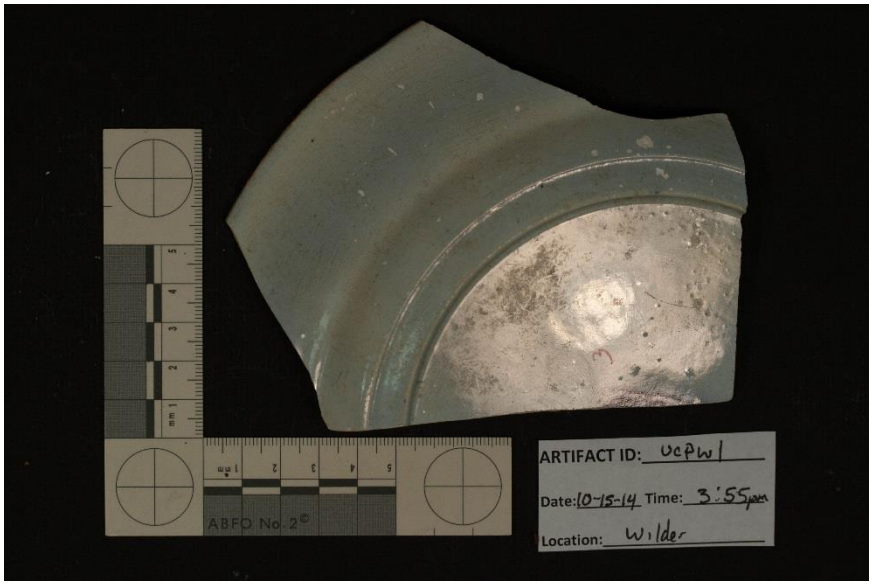

Figure 5.4: Unmodified image of the reverse side of UCPW1

Interestingly, the '3' marking written on the underside of UCPW1 in Sharpie ©, seen in Figure 5.4, completely disappears under infrared imaging in Figure 5.5. For researchers seeking to image an artifact that has previously been marked with an alcohol-based marker like a standard Sharpie ©, infrared would be a useful tool in obtaining a clear image and removing the markings from view without physically needing to treat the marks.

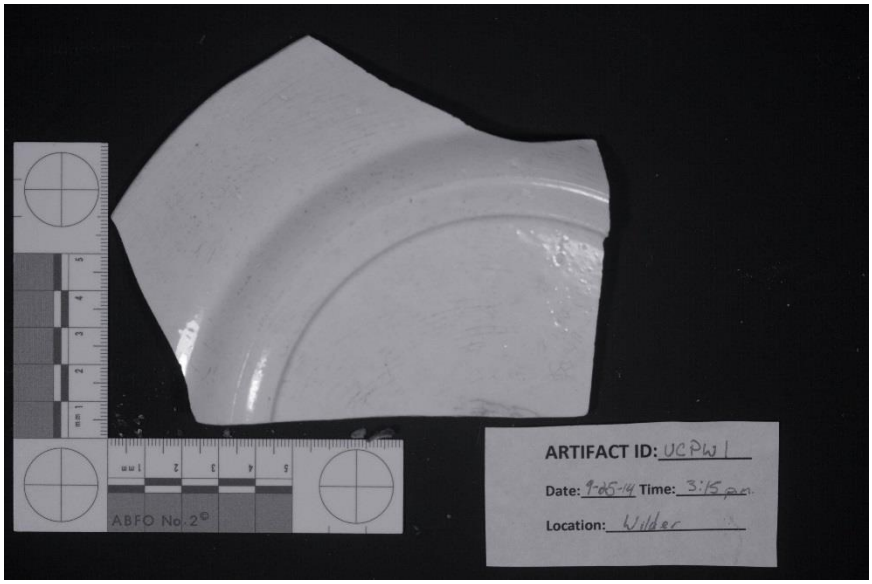

Figure 5.5: Infrared image of the reverse side of UCPW1

Conclusions for UCPW1

UCPW1 offers a lot of insight into the capabilities of infrared imaging on ceramics featuring printed designs. Under infrared conditions, the printed image becomes clearer and reveals details that may be hidden underneath by penetrating the thinner areas of pigment in the design. This does not come without risk, however. Smaller designs risk being obscured through infrared, and care must be taken to note the loss of any details.

The infrared imaging if UCPW1 also demonstrates the effectiveness of removing alcohol-based marker notations from artifacts without having to physically remove them. From UCPW1, no conclusions can be drawn as to the spectrum of ink types that infrared is able to obscure, however alcohol-based inks prove easily penetrated by IR wavelengths.

In conclusion, infrared imaging proves to be successful in resolving clearer, and potentially hidden design features in pearlware and other similarly print design ceramics. The potential also exists in using IR as a tool to remove marks from specific types of inks on artifacts for diagnostic imaging.

UCP2

UCP2 features the bottom well portion of a porcelain bowl or cup, also recovered from A&M excavations of Port Royal, Jamaica. A small, blue, hand drawn flower decorates the bottom of the well, surrounded by a blue circle that defines the bottom of the vessel. The flower is filled with three blue dots, one covering the center of the flower petal and the other two filling each of two leaves.

On the reverse side, the rim base of UCP2 remains intact. Small areas of iron corrosion discoloration are visible on the underside of the ceramic, confined to the area inside the rim base. Moving away from the base, remnants of exterior blue decorative elements are visible, consisting of parts of a circle, and, most likely, a floral design similar as to the interior of the piece. The non-decorated areas of the porcelain show up as a soft blue color, likely from the use of cobalt blue in the decorative process.

Figure 5.6: Unmodified image of UCP2

Under normal photographic conditions, the drawn designs of UCP2 are clearly visible, as seen in Figures 5.6 and 5.8. However, under infrared conditions, a substantial visual change takes place to the appearance of UCP2. On the inside face, seen in Figure 5.7, the circle inscribing the flower and the flower's three fill dots disappear from view. The flower itself is further obscured, showing neither the clarity nor completeness of Figure 5.6.

A similar effect continues on the underside of UCP2, shown in Figure 5.9. However, rather than just obscuring elements of the cobalt blue designs, the infrared imaging has completely removed any trace of their application. The retention or disappearance of designs under infrared may be related to the thickness of the application of cobalt blue in a particular design. Further research outside the scope of this thesis would be required to describe specific causes with certainty.

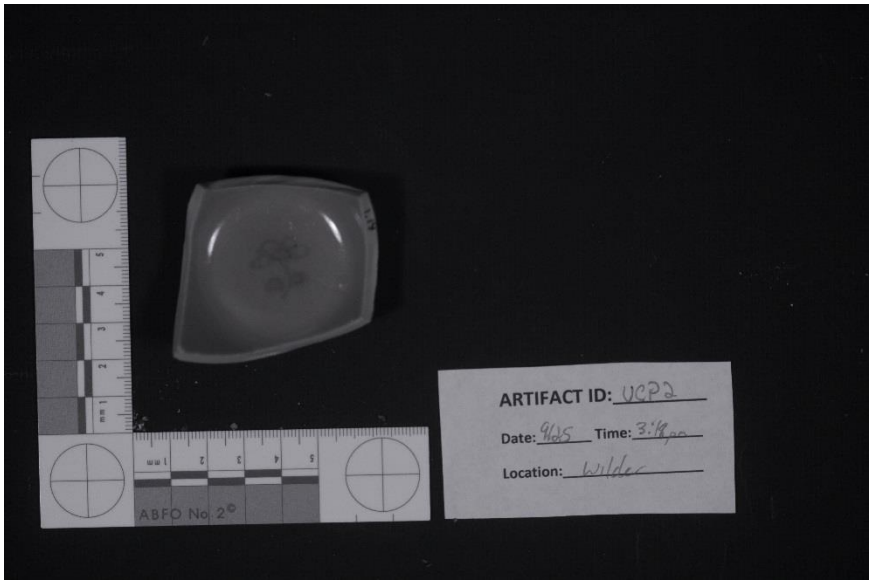

Figure 5.7: Infrared image of UCP2

Coinciding with the disappearance of artistic elements in UCP2, infrared imaging has also caused a darkening of the surrounding ceramic, from a light blue to a considerably darker shade. While it is understood that the nature of colors can change due to the desaturation of the photograph from infrared capture, this color change is atypical of that transformation. It appears, when compared to the bright color of the infrared photographs of UCPW1, seen in Figures 5.3 and 5.5, that infrared waves may be more heavily absorbed, resulting in a darker return to the camera sensor.

In addition to the loss of design features and darkened appearance of the ceramic, the spots of iron corrosion visible on the bottom of UCP2 are not visible under infrared.

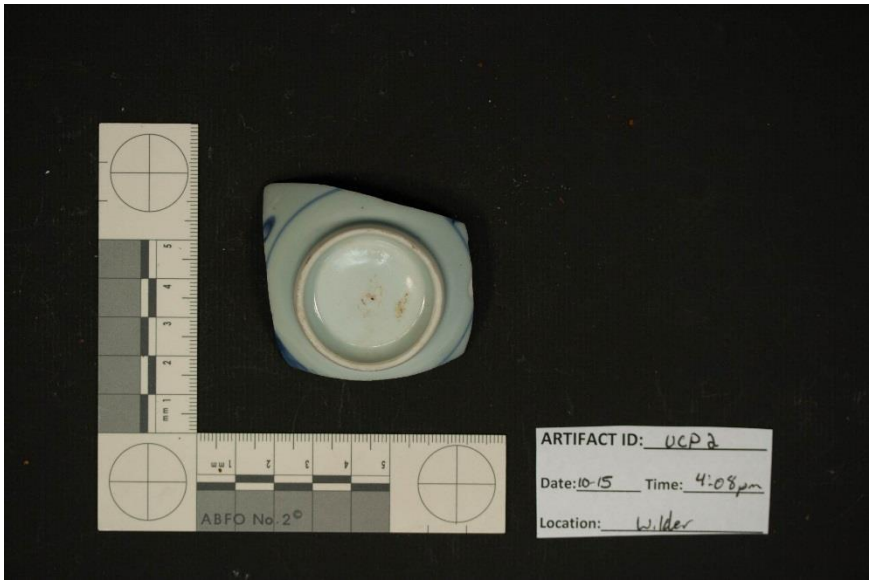

Figure 5.8: Unmodified image of the reverse side of UCP2

Figure 5.9: Infrared image of the reverse side of UCP2

Conclusions for UCP2

UCP2 offers intriguing results when compared to UCPW1. Both types of ceramic have their designs made out of cobalt blue, a pigment made using the cobalt salts of alumina, or aluminum oxide. In UCPW1, a sample of pearlware, the cobalt blue image retains its integrity well under infrared imaging. The porcelain piece, UCP2, however, images poorly under the same conditions even though it also has designs created with cobalt blue.

Discounting the differences between the lighter ceramic background of UCPW1 and the darker UCP2, the largest difference may lay in the thickness of the layer of cobalt blue applied in creating the design. UCPW1 suffered the same disappearance of detail seen in UCP2, albeit in a smaller degree, in lighter lines throughout its 'blue willow' features. If UCP2's designs used only a thin layer of cobalt blue, it is likely the infrared light passes completely through, causing the floral and circle designs to be invisible to the camera sensor.

Overall, UCP2 did not image well under infrared conditions. Diagnostic designs and iron corrosion stains failed to appear after being imaged with the infrared camera and the underlying ceramic background became much darker. More information, with these conditions and equipment, was captured using unmodified, normal photography.

UCWW3

UCWW3 is a piece of whiteware excavated from Port Royal, Jamaica. It is unknown what type of ceramic the sherd comes from. Similar to UCPW1 and UCP2, UCWW3 features a blue floral design that dominates the majority of the piece (Figure 5.10). The design shows obvious fading, staining and cracking of the surface. On the left side of the piece, a brown area of unknown damage is visible.

The rear of UCWW3 is bare, minus similar surface cracks as to the front. These cracks are highlighted with a rust-colored stain that causes them to stand out against the off-white background of the ceramic. The cause of this staining is unknown.

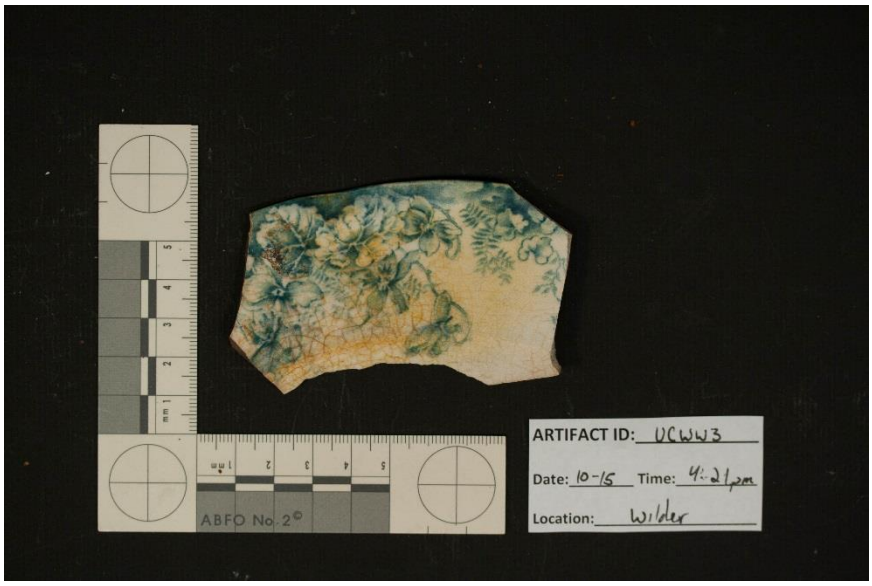

Figure 5.10: Unmodified image of UWCC3

UCWW3 did not respond well to infrared photography. The entirety of the floral image on the sherd disappeared when imaged with the infrared camera (Figure 5.11).

Areas of surface cracking and most of the brown area of damage are still visible, however, the floral design is not. Judging by the already faded state of the design, it is likely the blue pigment is not thick enough to absorb the infrared light needed to appear in an infrared image.

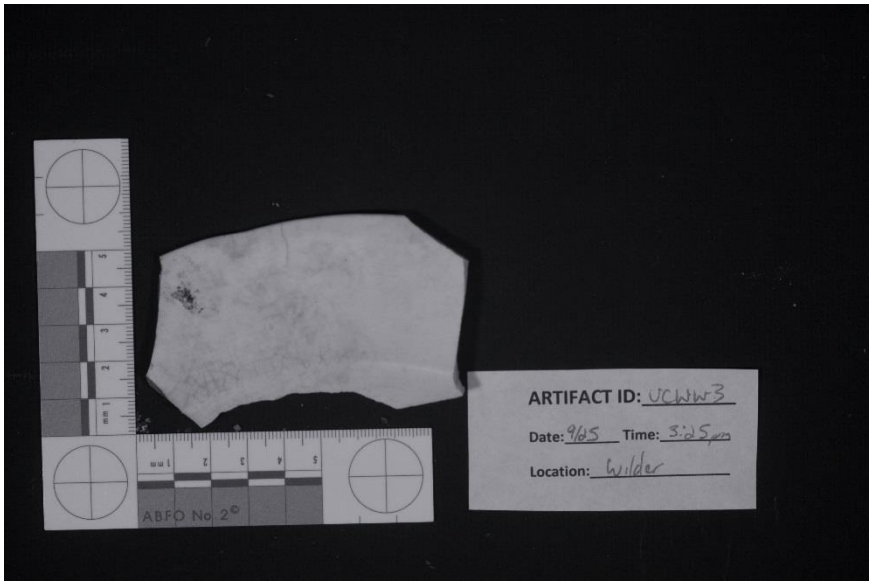

Figure 5.11: Infrared image of UCWW3

The reverse side of UCWW3 suffers detail loss as well. The stained surface cracking shown in Figure 5.12 does not show up in the infrared image, Figure 5.13. The likely cause of this is the removal of the rust-colored stains from view. These stains cause the cracks to become clearly visible to the naked eye, and without the benefit of their aid, the cracks are undetectable in imagery.

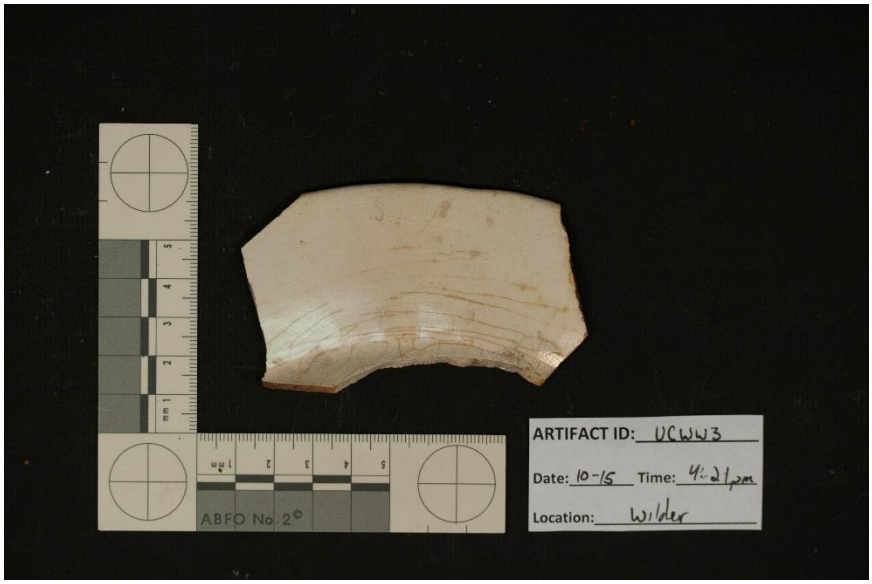

Figure 5.12: Unmodified image of the reverse side of UCWW3

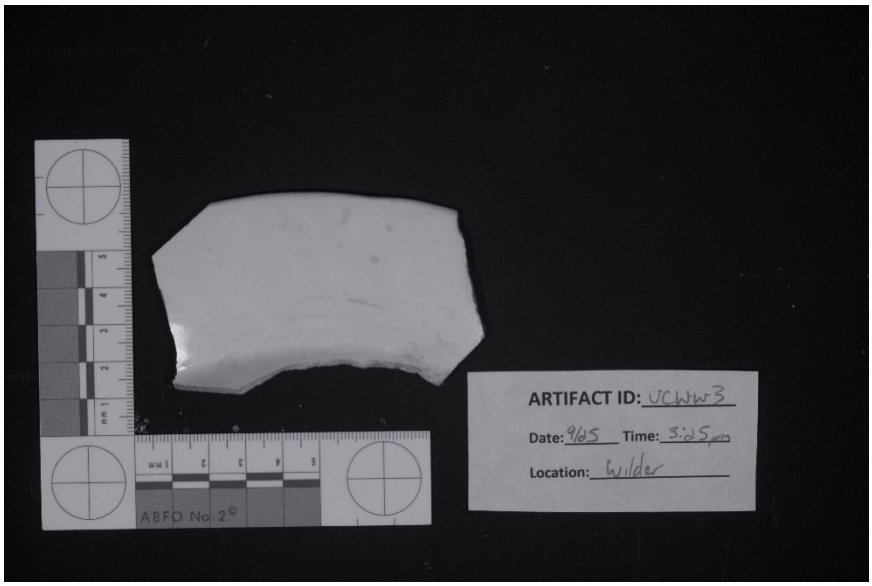

Figure 5.13: Infrared image of the reverse side of UCWW3

Conclusions for UCWW3

UCWW3 responded poorly to infrared photography. As seen between Figures 5.10 and 5.11, the image and staining patterns visible under normal conditions and with the naked eye completely disappear when imaged with a camera modified for infrared. Similar results appear for the reverse side of UCWW3, where the removal of surface crack staining makes them impossible to detect in Figure 5.13. This may be useful for researchers seeking to image areas of whiteware without similarly stained surface cracks, however, for recording artifacts in their current state, infrared is not recommended.

UCCW4

UCCW4 features a rim sherd of creamware, also known as Queen's ware. A lead-glazed earthenware, it was developed by Josiah Wedgwood in 1762 and remained immensely popular from 1770 until 1800, with variations continuing until 1820 (Hamilton, 2015).

The creamware sherd has a soft-yellow, cream color base to its ceramic. Along the rim, a worn and faded brown leaf pattern survives, followed by a similarly colored geometric design of lines, ovals, and dots. Underneath these designs, the remains of a green-colored line that appears to have circled the entire rim of the vessel can be seen where it has not eroded or chipped away. The rear of UCCW4 is completely devoid of any diagnostic markings.

In Figure 5.14, the decorative pattern of UCCW4 can be seen. The leaves, most of which have chipped or faded substantially, can still be seen due to the stained outline that remains. Similar effects continue for the geometric pattern and green line below.

Figure 5.14: Unmodified image of UCCW4

When imaged under infrared, UCCW4 did not show much discernable change. The largest difference, seen in Figure 5.15, is the loss of the stained leaf outlines where the design has eroded away and the loss of identifying colors for the green line on the outermost edge of the rim. Losing these details make interpreting the pattern of the design on UCCW4 more difficult.

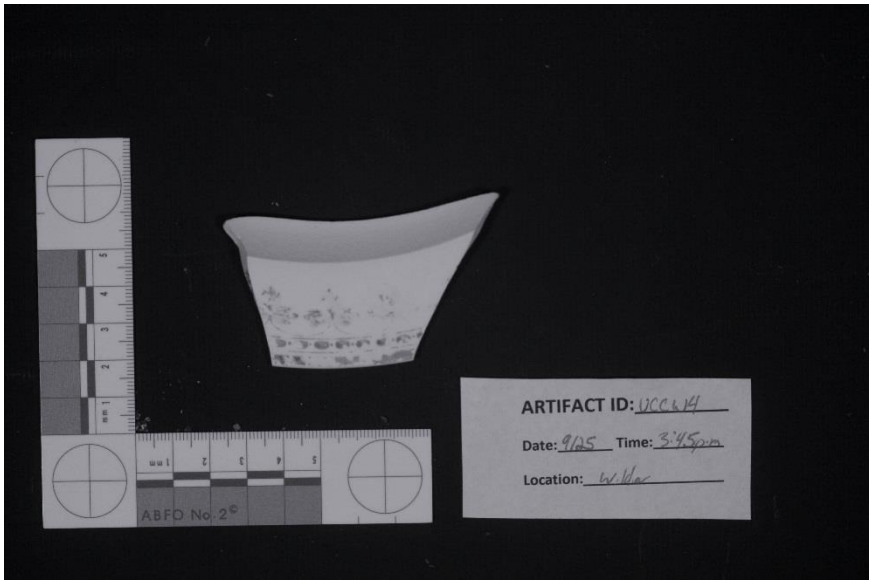

Figure 5.15: Infrared image of UCCW4

Conclusions for UCCW4

While little change was detected for imaging of the creamware sample UCCW4 using infrared, the change that occurred was detrimental to the overall analysis of the artifact. Trace stains of the rim pattern become obscured during infrared imaging and would not make good reference for diagnostic records of the artifact. Additionally, no new information is revealed through using infrared on this piece of creamware. Infrared imaging is not recommended.

UCSW5

UCSW5 is a piece of trailed slipware, characterized by a red to brown body and decorated by a brown and yellow slip with brown stripes. Popular between the late 16th through early 19th centuries, slipware of this type was used in most cases as tableware

and other utilitarian dishes (Hamilton, 2015b). The top (outer) surface, shown in Figure 5.16, is the only surface to be covered by the striped slip. The reverse surface retains the original reddish-brown color and rough texture of the true surface of the vessel when created.

Figure 5.16: Unmodified image of UCSW5

Comparisons of UCSW5's unmodified and infrared images proved inconclusive. The infrared image of UCSW5's slipped face, Figure 5.17, retains all of the same features seen in Figure 5.16 without revealing any new information. The thickness of each stripe remains consistent, proving more resistant to the penetrative power of infrared wavelengths than its pearlware, porcelain, and creamware counterparts.

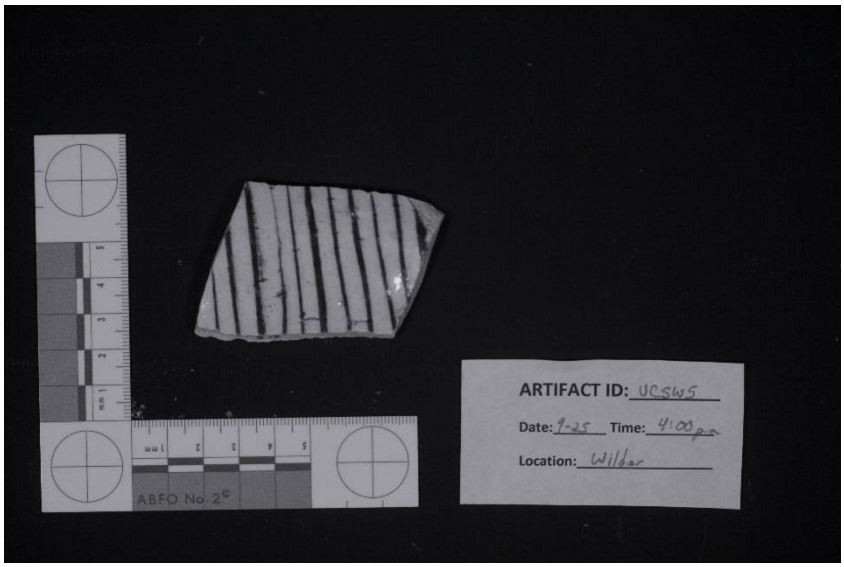

Figure 5.17: Infrared image of UCSW5

The reverse of UCSW5 does not contain any unique or diagnostic features apart from its reddish-brown body. When viewed between normal photography and infrared (Figures 5.18 and 5.19, respectively), no change is observed between the two.

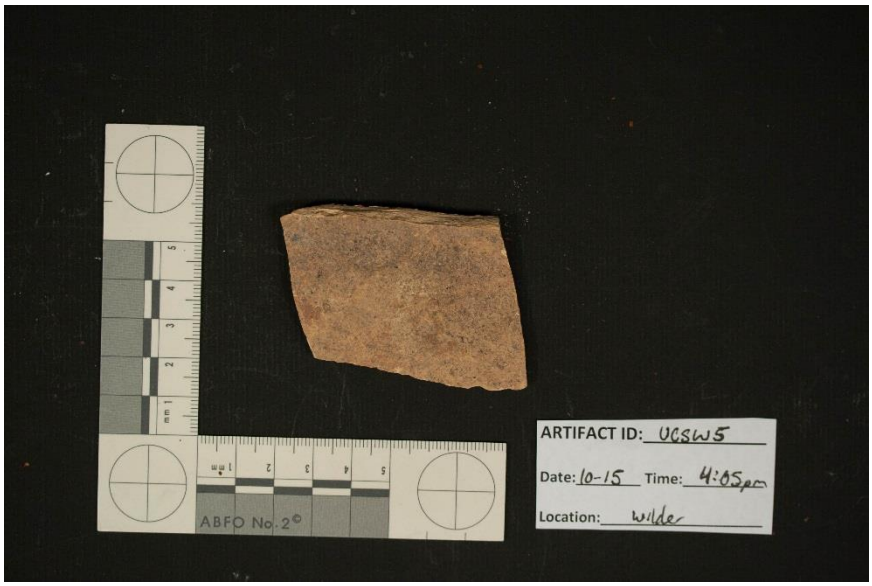

Figure 5.18: Unmodified image of the reverse of UCSW5

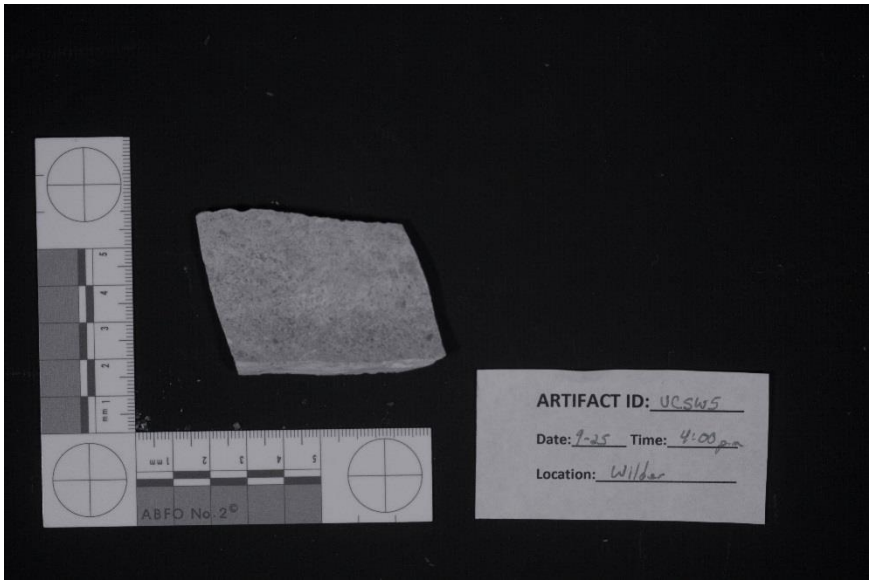

Figure 5.19: Infrared image of the reverse of UCSW5

Conclusions for UCSW5

Little to no change was observed between photographing the slipware sample UCSW5 in normal light and infrared. Both the slip and natural surfaces prove resistant to the penetrative power of the longer infrared wavelengths, offering no benefit to using infrared photography in place of normal photographic methods.

UCTE6

UCTE6 represents a sample of tin enameled ware, recovered from Texas A&M excavations in Port Royal, Jamaica. The sherd used in this study features a blue, hand painted design, known to end around AD 1690 (Hamilton, 2015). The glaze appears light blue in color and is uniform throughout the entirety of the piece.

Not enough of the design remains to identify it with certainty, but it appears to be a floral pattern of some kind with an additional line outside (Figure 5.20).

The rear of UCTE6 is unremarkable for diagnostic features. Continuing the pale blue glaze from the design side, the only markings visible are 'NS 2-1', painted on as identification by archaeologists following its excavation. Two areas of damage are visible where the ceramic has broken in its deposition environment. Visible traces of dirt can be seen covering the reverse side.

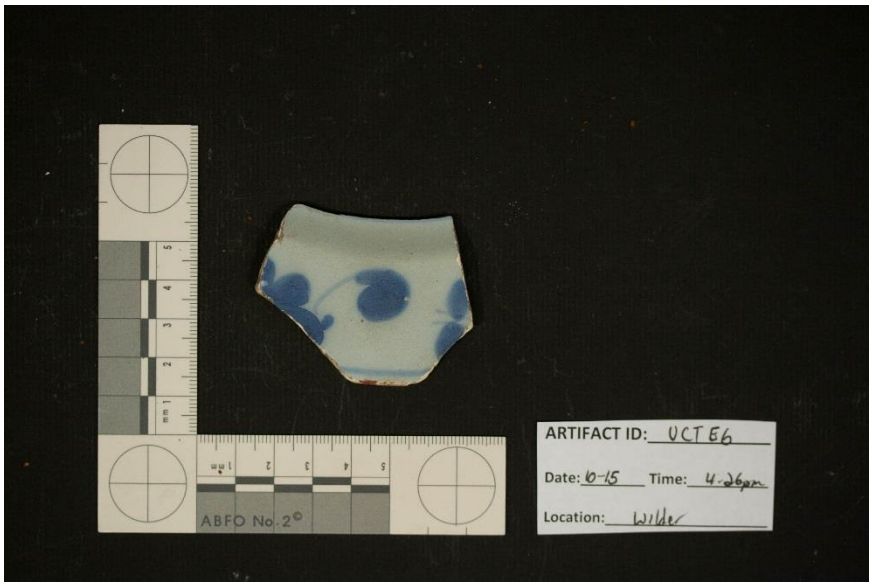

Figure 5.20: Unmodified image of UCTE6

When examined with the infrared camera, UCTE6 imaged poorly in relation to its unmodified counterpart. The blue decorate elements are nearly invisible in Figure 5.21. Trace outlines are visible in the center and left side of the image, but the line and design on the right have completely disappeared.

This result follows trends seen in UCPW1, UCP2, and UCWW3 where decorative elements printed or painted on in blue pigments have been penetrated in part, or in whole, by infrared waves and are obscured in the infrared image. Whether or not this holds true for all blue pigmented designs of the printed or painted type is uncertain. Further research is required to better define the scope and cause of this phenomenon on archaeological ceramics.

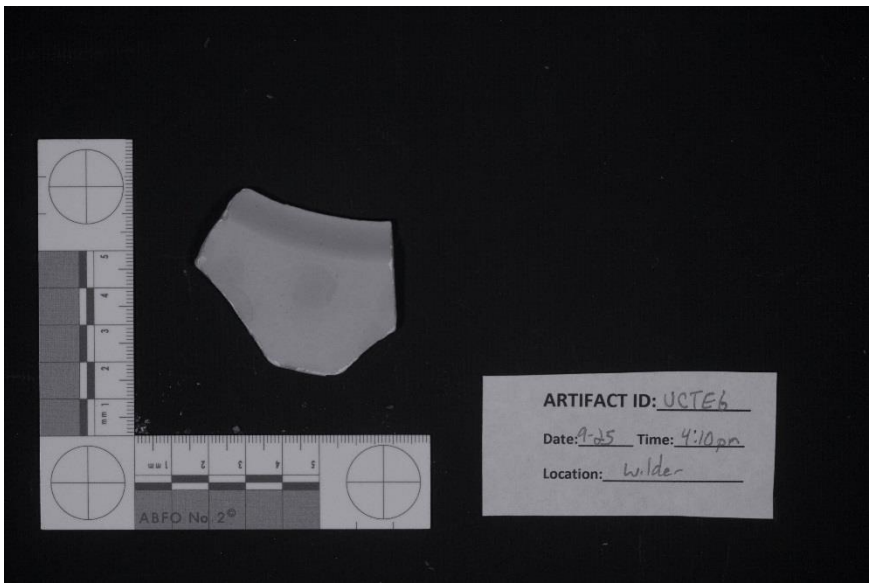

Figure 5.21: Infrared image of UCTE6

The reverse side of UCTE6 (Figures 5.22 and 5.23) shows little change between unmodified and infrared photography. The dirt mentioned earlier disappears from view, however, the painted identification ‘NS 2-1’ remains, due to the paint used absorbing infrared waves.

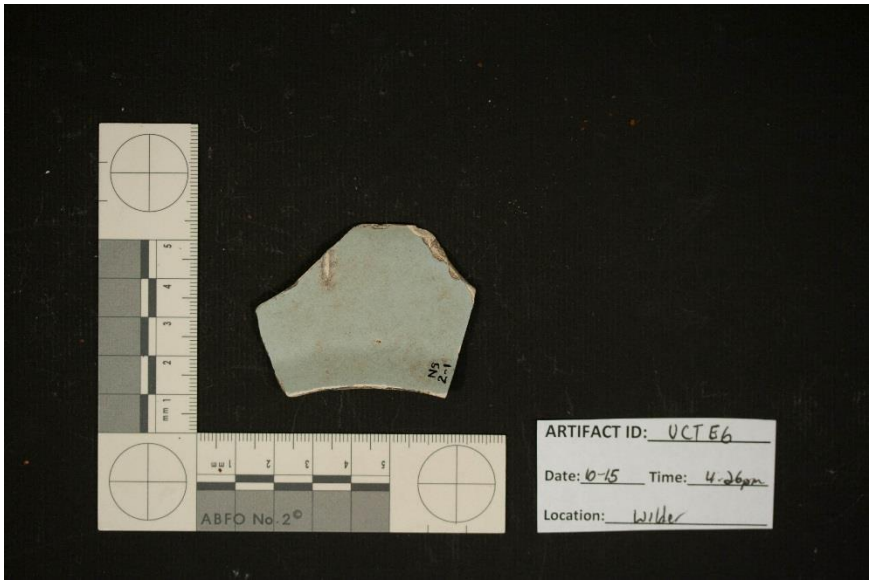

Figure 5.22: Unmodified image of the reverse side of UCTE6

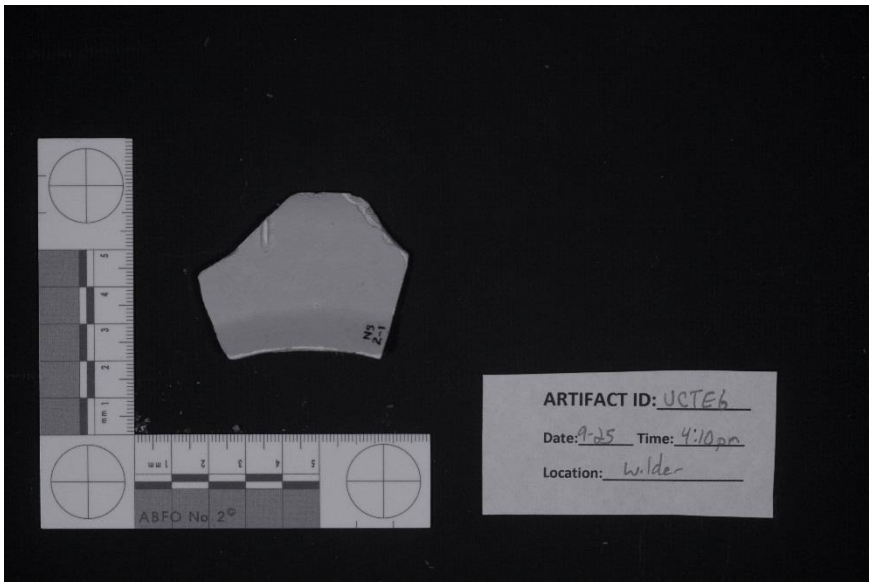

Figure 5.23: Infrared image of the reverse side of UCTE6

Conclusions for UCTE6

Tin enameled wear suffers from the same loss of printed and painted designs seen in the pearlware, porcelain, and whiteware samples. It is impossible to extend this trend onto other similar ceramics without further testing and better understanding the compositional make-up of each piece. Caution should be used if purchasing or converting a dSLR for the infrared imaging of similar ceramics. Infrared imaging is not recommended for use with this type of tin enameled ware.

UCStW7

The small, triangular UCStW7 was selected as the sample for stoneware. Tan on both surfaces, the exterior surface has a dimpled texture to it, evidenced by the lighter areas in Figure 5.24. On the reverse, the entire piece is smooth and uniform in color without any discernable imperfections.

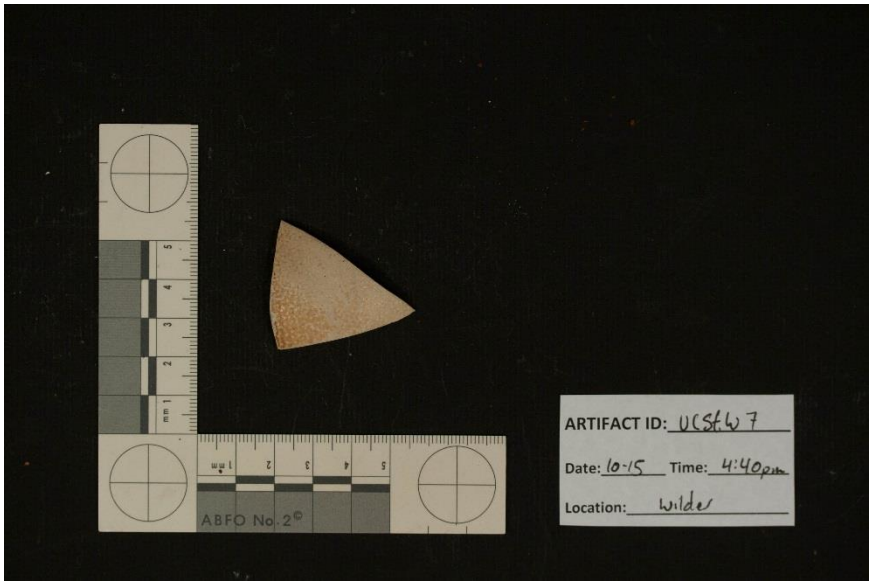

Figure 5.24: Unmodified image of UCStW7

In infrared, these characteristics do not change, with the exception of the lighter, dimpled areas on the exterior surface becoming uniform with the surrounding ceramic matrix. As seen in Figure 5.25, the exterior surface of UCStW7 is completely devoid of any identifying characteristics. The uniform response likely has to do with the nature of the glaze and how it does not vary over the surface of UCStW7 in color or depth. A larger, more varied piece of stoneware may yield different results.

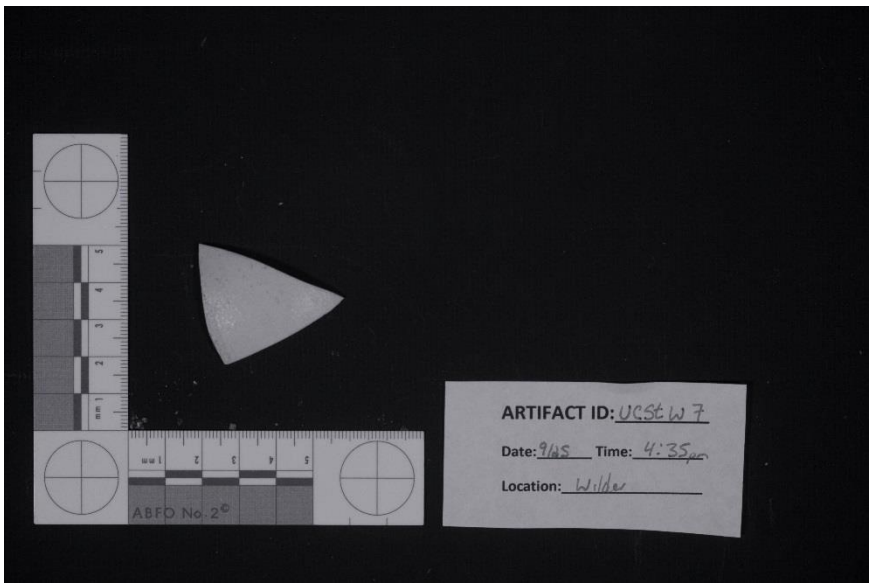

Figure 5.25: Infrared image of UCStW7

The reverse side of UCStW7 yields similar results as to the exterior surface. Having already appeared uniform in color and texture, the penetrative power of the infrared waves act evenly over the entire sherd, causing no detectable change once the waves are reflected and processed by the camera sensor. This can be seen in Figures 5.26 and 5.27.

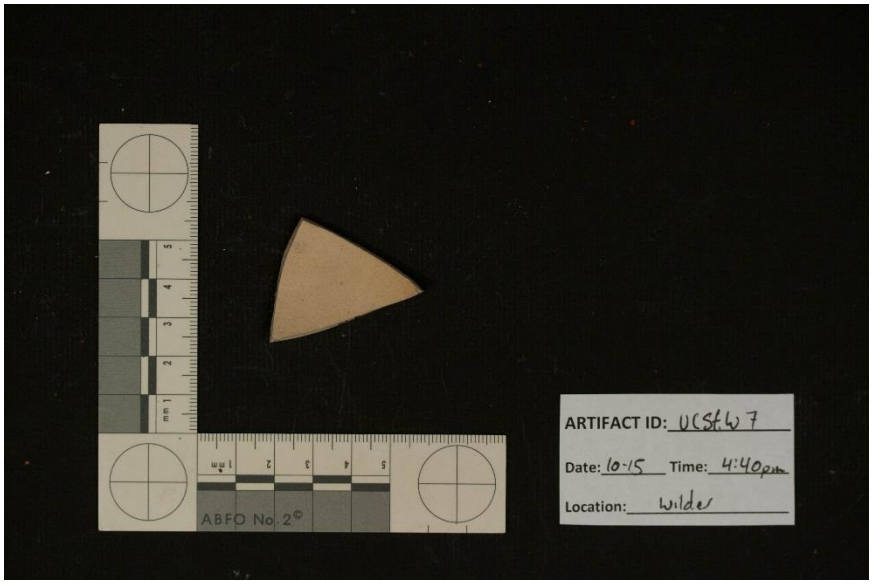

Figure 5.26: Unmodified image of the reverse side of UCStW7

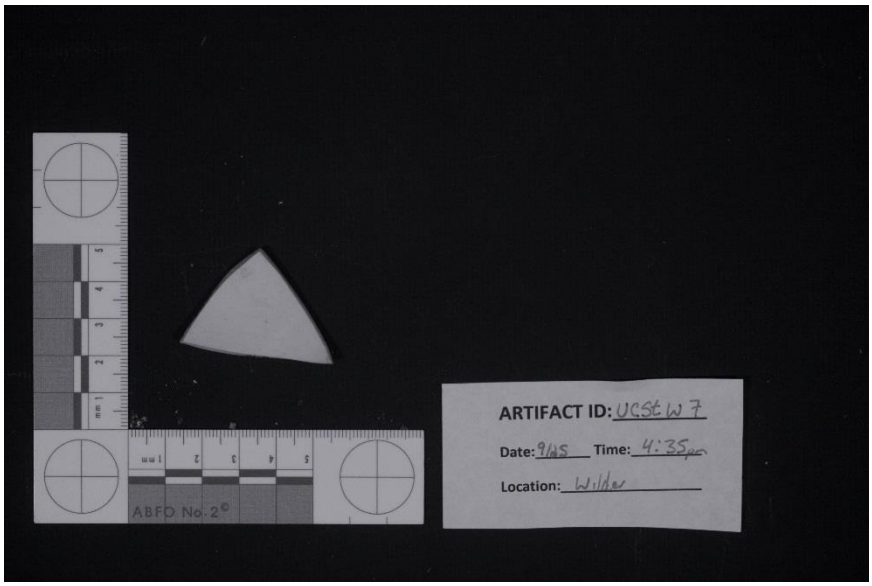

Figure 5.27: Infrared image of the reverse side of UCStW7

Conclusions for UCStW7

No visible differences were detected between the unmodified and infrared imaging of UCStW7 other than the dimpled areas becoming more uniform in color to the

surrounding ceramic body. At least in the case of UCStW7, infrared imaging does not appear to be a useful solution in examining stoneware ceramics.

UCCE8

UCCE8 is a large piece of unglazed coarse earthenware. The exterior surface, seen in Figure 5.28, has a reddish-brown body spotted with red and white patches of sea encrustations. Small ridges are visible running horizontally across the sherd, appearing to be where coils of clay were added to create the final ceramic vessel. On the reverse side, UCCE8 is a sandy color. Coating the lower left corner and parts of the left side of the sherd are a series of black stains. The origin of these stains is unknown.

Figure 5.28: Unmodified image of UCCE8

After undergoing infrared imaging, UCCE8 does not appear to show any additional diagnostic characteristics nor lose any substantial detail. The largest change observed stems from the coloration change of the residual red and white encrustations. Rather than standing out prominently, they fade into the background once imaged in infrared, seen in Figure 5.29.

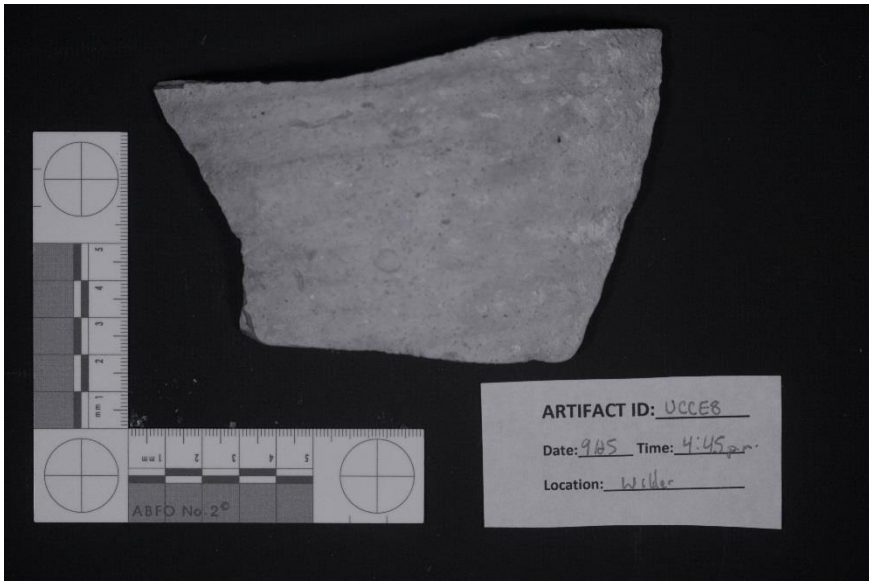

Figure 5.29: Infrared image of UCCE8

The reverse side of UCCE8, Figures 5.30 and 5.31, remains consistent in registering no change between the unmodified photograph and infrared image. The density, visibility, and expanse of the black stains remains constant between both photographs, showing no signs of penetration by NIR waves.

Figure 5.30: Unmodified image of the reverse side of UCCE8

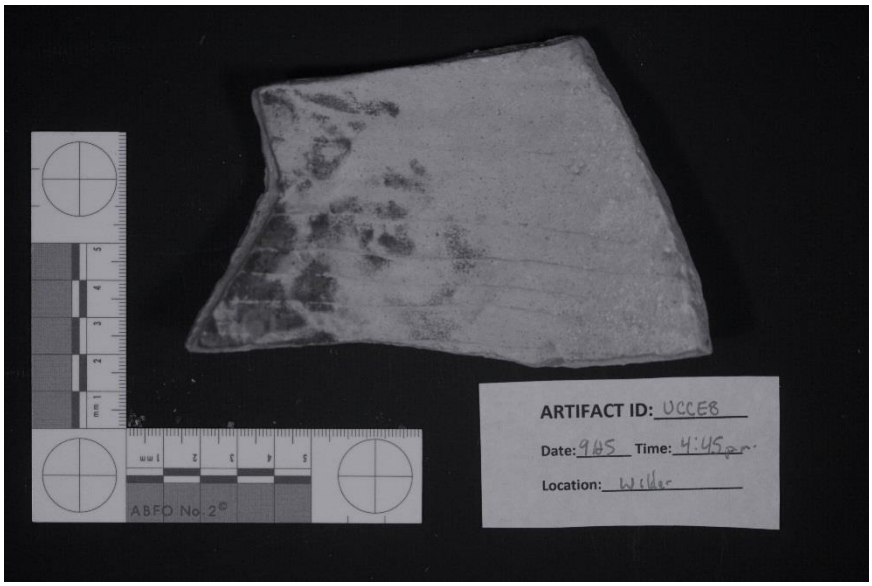

Figure 5.31: Infrared image of the reverse side of UCCE8

Conclusions for UCCE8

UCCE8 does not reveal any hidden information under examination with infrared photography. The only notable changes that occurred when unmodified and infrared images were compared were the encrustations remaining on the exterior of UCCE8 becoming less visible. The black stains observed on the reverse side failed to change in their clarity or coverage, evidence whatever substance remains absorbs NIR waves. From these comparisons, it is apparent that coarse earthenware of this style is not responsive to NIR photography.

UCWC9

The final ceramic artifact selected in this study was UCWC9, the bowl of a clay pipe recovered from Port Royal, Jamaica. UCWC9 was found without its stem and shows evidence of use due to the black charring evident within the bowl. It is labeled 'PR 89 654-4', the identification code given to it after its excavation by archaeologists. Other than the missing stem and evidence of charring, UCWC9 suffers numerous nicks and gouges across its surface, including a substantial piece missing from the heel. Figure 5.32 gives the unmodified photographic overview of UCWC9.

Upon comparison, no change takes place under infrared of the white clay of UCWC9. The clay remains uniform in color, displaying the same imperfections that are visible under normal photography conditions when photographed by the modified camera (Figure 5.33).

Figure 5.32: Unmodified image of UCWC9

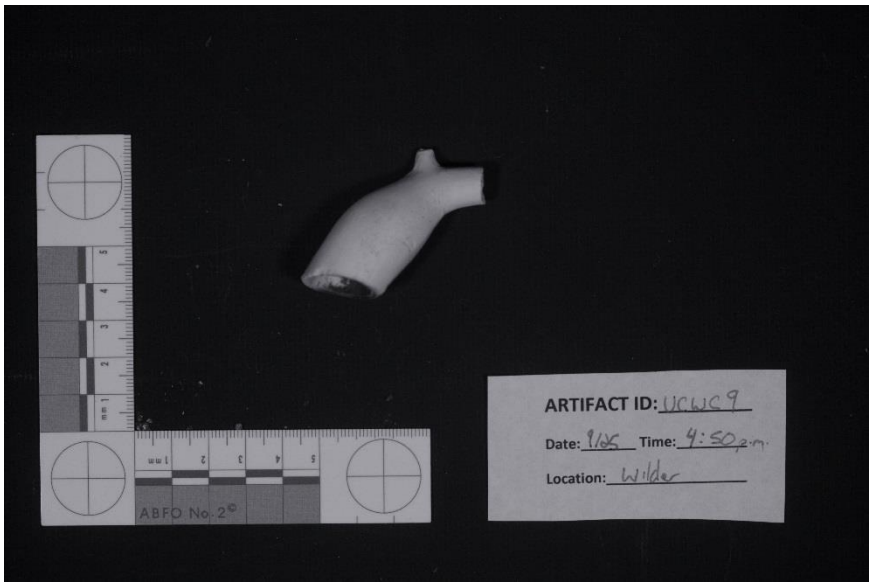

Figure 5.33: Infrared image of UCWC9

The charred areas of the pipe bowls are of particular interest. No difference is seen between the burned areas of clay in Figures 5.32 and 5.33. However, the reverse side of the bowl show noticeable changes. In Figure 5.34, the closest edge to the camera

shows a range of color for the burned areas of the pipe bowl, ranging from brown to black. These changes show the intensity of the heat in that localized area on the pipe. When comparing the same areas in infrared in Figure 5.35, these subtle changes in color are more difficult to detect. Some portions appearing to be in better shape than shown with unmodified photography in Figure 5.34.

5.34: Unmodified image of the reverse side of UCWC9

Possible causes for this change may have to do with the depth of the burned areas and how long they were exposed to increased temperatures during the times the pipe was used to smoke tobacco. Places along the pipe rim not subject to higher temperatures for longer periods would contain only a small depth of charring into the clay, seen as the brown areas, while the black areas likely held sustained heat for a prolonged time. The changes in this depth over time make the more heavily charred sections less susceptible

to penetration of NIR radiation, not allowing it to reflect to the camera sensor and image areas underneath. The brown areas, in this case, are not yet deep enough to resist the infrared waves from passing through, obscuring them from the sensor.

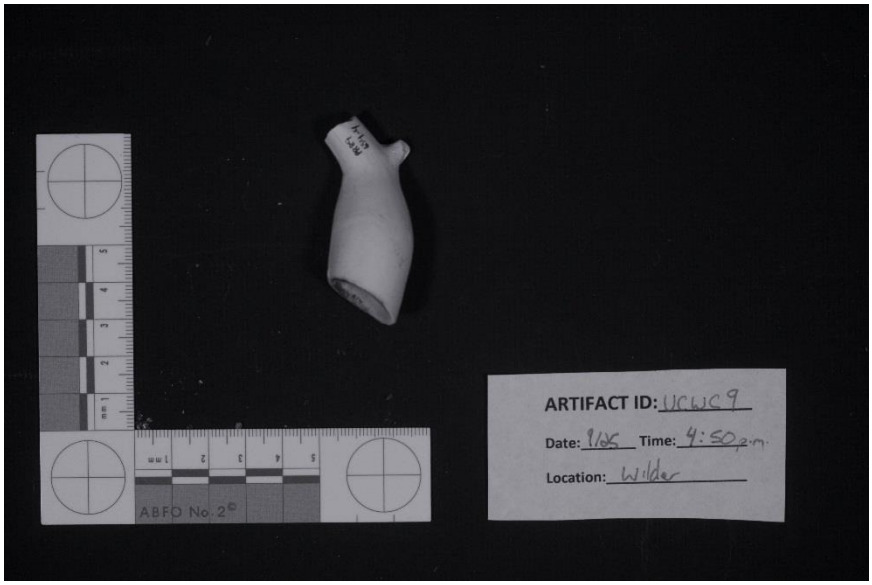

Figure 5.35: Infrared image of the reverse side of UCWC9

Conclusions for UCWC9

Infrared imaging did not show any noticeable change to the appearance of the white clay body of UCWC9. However, the more lightly burned areas of the pipe bowl were more likely to be obscured through the use of infrared photography than more deeply charred areas. This could prove useful to researchers attempting to determine burn usage of clay pipes, using the penetrative power of NIR wavelengths to map out heavily burned areas in comparison to those that have minimal use. Infrared imaging has the potential to be useful in the study of previously used clay pipes.

Conclusions for Ceramics

The capabilities of NIR photography for ceramics vary widely depending on the type of ceramic to be examined. UCPW1, the 'blue willow' pearlware, showed the most promise, clarifying the printed design and better exposing the design for identification. Other ceramics making use of cobalt blue for their designs, however, did not fare well under NIR imaging.

On the other hand, coarser, more heavily glazed ceramics proved to show little change between being photographed by 'normal' and infrared camera units. It is likely the unvaried nature of their design and lack of decorative elements leave little for infrared imaging to reveal below the surface. In other cases, such as UCSW5, the glaze appears thick enough and of the right pigments to prevent the penetration of IR radiation.

In the case of UCWC9, infrared photography did not enhance any part of the ceramic, but instead offered insight into the use of the bowl of the clay pipe. Mapping out burn patterns may prove useful to researchers attempting to recreate how similar clay pipes were used in historical periods.

No one answer adequately describes the capabilities of infrared photography on ceramics. With such a wide range of ceramic types, methods, uses, and deposition environments, it comes as no surprise that the results vary. Final recommendations on the usefulness of infrared photography on each artifact are listed on the table shown in Figure 5.36.

ARTIFACT ID	ARTIFACT TYPE	SPECIFIC TYPE	ID EXPLANATION	RATING: IR vs VISIBLE
CERAMICS				
UCPW1	Ceramic	Pearlware	Unconserved Ceramic Pearl Ware	Recommended
UCP2	Ceramic	Porcelain	Unconserved Ceramic Porcelain	Not Recommended
UCWW3	Ceramic	Whiteware	Unconserved Ceramic White Ware	Not Recommended
UCCW4	Ceramic	Creamware	Unconserved Ceramic Cream Ware	Not Recommended
UCSW5	Ceramic	Slipware	Unconserved Ceramic Slip Ware	No Change
UCTE6	Ceramic	Tin Enamel	Unconserved Ceramic Tin Enamel	Not Recommended
UCStW7	Ceramic	Stoneware	Unconserved Ceramic Stone Ware	No Change
UCCE8	Ceramic	Coarse Earthenware	Unconserved Ceramic Coarse Earthenware	No Change
UCWC9	Ceramic	White Clay	Unconserved Ceramic White Clay	Recommended

Figure 5.36: Table of final recommendations for ceramics

CHAPTER VI

METALS

Infrared imaging of archaeological metals, particularly those from underwater deposition environments, have not been studied in detail. In this chapter, a collection of nine objects with a variety of compositions, deposition environments, and conservation work were examined to determine their visual response to infrared. Among the metals tested were brass, iron, pewter, lead, and silver. Each conservation treatment described follows recommendations put forth by Hamiltion (2010). Figure 6.1 lists and identifies the artifacts seen throughout this chapter.

Specific causes for imaging changes between NIR and conventional photographs, if any, is mostly unknown. The goal of this chapter is to visually compare the two photographic methods and determine if NIR imaging is a useful tool under the imaging conditions in this thesis for the selected artifacts.

CMPER1

CMPER1 features the handle remains of a pewter spoon recovered from Port Royal, Jamaica. The obverse side of the handle is ornately decorated with scroll work and other design features. Pewter recovered from an underwater archaeological context often suffers from varying degrees of corrosion, depending on the pH of the surrounding environment (Gotelipe-Miller, 1990; 37). However, once removed from this

ARTIFACT ID	ARTIFACT TYPE	SPECIFIC TYPE	CONSERVATION METHOD	ID EXPLANATION	IMAGING LOCATION
METALS					
CMPER1	Metal	Pewter	Electrolydic Reduction	Conserved Metal Pewter Electrolydic Reduction	Wilder
UMSC2	Metal	Silver	Unconserved	Unconserved Metal Silver Coin	Riverside
UMBB3	Metal	Cupreous (Brass)	Unconserved	Unconserved Metal Brass Buckle	Riverside
UMWM4	Metal	White Metal	Unconserved	Unconserved Metal White Metal	Riverside
UMC5	Metal	Cupreous and Wood	Unconserved	Unconserved Metal Cupreous	Riverside
UMLB6	Metal	Lead	Unconserved	Unconserved Metal Lead Ball	Riverside
UMIC7	Metal	Iron Concretion	Unconserved	Unconserved Metal Iron Concretion	Riverside
UMISD8	Metal	Iron with wood	Unconserved	Unconserved Metal Iron Spike Dry	Riverside
CMIERT9	OMITTED				
CMLBER10	Metal	Lead	Electrolydic Reduction, Tannic Acid, and Microcrystalline wax	Conserved Metal Lead Bar Electrolydic Reduction	Wilder

Figure 6.1: Metal artifacts examined for Chapter VI.

environment, the corrosion products of pewter are stable, no longer actively attacking the underlying metal (Hamilton, 2010; 85). CMPER1 underwent electrolytic reduction

(ER) to remove the corrosion for aesthetic reasons. Its appearance following ER can be seen in Figure 6.2.

The reverse of CMPER1 (Figure 6.4) is largely unremarkable. “Pock marks” are visible where corrosion has attacked the metal, as described by Peal (1983; 37) and Hornsby (1983; 372-373). No decorative elements adorn this side. The markings ‘PR89 764-5’, used by the excavating team to track the artifact, are visible midway down the handle, written in black paint. It is unknown how this paint will react to IR, and whether it will disappear similar to the ceramic UCPW1.

Figure 6.2: Unmodified image of CMPER1

When examined under infrared, the decorative side of CMPER1 showed no change between conventional and infrared photography. The infrared image of the obverse of CMPER1, Figure 6.3, shows no distinctive change in comparison to its

conventional counterpart, seen in Figure 6.2. With no corrosion or pigments to see through on the surface of the pewter spoon, infrared does not have a medium it fully penetrates. Instead, the original surface of the pewter spoon is returned to the camera sensor.

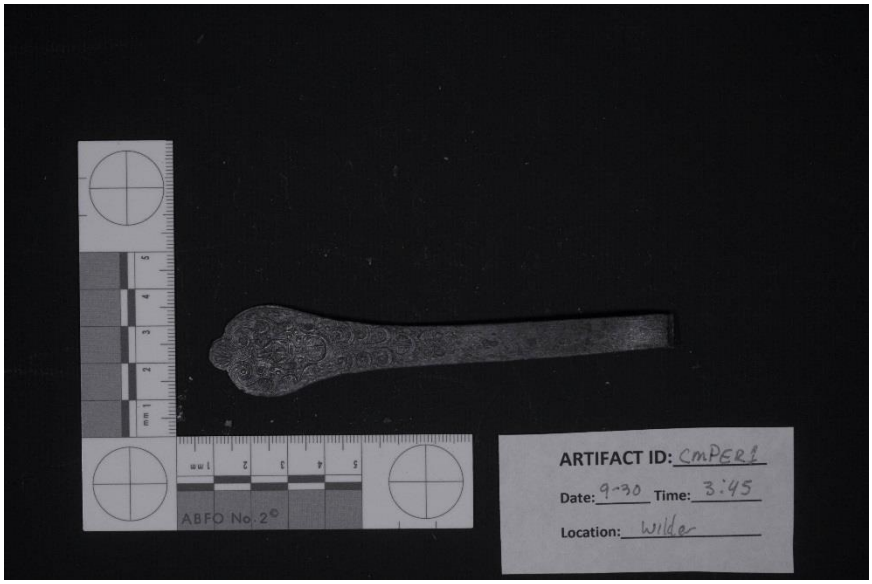

Figure 6.3: Infrared image of CMPER1

Results were similar on the reverse side. The “pock marks”, mentioned previously, show no apparent difference between unmodified (Figure 6.4) and infrared (Figure 6.5) images. Interestingly, the written archaeological identification code ‘PR89 764-5’ does not disappear as similar markings did in the pearlware ceramic UCPW1. The chemical make-up of the ink used was sufficient enough to absorb the IR waves as they struck the writing and be seen on the final image.

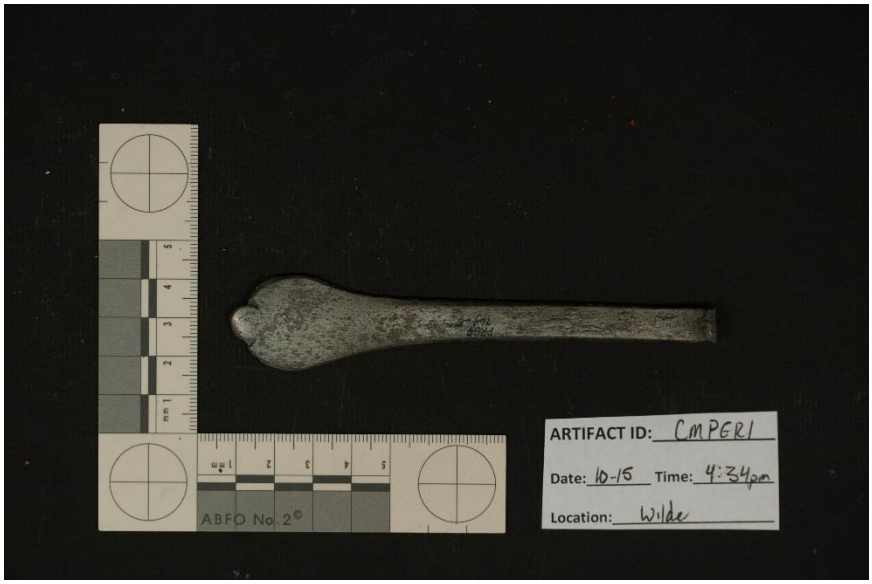

Figure 6.4: Unmodified image of the reverse side of CMPER1

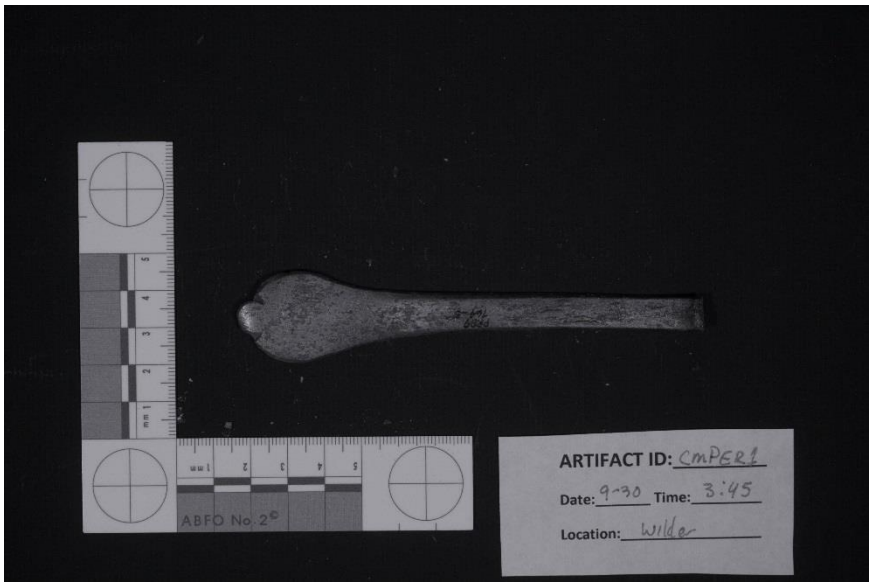

Figure 6.5: Infrared image of the reverse side of CMPER1

Conclusions for CMPER1

In the case of CMPER1, pewter treated through electrolytic reduction did not show any meaningful change between conventional and infrared photography. Had corrosion still been present on the surface, it may have been possible to see through it with infrared, depending on the chemical make-up and thickness. However, further tests would be necessary to verify as such.

The identification marks left by archaeologists remained throughout both images, unlike the results noted in Chapter V for UCPW1. Depending on the chemical make-up of the ink or paint used, variation in the clarity of post-excavation markings appear to occur. If researchers desire the marks to remain through the infrared photography process, test photos with particular inks and paints will need to be conducted to measure their response to NIR.

Infrared imaging for pewter artifacts similar to CMPER1, in that they have uniform color and no surface corrosion, are not recommended due to the lack of visible change observed.

UMSC2

A small, unconserved silver coin recovered from a terrestrial site was selected to test the compatibility of the NIR camera with silver. The coin itself is a Mexican Republic Cap and Rays 8-Reales coin of unknown date. On the obverse (Figure 6.6), the traditional image of a Mexican golden eagle perched upon a prickly pear cactus with a snake held in its mouth can be seen. An area of black corrosion (also known as tarnish)

covers parts of the right wing (on the left side of the coin) and the branch to the right of the eagle's feet. Otherwise, the coin shows some use wear, particularly on the embossed lettering that reads 'Republica Mexicana'.

The reverse side of the coin (Figure 6.8) carries the 'Cap and Rays' design – a cap with numerous rays of light emanating from it. Lettering enumerating the mint location and date, which cannot be easily read, is located underneath this design. Several areas of silver corrosion mar the surface, located to the left, right, and above the cap in the center of the coin.

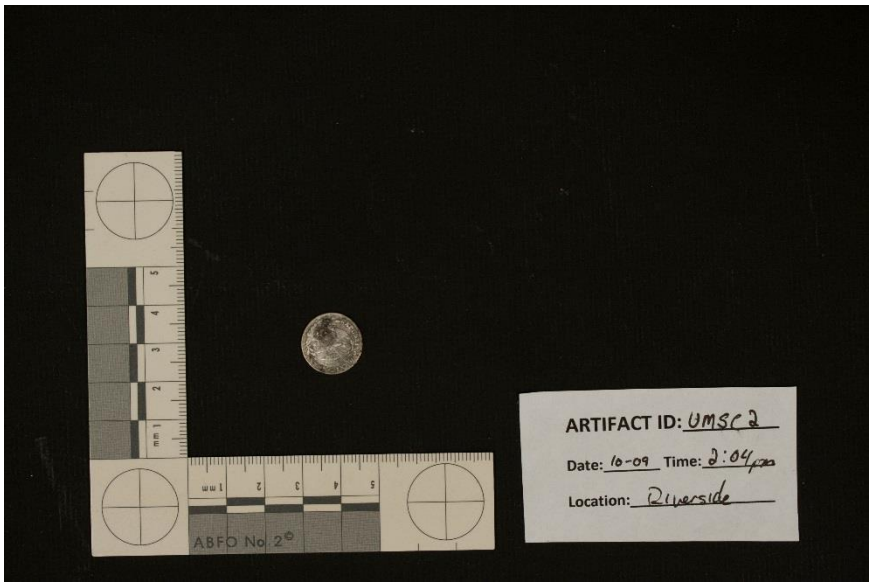

Figure 6.6: Unmodified image of the obverse of UMSC2

Surprisingly, no change was observed on the obverse side of the coin. Unlike iron corrosion stains seen on pottery in Chapter V and paper in Chapter VII, the silver corrosion product was not penetrated by NIR imaging. No additional clarity of the

underlying coin details was detected through visual analysis. However, it is important to note silver tarnish has a different chemical make-up. Iron corrosion is an iron oxide, while silver corrodes into a silver sulfide. It is unknown what, if any, effect this difference may have on the ability of the NIR camera to penetrate corrosion products, but is worth noting for future research.

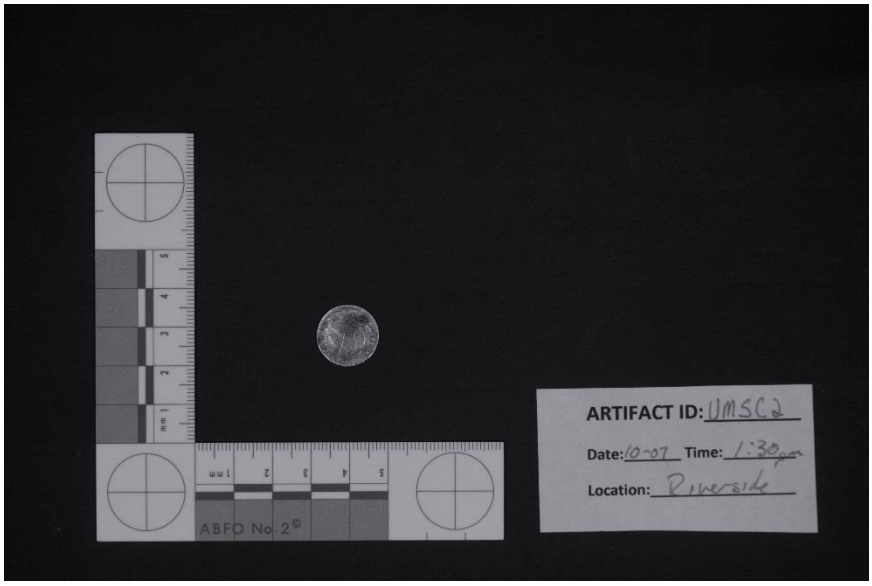

Figure 6.7: Infrared image of the obverse of UMSC2

The corrosion on the reverse side of UMSC2 (Figures 6.8 and 6.9) similarly responds to NIR imaging. Here, the corrosion is not as dense in a single area as the obverse side, so the infrared camera is able to marginally improve the sight through the lighter spots of corrosion. Despite this, the three distinct spots still remain. It appears the resistivity of silver sulfide to NIR photography is a combination of chemistry and density of the corrosion area.

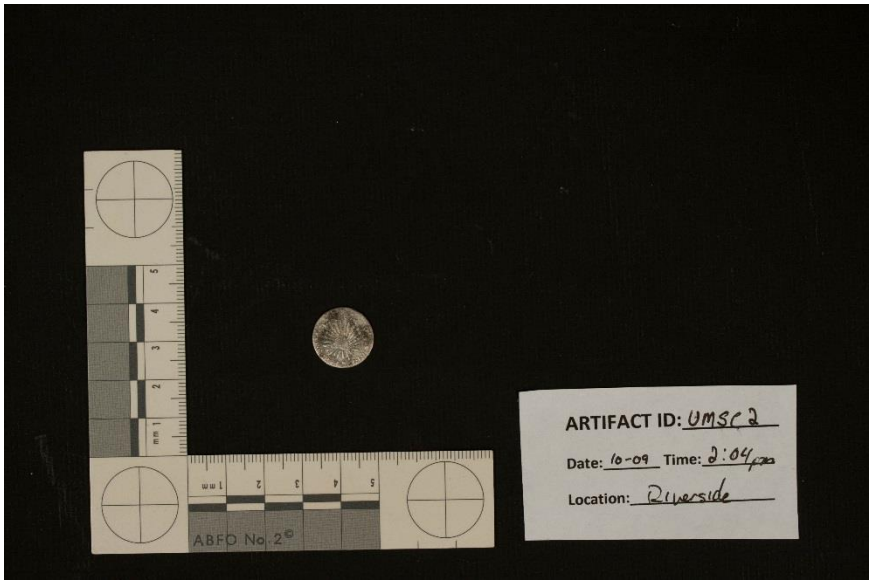

Figure 6.8: Unmodified image of the reverse of UMSC2

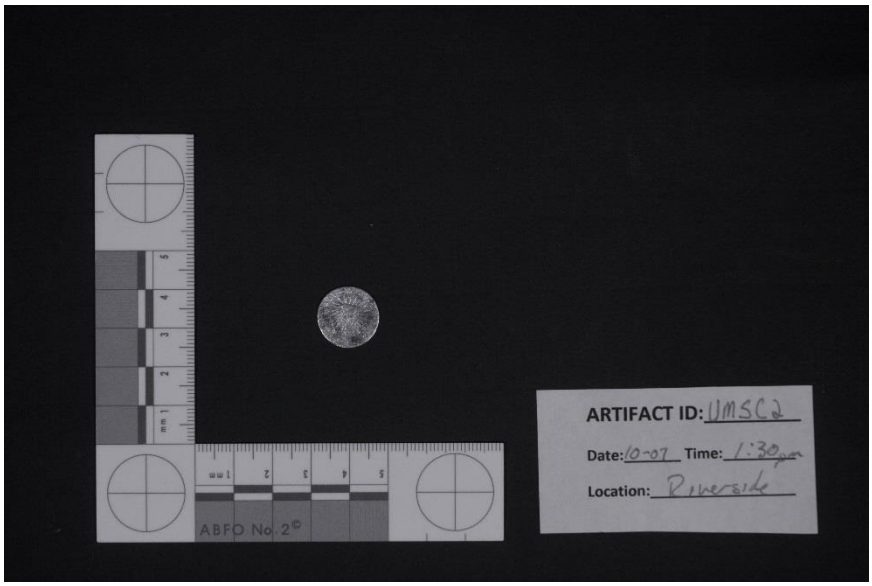

Figure 6.9: Infrared image of the reverse of UMSC2

Conclusions for UMSC2

The use of NIR photography on UMSC2 did not produce any significant changes. Vision through the silver sulfide corrosion was marginal, at best, and the rest of the coin appeared the same under both conventional and infrared. The differing chemical make-up of silver tarnish as compared to iron oxide stains, which NIR successfully penetrated in UCP2 and UTPGI1, may be a possible cause. If very thin layers of silver corrosion are present on an artifact, NIR may have promise, however in artifacts similar to UMSC2, infrared imaging cannot be recommended for use due to the lack of change.

UMBB3

UMBB3 is a corroded, unconserved brass buckle from a terrestrial site (Figure 6.10). Due to its darker appearance, it was imaged on a white card to separate it from the black background. Overall, the buckle has a mottled appearance to its surface, showing signs of obvious corrosion throughout. The middle of the buckle shows areas of iron corrosion, likely from contact of an iron post. Up close, the surface is pitted, both visually and to the touch. The reverse side of UMBB3 appears similar to the front, with a mottled color, iron corrosion products in the center crosspiece, and pitting. While the exact composition is unknown, most brass is made of an alloy of copper, zinc, and often, lead (Hamilton, 2010).

Figure 6.10: Unmodified image of UMBB3

Under infrared, the results from UMBB3 are promising. On the top side of the buckle, the infrared photograph differentiates the corroded areas from the original surface, for both the brass itself and rust stained areas. In the image (Figure 6.11), areas with the remaining original surface show up dark, while more heavily corroded colors image as a matte gray or brighter. Of particular interest is the center crosspiece. In its center, a horseshoe shaped area of red oxide rust is present. This spot, the most corroded of UMBB3, shows up even more brightly.

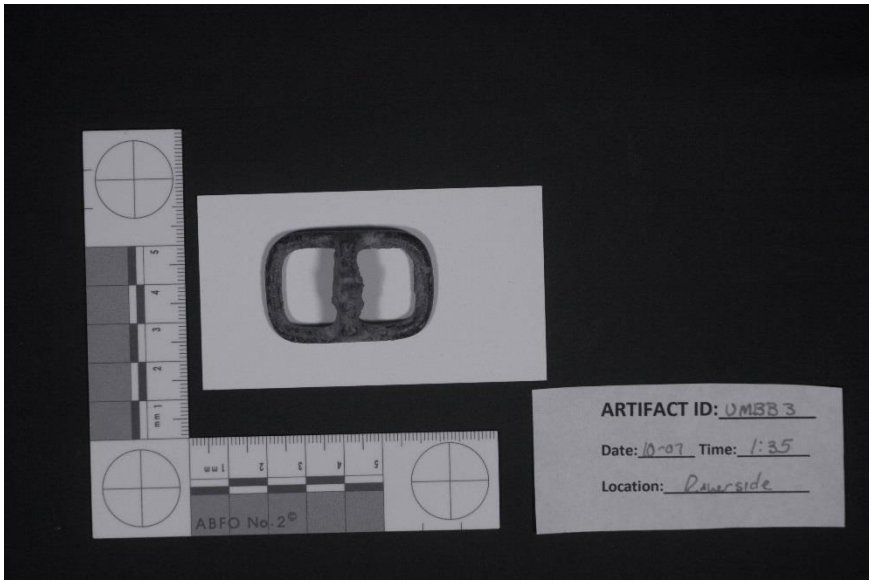

Figure 6.11: Infrared image of UMBB3

Infrared coloration on the rear of the buckle is consistent with the front. Sections of the original surface, most visible on the outer edge of the oval buckle, appear almost black in relation to the corroded areas. Underneath the center crosspiece, the heaviest of the corrosion is well differentiated from its surroundings. The visual separation of areas more heavily affected by corrosion is useful for conservators in determining the extent an artifact has been altered in its time underwater. The reverse side of UMBB3 can be seen in Figures 6.12 and 6.13.

Figure 6.12: Unmodified image of the reverse side of UMBB3

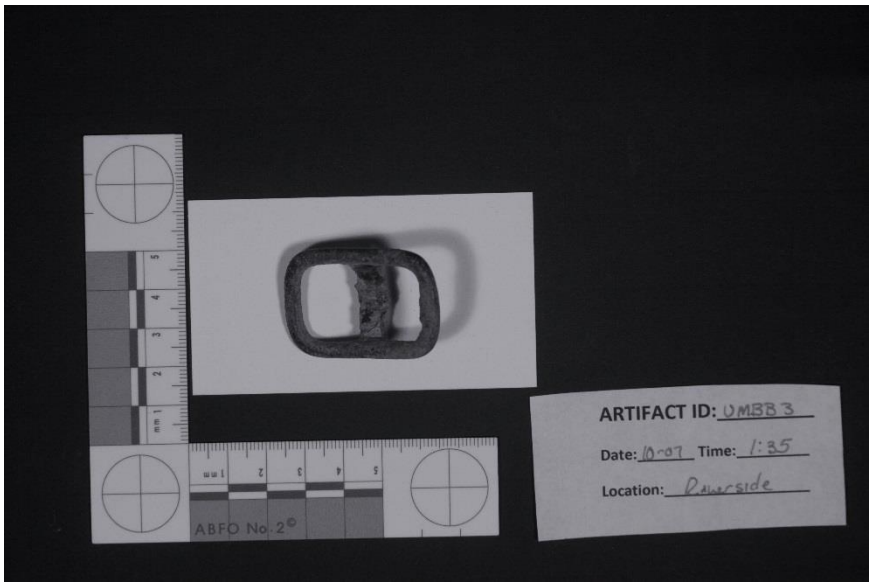

Figure 6.13: Infrared image of the reverse side of UMBB3

Conclusions for UMBB3

Infrared photography of the brass buckle, UMBB3, shows clear differentiation of the original surface of the artifact and areas of corrosion. As a general rule, the corrosion resistivity of brass and other alloys containing zinc decreases as the percentage of zinc increases above 15 % (Roberge, 2006). The alloy content of UMBB3 is unknown. However, future comparisons of brass alloys containing varying levels of zinc may prove useful in determining the ability of NIR photography to differentiate heavier corrosion patterns from more susceptible alloys. As it stands in this thesis, infrared imaging proves useful in tracing corrosion patterns throughout UMBB3 and is recommended as an analytical tool for imaging similar artifacts.

UMWM4

UMWM4 is a small, heart-shaped lock of white metal excavated from a terrestrial site, awaiting conservation at Texas A&M's CRL[15]. At one time, the locket may have been plated by some other metal, however, at the time of this analysis, only the underlying white metal remained. The surface of UMWM4 is rough and pitted, showing a variety of dull brown and gold colors. The arched locking arm of the lock appears to be iron, likely to give it additional strength. In the lower center, a small keyhole rests, still filled with debris from its terrestrial environment (Figure 6.14).

---

[15] White metal is defined as "any of several light-colored alloys used especially as a base for plated silverware, ornaments, and novelties" by Merriam-Webster Dictionary Online. < http://www.merriam-webster.com/dictionary/white%20metal>.

The reverse side of UMWM4 has the same coloring as the front. However, a dark spot dominates the middle of the lock. It is unknown whether this area emerged from close proximity with another object or is a section of corrosion product. On the right side, a layer of glue and a white strip reading '2011.118.8' has been added to identify the excavation location of the lock. A small area of green patina is present just below these identification marks.

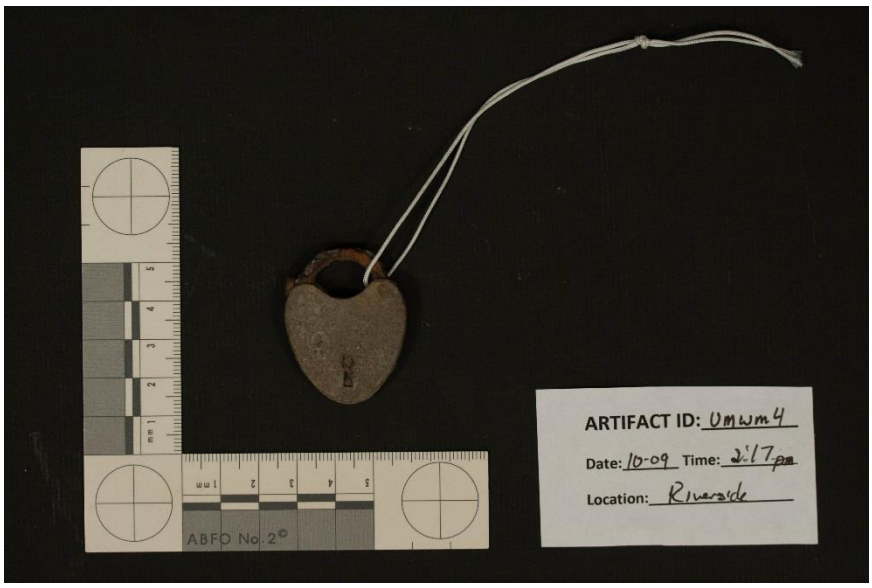

Figure 6.14: Unmodified image of UMWM4

Overall, little change is observed between infrared and conventional imaging. UMWM4 retains a uniform color under infrared (Figure 6.15), with only slight variation in the locking arch of the object. However, it appears this is more due to the desaturated nature of infrared rather than a change from the penetration of NIR waves. The corrosion

of the iron is more easily picked out in the unmodified photograph, Figure 6.14, than what can be seen from the modified camera.

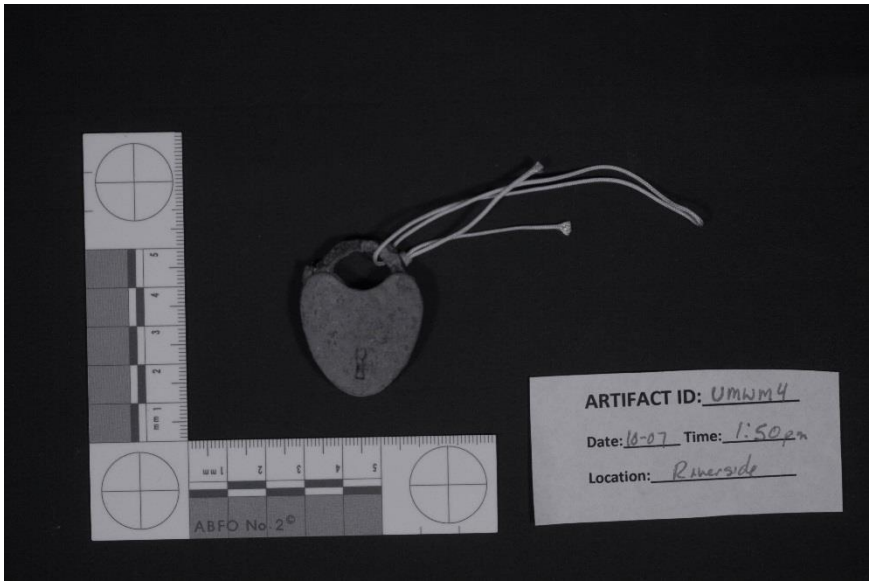

Figure 6.15: Infrared image of UMWM4

The color of the reverse side of UMWM4 appears more uniform under infrared. In the center, the dark spot still remains, unchanged in size and clarity from Figure 6.14. On the right, the glue, white strip, and numbers are all clearly visible, showing no signs of penetration by infrared waves. Below this area, the green patina has disappeared. No other differences were noted. Images of the back can be viewed in Figures 6.16 and 6.17.

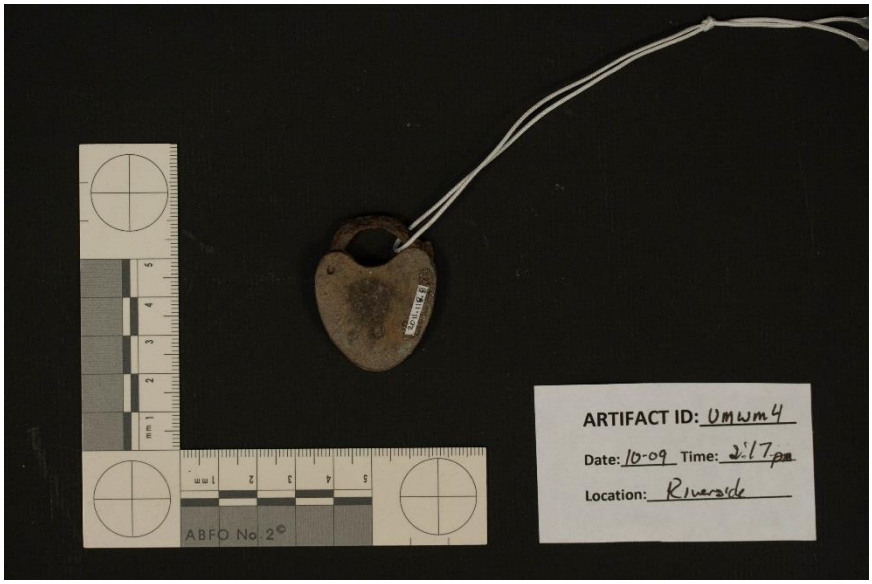

Figure 6.16: Unmodified image of the reverse of UMWM4

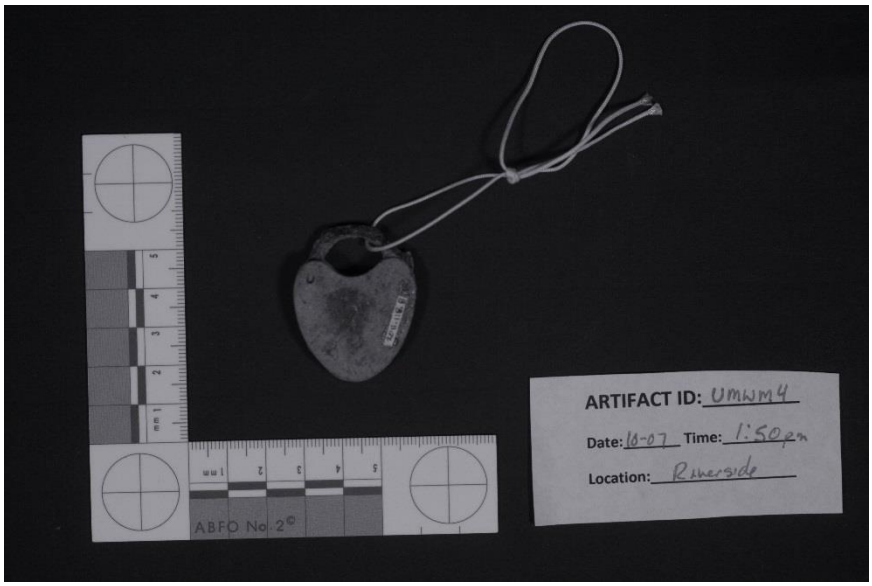

Figure 6.17: Infrared image of the reverse of UMWM4.

Conclusions for UMWM4

UMWM4 did not show any significant change when examined with NIR photography. While the coloration did become more uniform and the green patina disappeared, these were not widespread or drastic enough to warrant recommending infrared photography as a must for white metal. However, this may change depending on the composition of white metal, as it defines an entire range of possibilities rather than a specific alloy.

UMC5

UMC5 is a composite of an unknown cupreous metal and wood. At first glance, the most glaring feature of this piece is the 'blue-green' patina covering sections of the wood. The color of the corrosion is a clear sign of metals belonging to the cupreous family (copper, brass, bronze). It is unknown to the author why the flakes of patina collected so heavily on the wood, however, it appears to have been related to the hole seen near the bottom of the artifact (Figure 6.18).A large U-shaped loop has been driven through the wood, secured underneath by a second plate. It has not undergone conservation and was submerged in distilled water prior to imaging. Due to its uniformity on both and unique shape, it was chosen to have a top-down view for the second round of images. UMC5 was still wet when photographed.

The conventional and infrared images used for this object were imaged at slower speeds due to their darkness, as outlined in Chapter III. An interesting cause to this darkening, apart from the darker shading of the artifact, may be its wetness and the fact

the wood is still waterlogged. At 20ºC, water has a high IR absorption, especially at 760 nm and 970 nm below 1100 nm, the approximate maximum sensitivity of the CMOS sensor (Curcio and Petty, 1951). If similar objects are wet or waterlogged, test images should be performed to determine if those artifacts are affected.

Figure 6.18: Unmodified image of UMC5

UMC5 loses detail when imaged through NIR (Figure 6.19). The wettest areas of the wood imaged the darkest, as can be seen in the middle of Figure 6.19. It appears the quality of an IR photograph can be altered by the wetness of an object. More testing is needed to better quantify this phenomenon, but caution should be used when imaging wet artifacts.

The loss of the blue-green patina, a large change from conventional to infrared, is not due to the infrared waves themselves. Instead, the blending effect is a product of the

natural desaturation of the IR photograph. By desaturating figure 6.18, a similar visual response was generated. However, this did not account for the darkening of the wood. Corrosion on the top face of the looped metal ring was still visible in IR, but the lighter coloration changes on the surface facing the camera became more uniform and harder to identify.

Figure 6.19: Infrared image of UMC5

From the top (Figures 6.20 and 6.21), much of the traits described from the profile view remain the same. Wood is darker where wetter and thicker and the patina has faded into the background (due to desaturation). The top plate securing the ring, however, shows more clarity in mapping the corrosion in IR, particularly below the ring on the lower edge. More heavily corroded areas, similar to UMBB3, show up as a brighter grey color.

Figure 6.20: Unmodified top view of UMC5

Figure 6.21: Infrared top view of UMC5

Conclusion for UMC5

UMC5 offers a mixed response to IR. Different than other objects analyzed thus far, it is a composite artifact, containing both metal and wood. To take it one step further, this piece is also waterlogged from its storage in distilled water. Due to the absorptive nature of water to NIR waves, it throws a potential wrench into the imaging of waterlogged objects in infrared. However, NIR imaging may be useful for determining areas with the highest water density (would appear darker due to absorption of NIR waves). More research is required to determine the feasibility of such a method.

The desaturation of images in NIR caused issues with the clarity of the 'blue-green' patina present on a large section of the wood. Opposite of this, corrosion products were more easily discerned on the upper plate face of UMC5. Overall, it appears that conventional imaging is best for proper recording of composite cupreous and waterlogged wood objects.

UMLB6

UMLB6 (Figure 6.22) is a lead ball recovered from an underwater site and has not yet undergone conservation. Prior to imaging, the artifact was stored in distilled water and was still damp when imaged. The surface shows signs of corrosion and cracking. Typical lead corrosion types include lead chloride, lead sulfide, lead sulfate, lead carbonate and lead oxides (Hamilton, 2010; 85). An attachment of corrosion product juts out from one side of the ball, possibly where it had been previously connected to another artifact. It has a green coloration to it. The overall color is a dark

brown, while the cracks show lighter, almost white. Like UMBB3, UMLB6 was photographed on a white card to better distinguish it from the dark background. The exposure was also increased to compensate, following the methodology set forth earlier in this thesis.

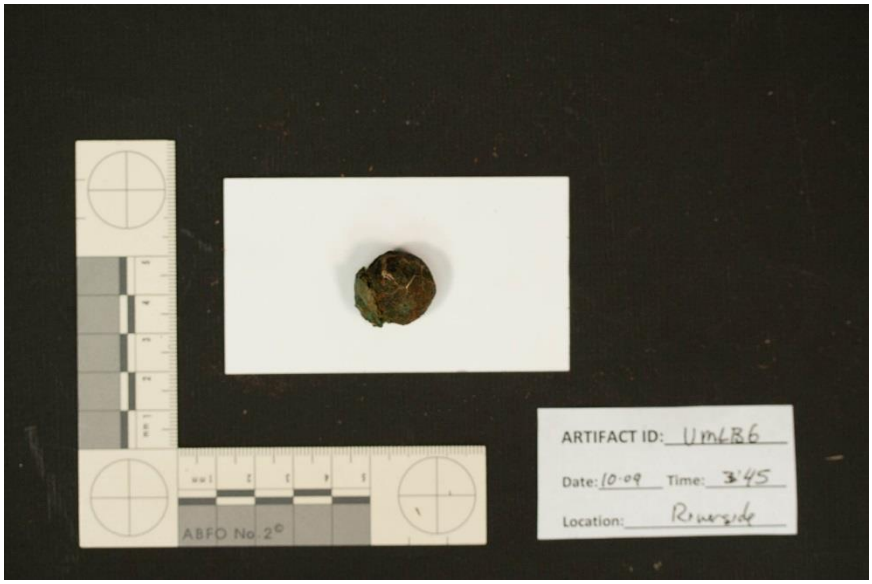

Figure 6.22: Unmodified image of UMLB6

Following imaging with the modified camera, UMLB6's surface became very dark, even when compared with the conventional photograph. However, the spaces between the surface cracks contrasted well with the darker surface. In Figure 6.23, these areas stood out more clearly than what was seen in Figure 6.22. It is not certain what causes this change, but the author hypothesizes the NIR is able to see the original grey lead surface between the cracks of the surface corrosion.

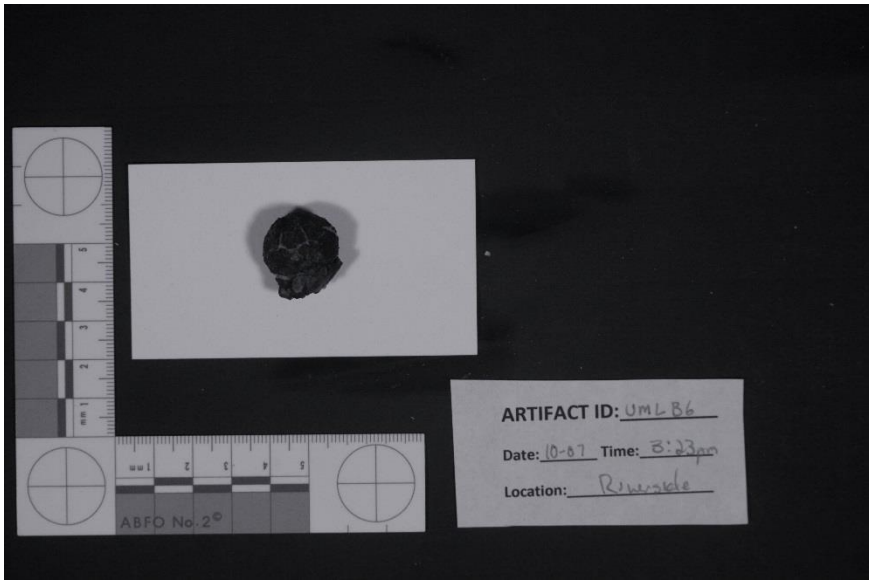

Figure 6.23: Infrared image of UMLB6

Conclusions for UMLB6

The surface of UMLB6 did not image well, rendering as a largely dark black mass, in part because of the lead corrosion and possibly aided by the dampness of the ball. Despite the lack of diagnostic change on the surface, NIR imaging was able to better decipher and display the pattern of cracks surrounding the ball. Being able to define these areas may help conservators in later removing the corroded areas or prevent them from detaching from the artifact during the conservation process. NIR photography is not useful for the overall recording of lead balls similar to UMLB6, but does provide possible benefit to more specific conservation treatment. In this case, NIR imaging is recommended.

UMIC7

UMIC7 differs from the other artifacts presented in this chapter. Rather than being a true archaeological artifact, meaning a historically made man-made object, this is a cast off remnant of iron corrosion that once encased the outside of an iron object. Like several other metal artifacts analyzed in this chapter, the exposure was modified in compliance with the established methodology in Chapter III. Iron is the most common metal found in underwater archaeological sites. UMIC7 was wet when photographed.

The appearance of UMIC7 changes from the interior side (the side closest to the iron object) to the outer surface. On the interior, Figure 6.24, the surface is bright orange and relatively flat in contour. Darker orange areas can be seen in the interior. The exterior of UMIC7 is much rougher. Height varies substantially across its surface and is colored closer to brown rather than red or orange. A small piece of white encrustation remains on the piece's left side.

Figure 6.24: Unmodified interior of UMIC7

When photographed with the modified NIR camera, UMIC7 did not image well. The infrared photograph, Figure 6.25, showed little differentiation between the different shades of orange seen in Figure 6.24. The subtleties of change across its surface were lost, instead rendering as a uniform dark grey in color. However, these same traits emerge when Figure 6.24 is desaturated. It appears the lack of contrast in the IR is not a product of differing wavelengths as it is the natural desaturation of the image, similar to UMC5. Even with this uniformity, Figure 6.25 does show the darker area of corrosion in the center as well as the conventional photograph.

Figure 6.25: Infrared image of the interior of UMIC7

The exterior of UMIC7 (Figures 6.26 and 6.27) shows no significant change between unmodified and infrared. The white, string-like, encrustation is still clearly visible, showing no degradation in clarity or color. Shading of different areas of corrosion remains consistent between light and dark, resisting the uniformity seen on the interior side. These results are somewhat surprising, seeing the ability of infrared to penetrate iron stains in numerous other artifacts. However, the thickness of the iron corrosion product and the lack of any substantial difference underneath the surface, not including the presence of water on the surface, likely contribute to the lackluster response.

Figure 6.26: Unmodified image of the exterior of UMIC7

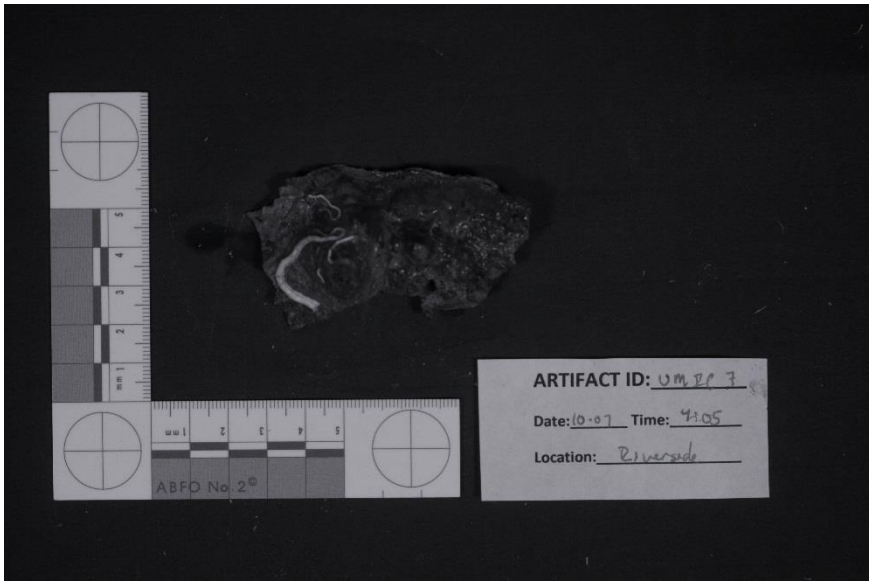

Figure 6.27: Infrared image of the exterior of UMIC7.

Conclusions for UMIC7

Overall, NIR photography does not provide any significant information over conventional imaging. The desaturation caused by the infrared photography process causes subtle color information to be lost. On the exterior, the camera was not able to penetrate the iron corrosion to any significant degree, leaving the white encrustation visible in Figure 6.27. The response of a separate piece of iron corrosion differs from what has been seen in previous artifacts with iron stains, which NIR was able to see right through. Factors influencing this change are likely related to the thickness of UMIC7's corrosion layer and the lack of any characteristics to image underneath the surface other than additional corrosion layers. UMIC7 and similar iron corrosion standalone pieces are not recommended for NIR imaging due to lack of substantial change.

UMISD8

UMISD8 features the remnants of an iron spike encased in wood and iron encrustation that has not yet been conserved. The imaged section was removed from the top of a larger concretion to expose the spike and obtain measurements. Two spikes can be seen meeting perpendicular to each other with the remaining wood visible on the right side of the photograph. In Figure 6.28, the wood can be seen as a darker brown as opposed to the varying orange and oxide colors of the spikes themselves. The images have had their exposure times increased.

Figure 6.28: Unmodified image of UMISD8

Infrared imaging does not show any significant change in the iron corrosion pattern or visibility of iron spikes and wood in UMISD8. When the original photograph is desaturated, it proves to be nearly identical to the infrared image (Figure 6.29). This suggests a lack of uniform penetration by NIR waves, as there is no trend towards a uniform tone as seen in other artifacts that are more susceptible to penetration by IR. Instead, the NIR photograph retains varying shades of grey, similar to a desaturated image of UMISD8 (Figure 6.28).

Figure 6.29: Infrared image of UMISD8

Conclusions for UMISD8

UMISD8 did not show any meaningful visual differences between conventional and infrared photography. Corrosion lines appeared easier to follow in the unmodified image due to their coloration, some of which is lost in the desaturation of NIR. Changes in the tonality remain in Figure 6.29, however. The reasoning behind this is not certain, but the author hypothesizes it may be due to a lack of meaningful penetration of NIR waves (thus imaging of the surface, giving the NIR photograph a similar appearance to a desaturated conventional one), or the artifact not changing in composition close enough to the surface to elicit visible change. NIR photography for wood encased iron objects in concretion is not recommended due to perceived lack of change.

CMIERT9

CMIERT9 was omitted due to further analysis of the artifact proving it was not of the composition as originally recorded.

CMLBER10

CMLBER10 (Figure 6.30) is a large lead bar recovered during excavations at Port Royal, Jamaica. Overall, the artifact is a uniform grey color with punched round holes at each end. On its right side, white corrosion products can be seen where retreatment of the object is needed. On the reverse side, a long depression runs down the middle of the bar. Additional areas in need of retreatment due to corrosion are located on the right side and lower edge of CMLBER10. Initial conservation of this artifact was done through electrolytic reduction.

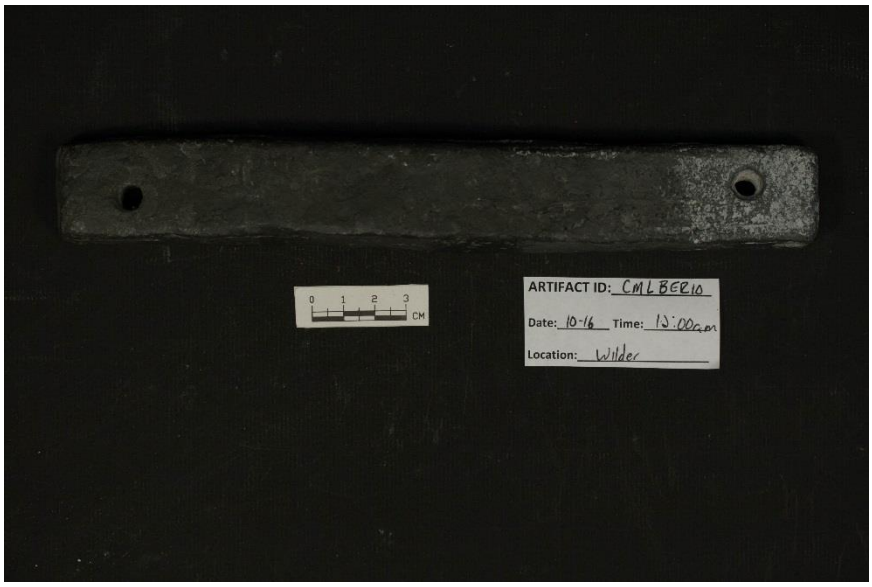

Figure 6.30: Unmodified image of CMLBER10.

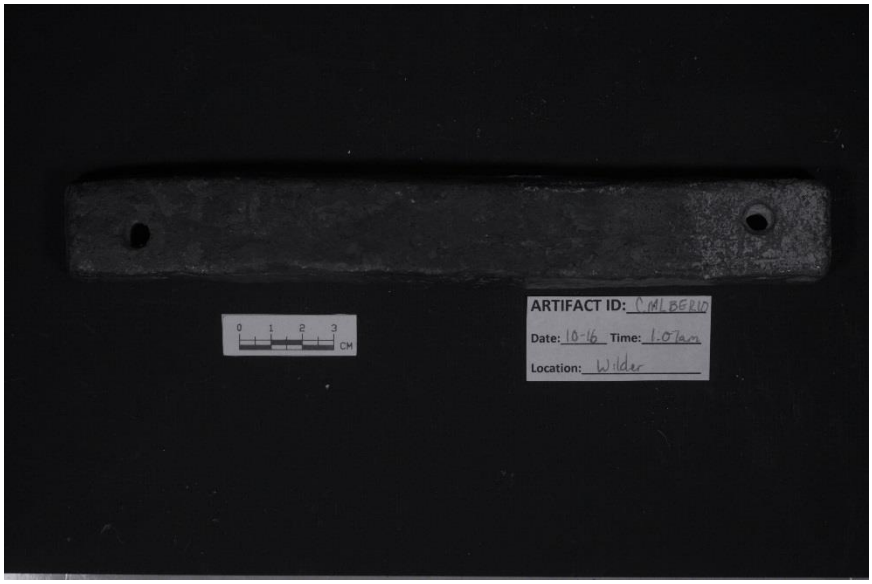

Figure 6.31: Infrared image of CMLBER10

No change was identified between conventional and NIR photographs of the lead bar. On both, wear markings and areas where surface corrosion is visible have not changed in clarity, color, or size. The reverse side (Figures 6.32 and 6.33), like the front, appears similar in both photographs. No hidden elements of lead are revealed by the use of NIR imaging.

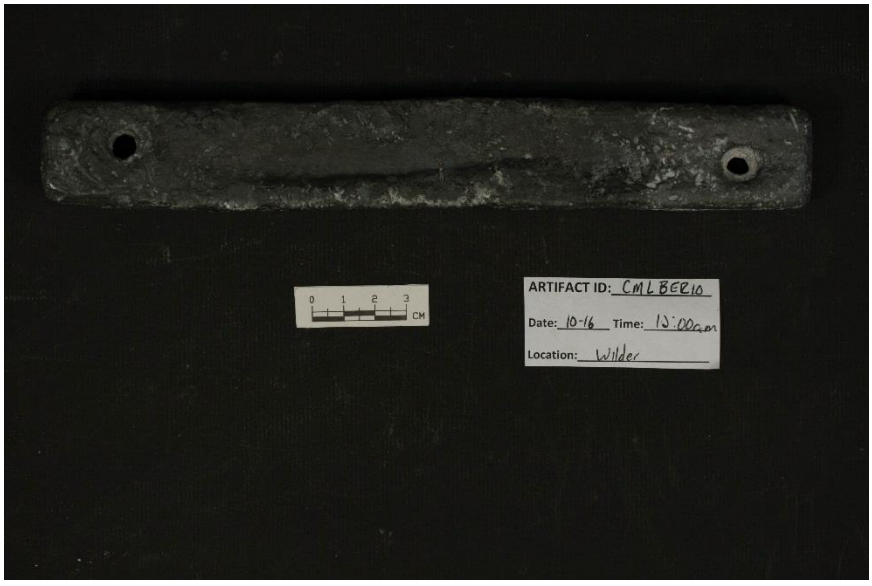

Figure 6.32: Unmodified image of the reverse of CMLBER10

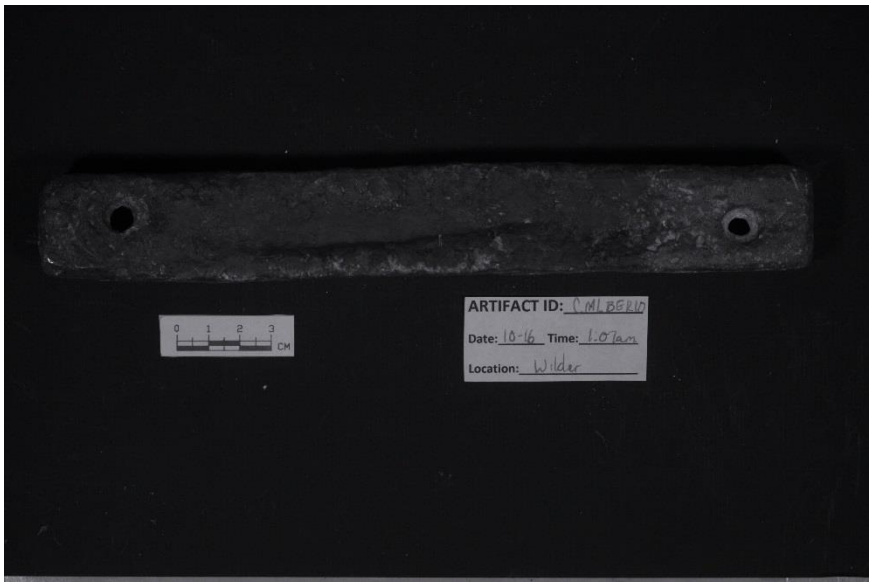

Figure 6.33: Infrared image of the reverse of CMLBER10

Conclusions for CMLBER10

No visual evidence of change was seen between the two imaging types for the lead bar CMLBER10. The density of lead and lack of potential hidden features on or near the surface are likely causes for the lack of any differences between conventional and NIR photography. Without any additional benefits from NIR, conventional photography offers the easiest solution to recording similar pieces of conserved lead.

Conclusions for Metals

Overall, most metals in this chapter proved to be largely unresponsive to NIR imaging. Of the nine artifacts examined, only two were able to be recommended to be worthwhile analyzing with NIR. The first, the brass buckle UMBB3, showed abilities to aid in the differentiation of original surface from corroded brass. It is unknown how the percentage of zinc affects the amount of corrosion of similar brass artifacts other than they are more susceptible to corrosion if containing greater than 15%. The second artifact to be recommended for imaging was UMLB6, a lead ball. A key component for recommending this object was the NIR camera's ability to highlight and better expose the cracking patterns of the surface of the ball. While the surface imaged worse in NIR than its conventional counterpart, the diagnostic use of NIR in conjunction with an unmodified camera is useful.

One artifact, UMC5, was not recommended for use with infrared imaging due to sub-par results. It appears the waterlogged nature of the wood absorbed portions of the NIR waves. In addition, the highly visible blue-green corrosion product become

completely obscured due to the black and white nature of the NIR photograph. UMC5 did show promise in better defining corroded areas on the top plate, however, the disadvantages caused by the other issues were too much to overcome. If only the cupreous parts had remained, then NIR may have been a viable option for UMC5.

The remaining six objects were rated as 'No Change', meaning they did not exhibit enough differences between conventional photographs, both colored and desaturated, and infrared images. Likely circumstances leading to this result include the density of the metal and corrosion products and the lack of sub-surface change that meaningfully differs from the surface. Pewter, silver, and iron all remained largely unchanged through the NIR photography process. Final results are listed in Figure 6.44.

Other non-conventional photographic techniques have been used successfully in the past for analyzing metals. One emerging with the advent of the digital age is Expanded Spectrum Photography (ESP), a technique related to high dynamic range (HDR) photography. This technique has been used to map the distribution of metallic oxides and numerous organic materials (Smith, 2010). Even though NIR did not prove groundbreaking in examining metals, other non-conventional photographic methods are worthy of examination by archaeologists.

ARTIFACT ID	ARTIFACT TYPE	SPECIFIC TYPE	ID EXPLANATION	RATING: IR vs VISIBLE
METALS				
CMPER1	Metal	Pewter	Conserved Metal Pewter Electrolydic Reduction	No Change
UMSC2	Metal	Silver	Unconserved Metal Silver Coin	No Change
UMBB3	Metal	Cupreous (Brass)	Unconserved Metal Brass Buckle	Recommended
UMWM4	Metal	White Metal	Unconserved Metal White Metal	No Change
UMC5	Metal	Cupreous and Wood	Unconserved Metal Cupreous	Not Recommended
UMLB6	Metal	Lead	Unconserved Metal Lead Ball	Recommended
UMIC7	Metal	Iron Concretion	Unconserved Metal Iron Concretion	No Change
UMISD8	Metal	Iron with wood	Unconserved Metal Iron Spike Dry	No Change
CMIERT9	OMITTED			
CMLBER10	Metal	Lead	Conserved Metal Lead Bar Electrolydic Reduction	No Change

Figure 6.34: Final results for metals

CHAPTER VII

TEXTILE AND PAPER

Two artifacts were imaged to analyze textile and paper. The first, UTPGI1, was an unconserved Bible printed in 1857, graciously donated for imaging by Dana Casey and her family. Throughout this book, hand-written notes in black ink, gall ink, and pencil were observed. Recently, much of the ink had begun to fade, leaving inscriptions difficult to read. Photographs of several pages of the best examples were taken. The book has not undergone conservation.

The second object photographed, CTRSO2, was a small piece of rope conserved using silicone oil. More information about the conservation techniques used to stabilize CTRSO2 can be found in "Methods of Conserving Archaeological Material from Underwater Sites" and "Silicone Oil: A New Technique for Preserving Waterlogged Rope" (Hamilton 2010; 28-29, Smith 1998). Figure 7.1 gives an overview of both artifacts.

ARTIFACT ID	ARTIFACT TYPE	SPECIFIC TYPE	CONSERVATION METHOD	ID EXPLANATION	IMAGING LOCATION
TEXTILE					
UTPGI1	Book	Paper	Unconserved	Unconserved Textile Paper Gall Ink	Wilder
CTRSO2	Textile	Rope	Silicone Oil	Conserved Textile Rope Silicone Oil	Riverside

Figure 7.1: Table with details of Chapter VII artifacts

UTPGI1

Three locations inside the Bible were chosen for photography, including the inside cover, reverse side of the title page, and a folded piece of scrap paper serving as a bookmark. The inside cover page contains a number of inscriptions written in different inks and hands. Much of it is illegible to the naked eye, however, certain names, dates, and phrases can be made out. Several stains line the binding of the book, as well as a large dirty area in the lower right-hand corner of the opposite title page. This is likely due to regularly handling and turning of the page in this location. It can be seen, unmodified, in Figure 7.2

On the inside of the title page, more illegible writing is visible. It does not appear to be of the same ink used on the previous page. Rather, upon inspection, it seems to be pencil of some kind. The print of the title page on the reverse side is visible through the blank page.

The folded insert of paper has twelve total lines of writing. Of these, ten appear to have been written with gall ink, due to their red-oxide coloration. The fourth and fifth lines, however, have been written with a blue ink of some kind. Noticeable age and wear of the slip of paper is obvious. None of the written words are readable, as the slip is only a fraction of a once larger piece.

Figure 7.2: Unmodified image of UTPGI1

Analysis of UTPGI1 showed a mixture of successes and failures for infrared photography of the artifact. Beginning on the inside cover and title page, the visibility of handwriting changed for the inscription written in the middle of Figure 7.2. Visible to the naked eye and 'normal' photography, this area fades from right to left. When examined under infrared (Figure 7.3), the same fading occurs. However, after being imaged in infrared, the clarity of this area is diminished significantly. The same trend of fading left to right continues, but rather than trailing off, the left side of this area has become completely obscured. This effect likely comes from the thickness of the remaining ink. Where it is thicker on the right, the infrared waves cannot fully penetrate, leaving behind a softer, but still visible return to the camera sensor where they were not absorbed. Despite some of this area still being visible, the quality has certainly diminished.

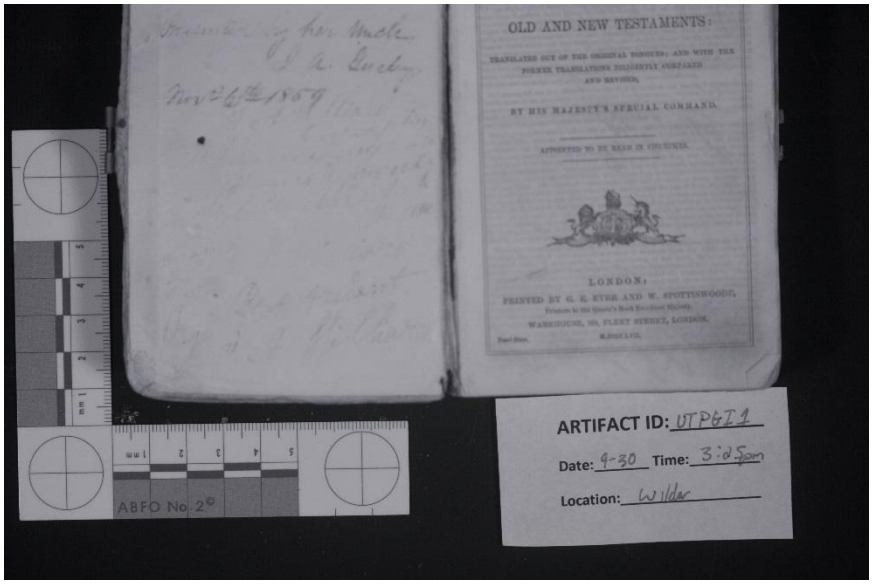

Figure 7.3: Infrared image of UTPGI1

Above this section, not much has changed. Both areas continue to exhibit similar visual properties in relation to the unmodified image. A significant change in the visibility of stains along the binding has changed, however. These stained areas, possibly the result of water damage, are completely invisible when imaged by infrared. This is a double-edged sword. On one hand, stained areas of paper may prove useful in diagnostic analyses to determine condition, environment, and other factors. However, at times, they obscure writing and other details that may hold vital information for researchers. The ability of infrared to see through light stains expands the diagnostic capabilities of researchers.

Moving to the reverse side of the title page, little has changed between the unmodified image, Figure 7.4, and infrared photograph, Figure 7.5. The hand-written areas, likely written in pencil, retain similar legibility across both spectra. Visibility

through the page to the printed title page previous is increased. It does not have a significant effect on the page being examined.

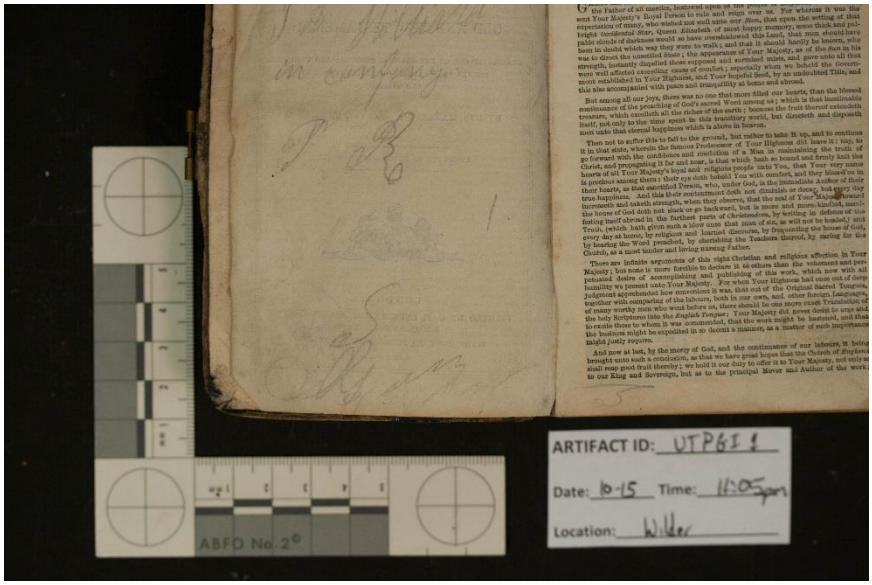

Figure 7.4: Unmodified image of the second page of UTPGI1

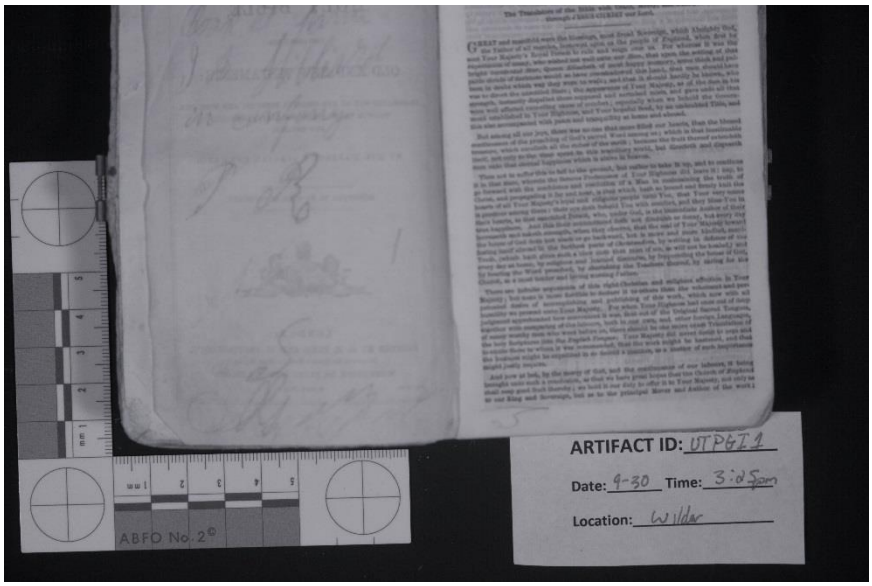

Figure 7.5: Infrared image of the second page of UTPGI1

The author observed an interesting stain related change on the opposing page. Located on the right hand side in the middle of a paragraph of text, a small rust stain was observed in Figure 7.4. It made the underlying text difficult to read. Once imaged by the infrared camera, the spot disappeared, reverting the text to a completely readable state, as if the stain did not exist. This ability of the infrared, similar to possible water stains on the previous pages, may prove useful for conservators attempting to read written inscriptions or printed letters under rust stains.

Final examination of UTPGI1 ended with a small, twelve-lined paper insert located within the pages of the book (Figure 7.6). Similar trends from the previous examined pages continue. Different ink types responded variably in their interaction with NIR waves from the camera. The red-colored gall ink and lighter blue ink on the fifth line faded substantially during imaging. On line four, the more heavily written, dark blue ink retained its detail (Figure 7.7).

Similar changes between inks were noted during the imaging phases of this research project. The author observed black inks of certain pens working well for the notation on ‘Artifact ID’ cards while others were completely transparent. This eliminates color as a deciding factor of the visibility of some inks over others. Different responses to infrared imaging have been used in the past to identify inks in works of all kinds. For example, Valeria Orlandini, a paper conservator at The Library of Congress, used multispectral imaging to aid in the identification of inks used in master drawings

(Orlandini 2005). Infrared imaging appears to have many useful applications in regards to inks and paper.

Figure 7.6: Unmodified image of the folded insert of UTPGI1

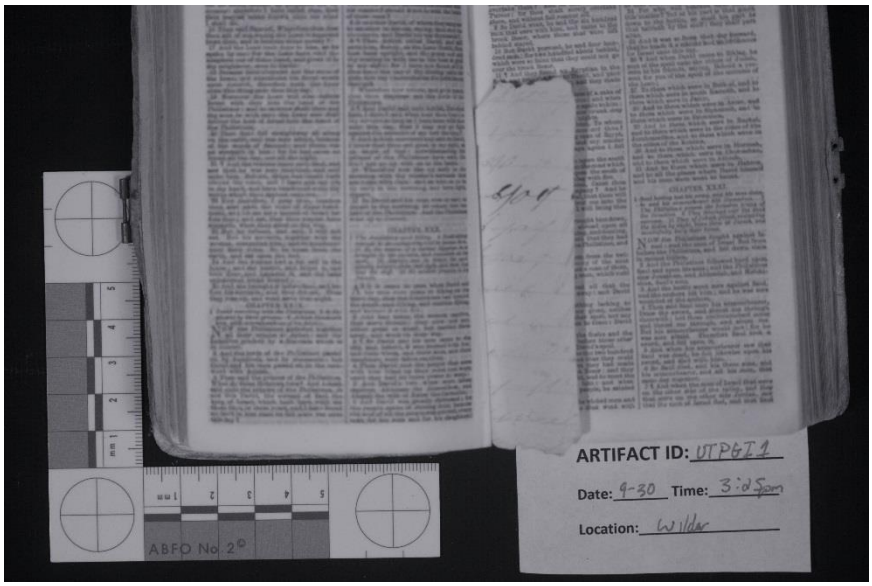

Figure 7.7: Infrared image of the folded insert of UTPGI1

Conclusions for UTPGI1

The results of NIR imaging of paper and inks on UTGPI1 showed success in several areas. NIR waves were able to penetrate and remove both water and rust staining on several pages, revealing areas underneath that were previously obscured. In addition, near-infrared photography identified inks that differed chemically from one another but held the same color, specifically in Figures 7.2 and 7.3. This differentiation acts as a marker for conservators, bringing notice that the inks may need different treatments for proper conservation.

NIR imaging was not without its troubles in analyzing inks and paper, however. The loss of some inks and stains in the imaging process can hamper proper documentation of some artifacts. Due to the helpful nature of some aspects of infrared photography and UTPGI1, the author recommends it as a useful tool. Despite this, caution is urged. Modified dSLRs should be used as a supplementary tool with similar artifacts, not as a standalone analysis.

CTRSO2

CTRSO2 consisted of a short segment of natural fiber rope from the excavation of *La Belle*, a shipwreck discovered in Matagorda Bay, Texas. After recovery, it was conserved using silicone oil, following methodology described by Dr. Donny Hamilton and Dr. C. Wayne Smith (Hamilton 2010, Smith 1998).

The fragment of rope had a mottled brown color overall, with brighter areas of the fibers emerging among the braid. Coloration differs slightly from front to back, with

the front, Figure 7.8, a darker brown and the rear showing areas of rust-red coloration. Dark brown stains appear on both sides. Whether these stains developed from the archaeological context or remain from the rope's construction is unknown. The rust-colored area on the reverse side, however, shows evidence of being closely associated with an iron object. The images used for CTRSO4 make use of the 'slower' photographic speeds outlined in CHAPTER III for darker artifacts.

Figure 7.8: Unmodified image of CTRSO2

The results from CTRSO2 and infrared are mixed. At first glance, it appears little change has taken place. The clarity of the rope fibers remains constant, as does the visibility of the brighter fibers within. What changes, however, is the ability to pick out the staining patterns mentioned earlier. In Figure 7.9, dark stains can be seen emanating from the left side of the image where the intertwined braids of the rope meet. These

stains, still visible in the unmodified photograph, are more easily recognized and defined under infrared.

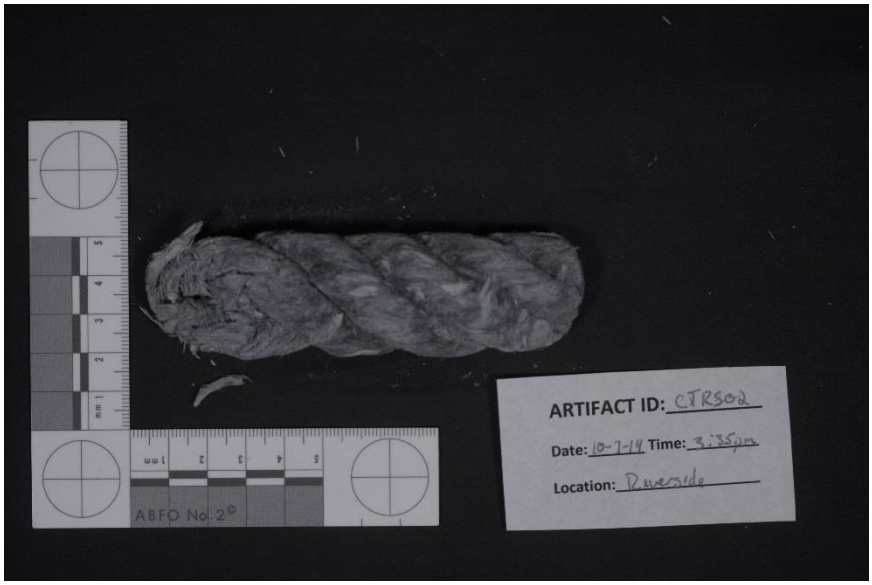

Figure 7.9: Infrared image of CTRSO2

Stain definition can also be seen on the reverse side. However, as seen on other artifacts, the iron staining does not stand out to the same degree in infrared as it does through 'normal' photography. Darker areas, where staining is present, do show up in Figure 7.11, however it does not show a hard boundary or the full extent of the area shown in Figure 7.10. It is likely that areas of the stain reside near the surface and have not penetrated more deeply into the fibers of the rope. The penetration of the NIR waves into the surface of the rope bypass staining near the surface, only revealing coloration changes in areas where the iron stain is deepest.

Figure 7.10: Unmodified image of the reverse side of CTRSO2

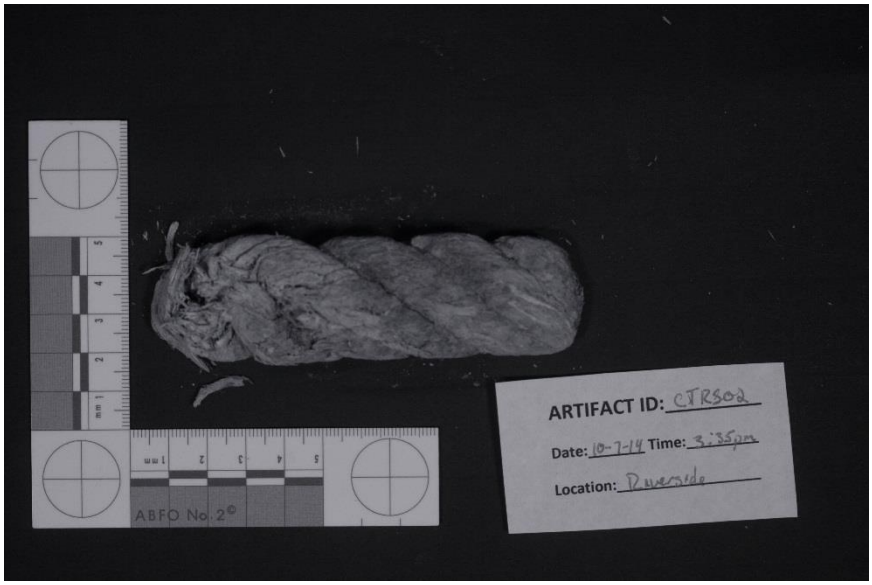

Figure 7.11: Infrared image of the reverse side of CTRSO2

The clarity of the staining through infrared imaging on the front side of CTRSO2, paired with the penetrative power of NIR through iron oxides, make a powerful combination. For non-iron based stains, NIR works well in defining the limit to which they extend, a useful tool for conservators who wish to map these stains or monitor their progress throughout the conservation process. On the reverse side, the smaller return of the rust staining in infrared can be combined with the unmodified image to better understand the extent of the iron staining pattern. The unmodified photograph records the entirety of the stained surface, while use of the infrared camera reveals areas the iron stain has penetrated deepest, bringing attention to areas that may require additional analysis or conservation.

Conclusions for CTRSO2

Infrared photography proved useful in limited applications with silicone oil treated rope. Non-iron stains showed up well in NIR images, while a combination of unmodified and infrared imaging proved useful for defining iron stains present on the textile. Major changes were not observed on CTRSO2 in comparison to UTPGI1. However, despite the lack of obvious change, the staining details the modified dSLR was able to record may prove useful for the imaging of similar textiles to CTRSO2 in conjunction with conventional photography. Infrared photography is recommended for textiles treated with silicone oil to analyze staining patterns. Expect best results when used in conjunction with other analytical methods.

Conclusions for Textile and Paper

Both UTPGI1 and CTRSO2 showed enough change between unmodified and NIR photographing for the author to recommend their use in the analyses of similar types of artifacts. This does not mean that infrared imaging alone provides enough detail to completely document these objects, but rather showed enough promise to expose details that were either previously unclear or invisible to unmodified imaging methods and the human eye. Figure 7.12 highlights the two artifacts and their final recommendations.

ARTIFACT ID	ARTIFACT TYPE	SPECIFIC TYPE	ID EXPLANATION	RATING: IR vs VISIBLE
TEXTILE				
UTPGI1	Textile/Book	Paper	Unconserved Textile Paper Gall Ink	Recommended
CTRSO2	Textile	Rope	Conserved Textile Rope Silicone Oil	Recommended

Figure 7.12: Final recommendations for textile and paper artifacts

For UTPGI1, conventional photography appears to be the safest and most reliable method to record most types of inks. However, infrared excels in seeing through stains that may have obscured areas of text, as well as the ability to differentiate between ink types. Combined, these two methods of imaging provide a clearer picture of both the contents and variability of UTPGI1 and similar artifacts.

CTRSO2 is not so obvious in its change between ‘normal’ and infrared imaging. The darker staining patterns on the ‘front’ side proved difficult to spot at first glance. Only after careful analysis were they visible to the author’s eyes. The rust stained area on the reverse side continued trends seen throughout other artifact groups – that infrared sees well through iron based stains. Like UTPGI1, this area was best imaged by both infrared and conventional methods simultaneously. The full extent of the stained area can be seen through conventional means, while the depth of the stain can be better quantified by use of the modified dSLR.

CHAPTER VIII

WOOD

The wooden remains of ships and other objects are often found in varying states of preservation at many underwater sites around the world. Study of these pieces allow archaeologists to determine how vessels were built, where it originated from, and the age it was built. Needless to say, any information an archaeologist can learn of archaeological wood is important. Despite this importance, little research into wood's reaction to NIR imaging has been done in the past by archaeologists. The following chapter examines seven wooden artifacts, both unconserved and conserved, to determine their visual response to a modified NIR dSLR. Conservation methods for these artifacts can be found in Hamilton (2010). Figure 8.1 lists the details of each artifact examined.

ARTIFACT ID	ARTIFACT TYPE	SPECIFIC TYPE	CONSERVATION METHOD	ID EXPLANATION	IMAGING LOCATION
WOOD					
UWSAD1	Wood	Soft Wood	Unconserved/ Air Dry	Unconserved Wood Soft Air Dry	Wilder
CWSPF2	Wood	Soft Wood	Polyethylene Glycol and Freeze Dried	Conserved Wood Soft PEG Freeze	Wilder
CWHP3	Wood	Hard Wood	Polyethylene Glycol	Conserved Wood Hard PEG	Wilder
CWHSO4	Wood	Hard Wood	Silicone Oil	Conserved Wood Hard Silicone Oil	Riverside
CWHSO5	Wood	Hard Wood	Silicone Oil	Conserve Wood Hard Silicone Oil	Riverside
CWSP6	Wood	Soft Wood	Polyethylene Glycol	Conserved Wood Soft PEG	Riverside
UWHAD7	Wood	Hard Wood	Unconserved/ Air Dry	Unconserved Wood Hard Air Dry	Wilder

Figure 8.1: Descriptions of the wooden artifacts analyzed in Chapter VIII.

UWSAD1

UWSAD1 is a small piece of archaeological wood prepared by the author by allowing it to air dry on a window sill of the Conservation Research Lab. The resulting piece shows obvious signs of shrinkage and deformation. Coloration of UWSAD1 is a uniform dull brown on the crosscut face (Figure 8.2) with a reddish to black tone on the natural sides of the wood (Figure 8.4). Wood grain or tree rings are not visible on the surface of UWSAD1. Only four pictures, two conventional and two infrared, are shown here. Additional photos can be found in APPENDIX II.

Figure 8.2: Unmodified image of UWSAD1

No change was seen in UWSAD1 when imaged with both conventional and infrared photography. The piece of wood appears to be a single color without any visible marking or coloration changes (Figure 8.3). Wood grain and tree rings remain unseen. It

is important to note that the considerable shrinkage of UWSAD1 during the air drying process has compacted the cut face of the wood. Any grain or tree rings that may have existed prior to its drying have been greatly displaced and altered, making imaging by any method unlikely for these features.

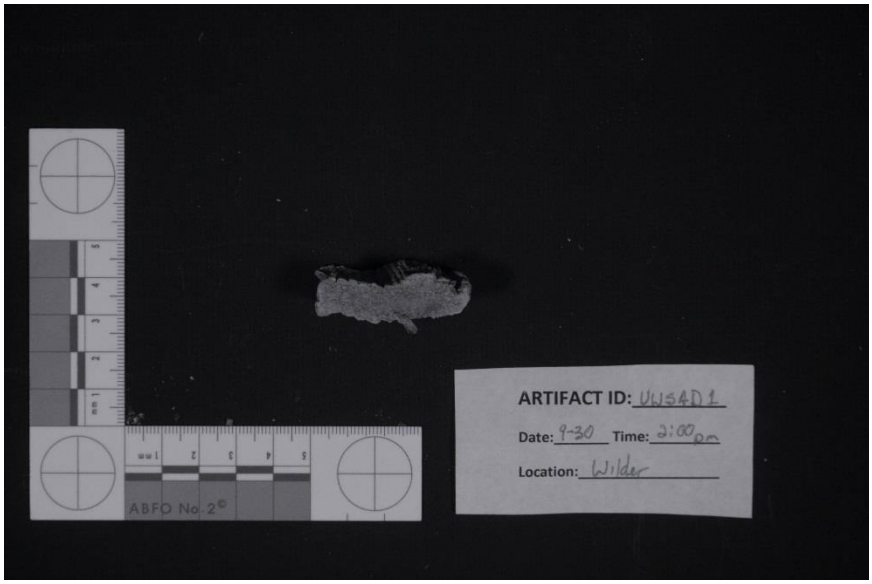

Figure 8.3: Infrared image of UWSAD1

The side of UWSAD1, while not suffering the same percentage of shrinkage as the cut face, still showed signs of substantial warping. However, under infrared, little difference was seen between unmodified and modified photos. The black coloration remains while the red areas have turned to a light grey, brighter than what is seen by a desaturated conventional photograph. This brightness is true for all areas of UWSAD1. Many of the metals examined in CHAPTER VI trended to imaging darker, while it

appears wood images on the lighter side. Photographs of the side of UWSAD1 can be seen in Figures 8.4 and 8.5.

Figure 8.4: Unmodified image of the side of UWSAD1

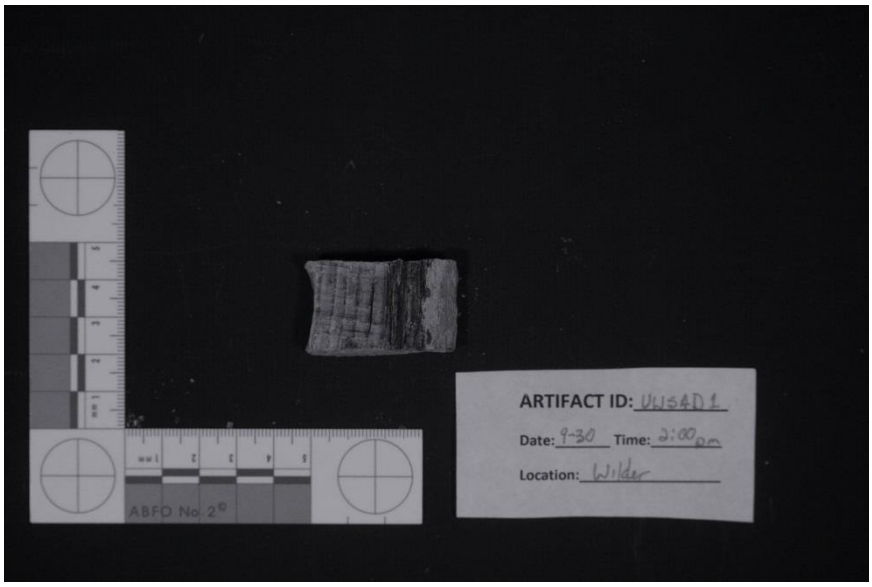

Figure 8.5: Infrared image of the side of UWSAD1

Conclusions for UWSAD1

UWSAD1 does not show any changes in visual characteristics when imaged with infrared. While it does appear to image more lightly underneath infrared conditions, no details such as wood grain or tree rings were revealed. It does not mean that NIR does not better visualize this information, but rather more likely due to the substantial warping of the artifact. A specimen with less shrinkage and warping will likely provide better information for the usefulness of NIR on wood.

CWSPF2

CWSPF2 (Figure 8.6) comes from the same archaeological site as UWSAD1. Rather than being allowed to air dry, this artifact was conserved by being bulked with polyethylene-glycol (PEG) and freeze-dried, following methods set forth by Hamilton (2010). The surface of the wood is dirty, with no diagnostic features easily visible on either of its sides. A split in the wood has occurred on the right side, extending from the edge towards the center. Coloration of the natural sides of CWSPF2 retain a similar rest-like red color, similar to UWSAD1. On the reverse side, a dark stain can be seen in the upper right corner of the artifact, straddling the split in the wood. The origin of this stain is unknown.

Figure 8.6: Unmodified image of CWSPF2

When used to image CWSPF2, NIR photography shows the ability to penetrate the surface layers of muck and grime obscuring details in the wood, clearly showing tree rings and stains that had not been visible previously (Figure 8.7). The rings begin on the left side of the image and grow as they emanate out to the right. Using this pattern, archaeologists can determine from which area of a tree this particular artifact was cut from. In addition, given a large enough piece, tree rings can aid researchers in determining the age and possible location of a piece of timber using dendrochronology.

In addition to revealing tree ring patterns in CWSPF2, NIR imaging also clarifies the extent of the staining seen near the split in the wood on the right side of the image. Staining patterns are important in the study of archaeological wood, particularly in wood

associated with shipbuilding. These stains can identify areas in which particular fasteners were used.

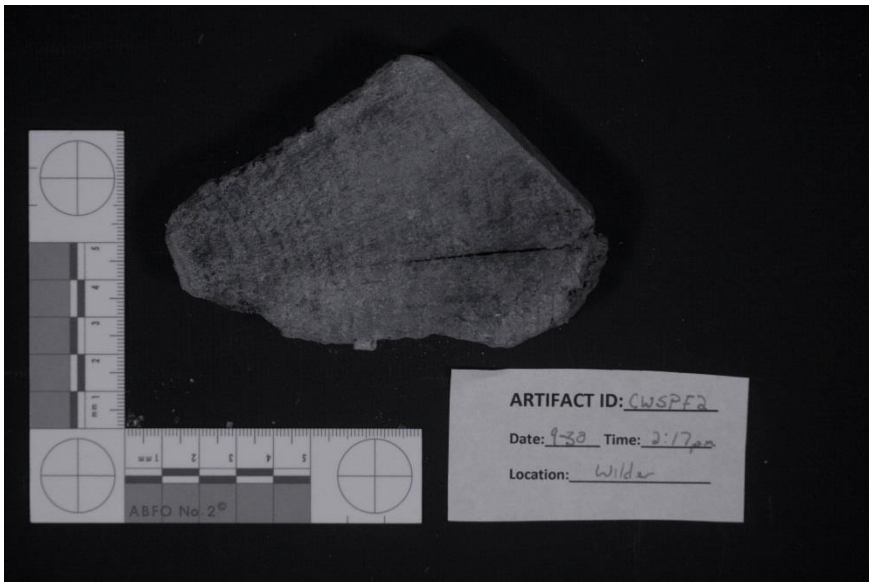

Figure 8.7: Infrared image of CWSPF2

The infrared image of reverse side of CWSPF2 (Figure 8.9) shows even more clarity in the imaging of tree rings that are not easily seen by conventional means (Figure 8.8). Unlike the initial side seen previously, the tree rings can be identified nearly edge to edge. The extent of a large stain bisected by the split in the artifact can be seen clearly. It is unknown to the author why tree rings appear more easily under infrared, but it is most likely a combination of the NIR camera being able to see through surface dirt and differing absorptive and reflective properties of tree rings and the surrounding wood. Rings formed during the growing season of a tree produce lighter colored, less dense wood. As the end of growing season approaches, however, a darker, denser wood is

formed, producing the darker rings seen in cross section of a tree. This density difference is hypothesized by the author to affect the clarity of how tree rings are imaged with NIR.

Figure 8.8: Unmodified image of the reverse of CWSPF2

Figure 8.9: Infrared image of the reverse of CWSPF2

Conclusions for CWSPF2

NIR photography of CWSPF2 both revealed tree ring patterns and clarified the position of large stains. The infrared waves were able to penetrate the surface layer of dirt and grime and provide important information for researchers studying similar pieces of wood. While the exact cause of the clarity of the rings in NIR is unknown, it is likely due to the ability of NIR to 'ignore' surface dirt in wood and the density differences between wood depending on the season. NIR imaging proves to be a useful tool in the study of wooden artifacts conserved with PEG and freeze-dried. Infrared photography is recommended for CWSPF2 and similar artifacts.

CWHP3

CWHP3 is a cross-section of a piece of hardwood that has been conserved using a heavy molecular weight of PEG. Large areas of white PEG remain in the large cavities of CWHP3, but do not fill the smaller pores of the wood (Figure 8.10). The cut face of the wood is dominated by a series of pores of various sizes, most elongated and running with the grain of the wood. Overall, CWHP3 is a dark brown in color, and does not show any evidence of its surface being obscured by dirt and grime. Rather, the reverse side and natural surface of the wood, is covered in a thin layer of PEG. Photos of this side are not included within this chapter, but may be found in APPENDIX I. No tree rings are visible, but the size of this particular piece of wood may be too small to adequately separate rings from the background. Another possibility is if the tree is tropical in origin, where tree rings are not visible to the human eye due to year-round rainfall.

The cut face of CWHP3 that is perpendicular to the grain of the wood also shows evidence of its larger pores being filled with PEG (Figure 8.12). Here, however, the pores are more circular, as they are seen in cross section perpendicular to their direction of travel. Coloration remains the same, with a darker brown area extending from the left towards the center.

Figure 8:10 Unmodified image of the parallel cut face of CWHP3

As seen in Figure 8.11, infrared imaging of CWHP3 substantially lightened the return of the wood. While little in the way of details changed, this lightening effect causes the porous nature of the piece to become easier to see and separate from the wood substrate behind it. When Figure 8.10 is desaturated, the same effect does not occur. The bright return is likely related to the ability of NIR waves to penetrate the surface of the

wood without meeting any subsurface features that actively absorb infrared waves, which would appear darker in the ensuing image.

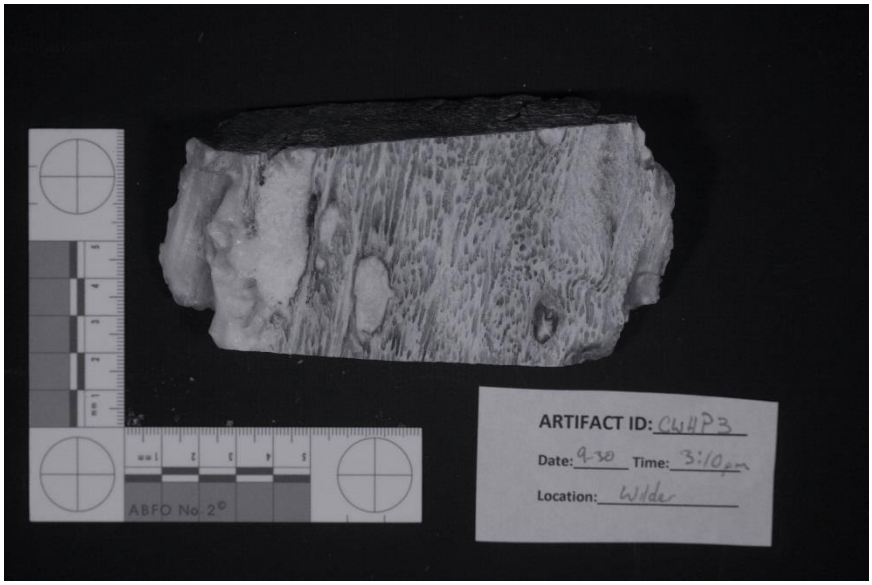

Figure 8.11: Infrared image of the parallel cut face of CWHP3

The lightening effect the NIR has on the wood, however, does make the areas of PEG more difficult to see. If trying to visually analyze the coverage of high molecular weight PEG, conventional imaging offers greater benefit. This does not extend to areas of PEG that have been covered in dirt, blending their bright white color in with the surrounding wood. In this case, dirty PEG is more visible through NIR because it can image underneath the grime obscuring the white coloration. If trying to map the run direction and lay out of the porous nature of this wood type, however, NIR holds the edge.

Similar trends continue on the perpendicular cut face of CWHP3 (Figures 8.12 and 8.13). Further clarity of the pours was observed, as well as a lightening of the surrounding wood matrix. The dark area traveling from the left side to center, can be reasonably differentiated. It appears this darkness is caused by a clustering of pores in these areas as well as unknown debris filling these holes. Larger pores can be seen to the lower right, filled with PEG.

Figure 8.12: Unmodified image of the perpendicular cut face of CWHP3

The outer bark covering of CWHP3 is also well defined in infrared, as seen in Figure 8.13. Both conventional and infrared photography image this areas as being distinct from the porous wood below it, however, the lightening of the shade of the wood allows its darker nature to be better visually represented.

Figure 8.13: Infrared image of the perpendicular cut face of CWHP3

Conclusions for CWHP3

NIR imaging of CWHP3 did not reveal hidden information like CWSPF2. However, it did increase the clarity of the porous nature of the wood, as well as reveal areas of PEG accumulation where its white color has been obscured by dirt and grime. If attempting to analyze areas in which PEG has accumulated and the artifact is clean, conventional photographic methods still provide the best contrast for inspection. The infrared imaging of CWHP3 also helped identify the line of the outer section of the tree in relation to the lighter colored wood inside, helping researchers determine area of the tree where the section of wood originated. NIR imaging is recommended for CWHP3 due to its ability to clarify the layout of the woods porous structure.

CWHSO4

CWHSO4 is a hardwood withy recovered from the *La Belle* shipwreck in Matagorda Bay, Texas. It was conserved using a silicone oil treatment developed by Dr. C. Wayne Smith and described in Hamilton (2010). The wood is not uniform in color, containing a variety of colored streaks and stains on both sides. On the upper face, the wood takes a reddish color, with a small orange stain in the lower left, likely from deposition near an iron object during its time underwater (Figure 8.14). Lighter colors dominate the reverse side, interrupted with darker bands of brown at the top and bottom of the artifact.

Figure 8.14: Unmodified image of CWHSO4

Greater detail in the staining patterns of CWHSO4 is revealed in the IR photograph (Figure 8.15). Bands of light and dark are easily definable, with two distinct

lighter bands appearing near the center of the artifact that were not clearly visible before. It is unknown to the author what causes these changes, however, potential sources include corrosion staining, the deposition of silicone oil, and varying densities of wood. Further analysis is required to better understand the processes causing coloration changes in CWHSO4.

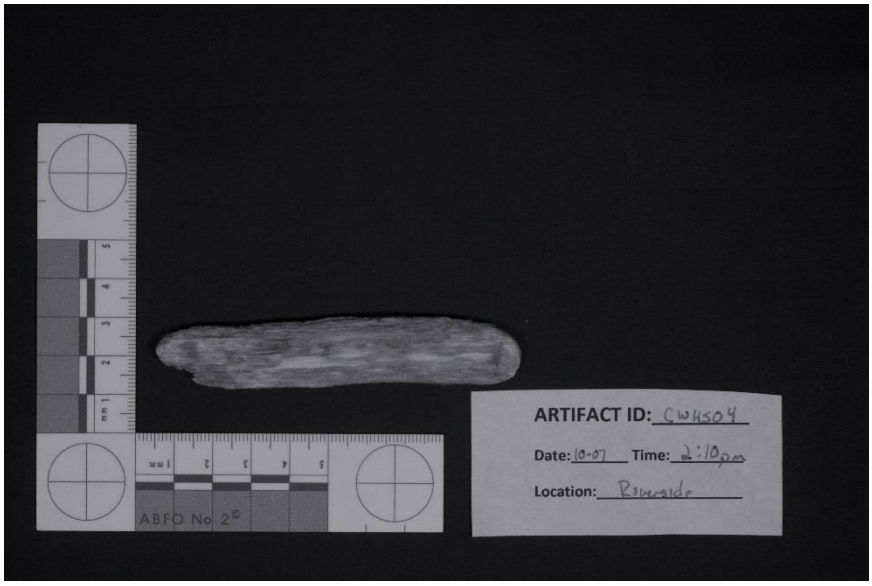

Figure 8.15: Infrared image of CWHSO4

The reverse side of CWHSO4 includes the same clarity in staining patterns. The dark brown bands mentioned earlier (Figure 8.16), remain dark at both the top and bottom of the wood withy. Other areas of the reverse side, which do not appear relatively bright under conventional means, become well separated in the NIR photograph (Figure 8.17). The ability to follow these changes may prove useful for conservators and other researchers studying wooden artifacts treated in silicone oil.

Figure 8.16: Unmodified image of the reverse of CWHSO4

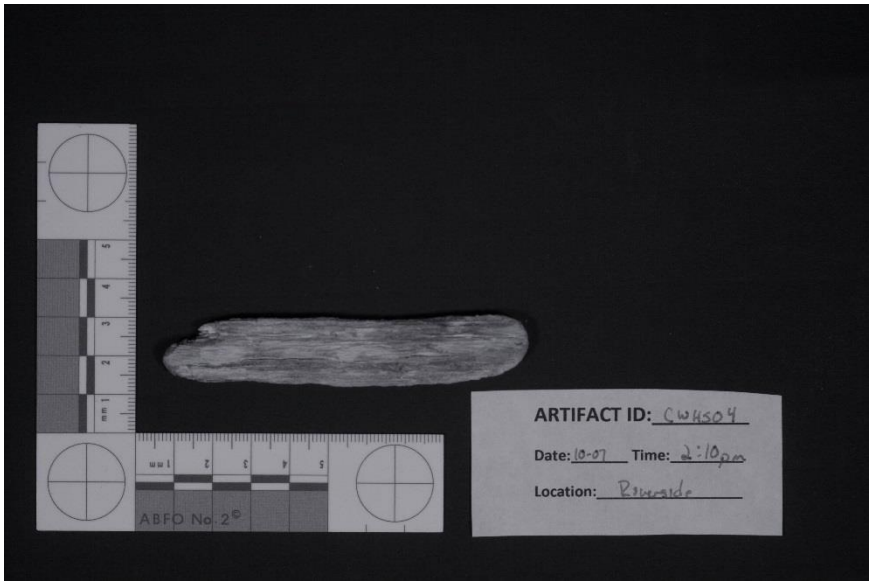

Figure 8.17: Infrared image of the reverse side of CWHSO4

Conclusions for CWHSO4

Imaging CWHSO4 with the modified Canon 20D in NIR showed significant changes in the clarity and definition of staining patterns on both sides. Current understanding of why these changes occur is unknown, but with further study, may prove of significance to archaeologists and conservators alike. Infrared imaging for silicone oil treated pieces of wood similar to CWHSO4 is recommended.

CWHSO5

CWHSO5 is a large piece of timber that has been conserved using silicone oil, using techniques similar to CWHSO4. On the upper face (Figure 8.18), a variety of different colors and staining can be seen, ranging from reds to black, which dominates the center of the artifact. The edges of CWHSO4 are heavily eroded, giving the object a non-symmetrical shape overall. Lines of the wood grain can be followed across CWHSO4 from left to right, but are obscured by the dark black stains in the center.

The opposite side of the timber (Figure 8.20), by contrast, is almost completely devoid of dark stains, with the exception of small areas of red near the upper edge and right side. This side has numerous surface holes, particularly towards the bottom center of the artifact. It is not known what caused the holes, whether deposition or marine activity.

Figure 8.18: Unmodified image of CWHSO5

The infrared imaging of CWHSO5 does not show the immediately apparent changes seen in its silicone treated counterpart, CWHSO4. Compared to a desaturated conventional image of the artifact, the infrared photograph (Figure 8.19) shows greater definition of the central black stain and other darker stains while still highlighting differences in areas where the red stains occur. In addition, the clarity of the grain lines in the wood is enhanced by a significant margin. It does not respond to NIR like tree rings seen previously, however. The grain has been eroded to some extent, creating a slight relief to its surface. This relief may be partially responsible for the increased clarity, but is unlikely due to the lack of equipment movement and change between the imaging of CWHSO5 with the two cameras. Some other factor or factors contribute to this phenomenon.

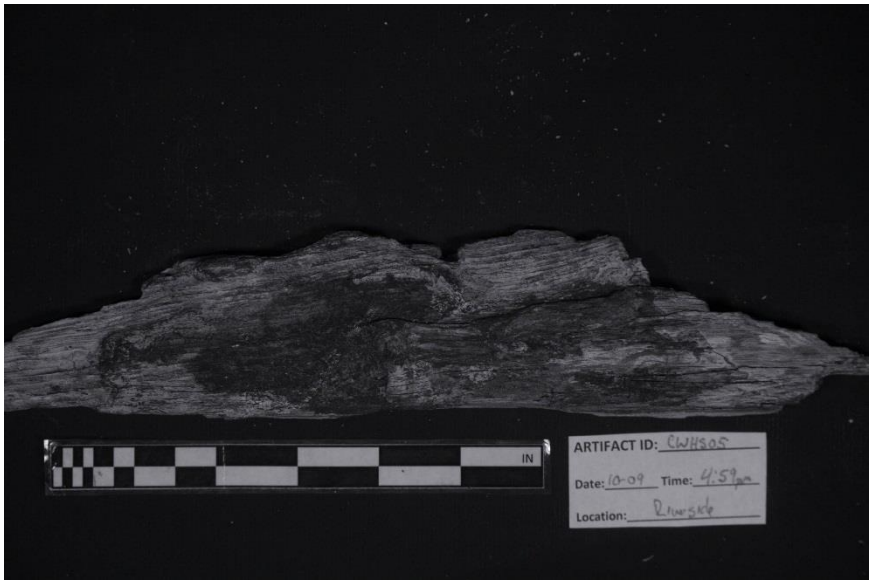

Figure 8.19: Infrared image of CWHSO5

Imaging of the reverse side of CWHSO5, seen in Figures 8.20 and 8.21, does not result in the same type of clarity and definition as seen on its front face. No major staining exists other than small red-orange patches near the edges. These areas are fully penetrated by the NIR waves and do not show up in the infrared image, Figure 8.21. Appearance of the wood grain lines is unaltered between the two photographs, as are the numerous holes and cavities that mar the surface of the object. It appears that NIR imaging works well on the front face and has little change on the rear of CWHSO5.

Figure 8.20: Unmodified image of the reverse of CWHSO5

Figure 8.21: Infrared image of the reverse of CWHSO5

Conclusions for CWHSO5

CWHSO5 responded well to NIR imaging on its upper face but failed to change when the opposite side was examined. As before, stains appear to render well on wood in most cases, despite the loss of a few lighter red stains on the back side. The unknown black stain proved quite resistant to NIR penetration, imaging darkly with a sharp boundary. Wood grain also stood out on the front face, clearly easier to distinguish with the eye than in the conventional photo. Reasons for a similar effect being absent on the opposite side is unknown, however changes in lighting have been ruled out due to a static setup. Infrared imaging is recommended for CWHSO5 on the basis of defining stains and increasing clarity of wood grain patterns.

CWSP6

CWSP6 is a block of soft wood treated with PEG. It is an unremarkable square shape lacking in any surface features. The artifact has a flat, dull brown color that covers its entire surface. This color is not uncommon for PEG treated wood, according to Hamilton. (Hamilton, 2010; 25). On the left side, a plastic artifact identification label reading ‘1335’ has been tacked into the surface with two small finishing nails. Visible wood grain runs from left to right, but no tree rings are visible. The reverse side proves as unremarkable as the front, with no distinguishing marks and a continuation of dull color.

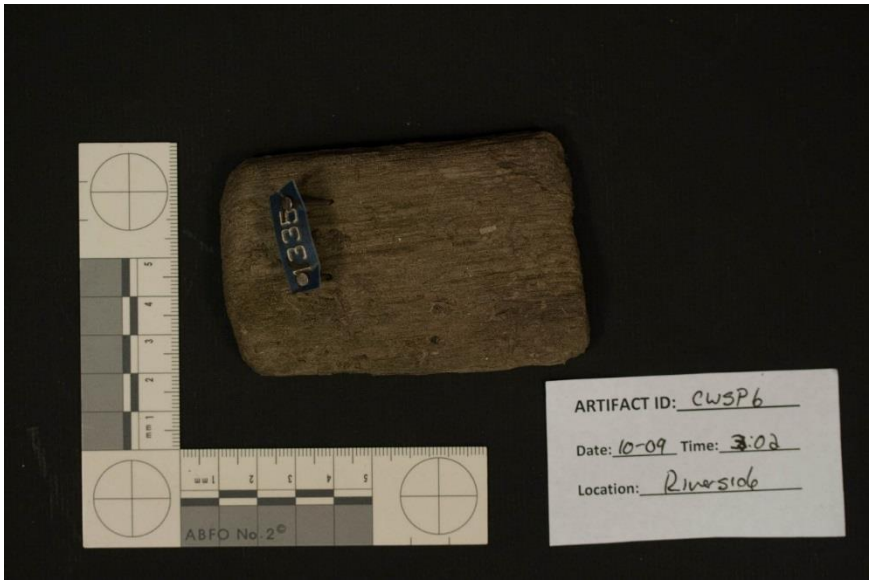

Figure 8.22: Unmodified image of CWSP6

NIR does not reveal any new features on CWSP6's initial face. The resulting photograph is bright grey in color, similar to wood colors seen in previous samples. Each feature seen in the conventional photograph (Figure 8.22), is repeated clearly in infrared (Figure 8.33). An interesting note unrelated to the wood is the color change of the identification tag. The blue pigment has been completely penetrated by NIR waves, resulting in a much brighter return. It does not affect the readability of the tag in any way, however it is interesting to note the change the NIR imaging has on coloration.

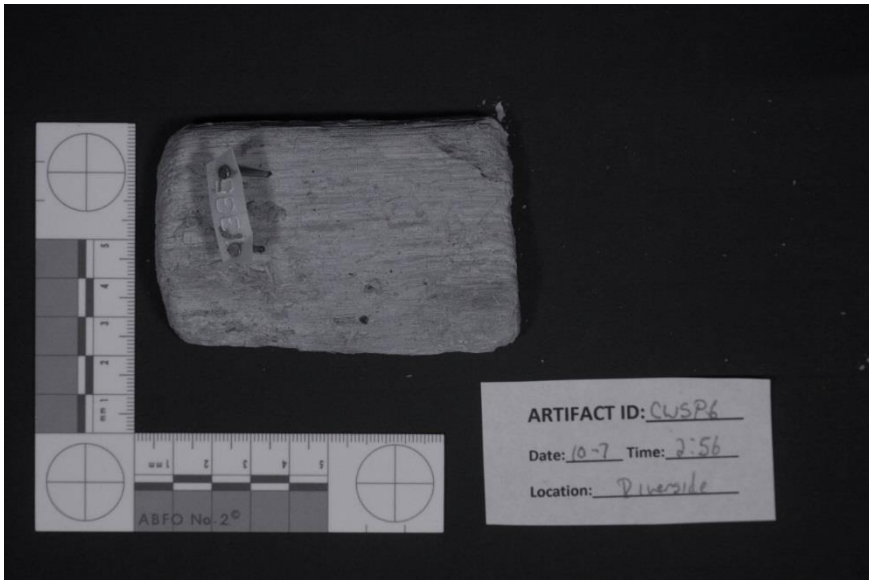

Figure 8.23: Infrared image of CWSP6

The rear of CWSP6 mirrors the front and does not reveal any new information. It retains the bright hue seen earlier, but is otherwise devoid of any changes. Images for this side of CWSP6 can be seen in Figures 8.24 and 8.25.

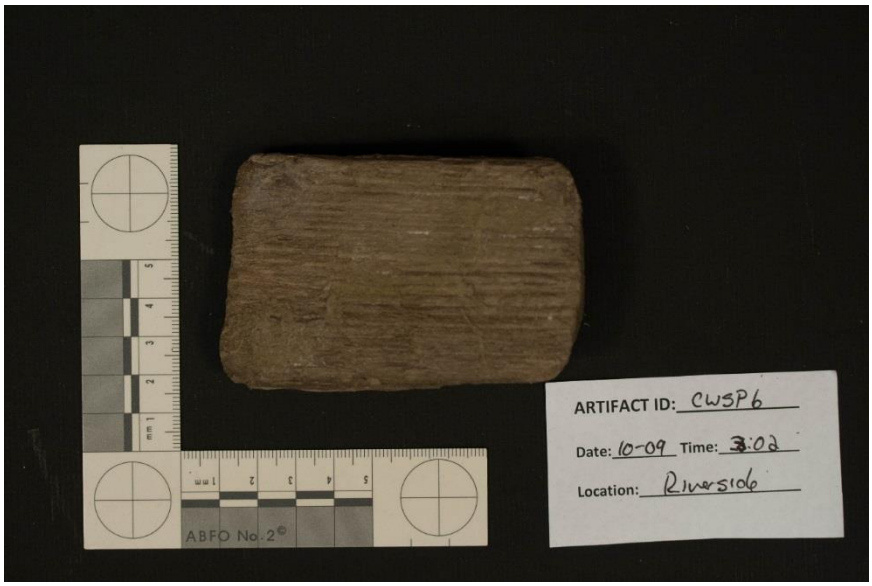

Figure 8.24: Unmodified image of the reverse of CWSP6

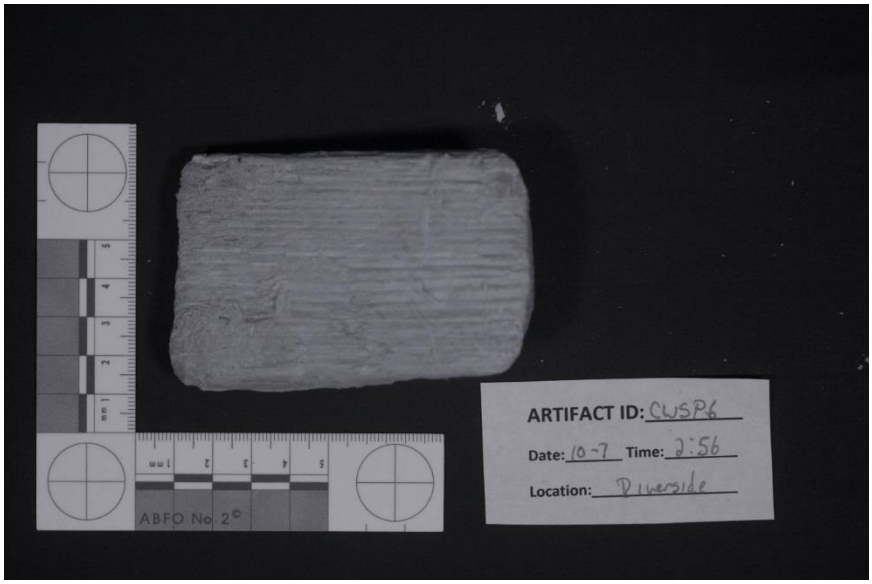

Figure 8.25: Infrared image of the reverse of CWSP6

Conclusions for CWSP6

Imaging CWSP6 with the modified NIR camera was inconclusive, showing no significant change from conventional images. While the wood did image brighter and the pigments from the plastic ID tag lost its hue, these are not compelling enough reasons to suggest using a NIR camera to image this artifact. Infrared imaging is not suggested due to the lack of perceivable change in CWSP6.

UWHAD7

UWHAD7 is a large piece of hardwood that was air dried and left unconserved. It is obvious from the lack of warping that it was not submerged long enough to become completely waterlogged, thus retaining its integrity. The interesting feature of UWHAD7 that stands out immediately is the presence of a treenail on its upper surface (Figure

8.26). This treenail has a grain that travels perpendicular to the ring structure of the main body of the artifact. On the main body of wood itself, a dark outer layer of bark followed by the lighter interior of the tree can be seen. Tree rings are visible on the interior, although areas of the object are dirty and stained, potentially making accurate counting difficult.

The reverse side of UWHAD7 shows similar properties. However, no treenail is present on this side. Instead, a dark, roughhewn groove takes its place. Like the first side, the inner surface contains visible tree rings emanating from a central point towards the bottom of the photograph, adjacent to the treenail groove. Other small marks mar its surface. Grey and black stains partially obscure tree rings to the right of where the treenail should be.

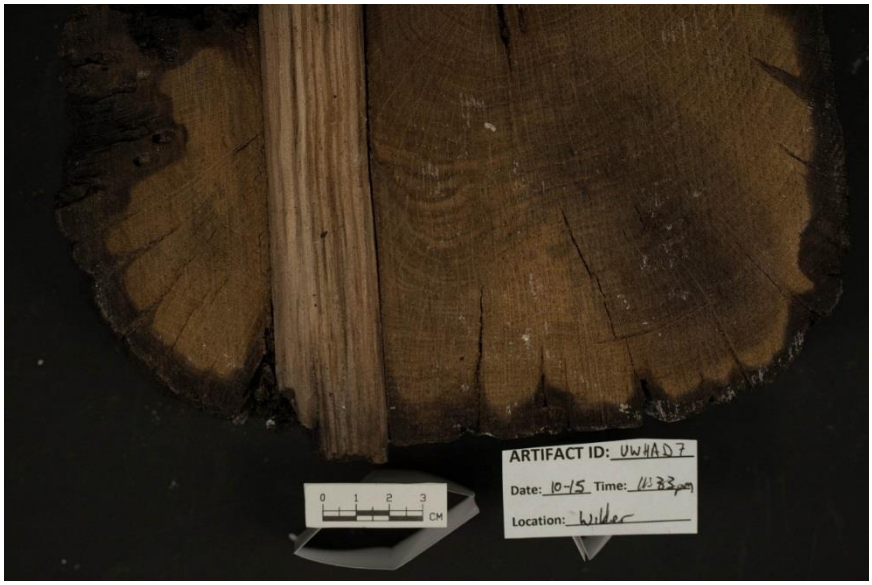

Figure 8.26: Unmodified image of UWHAD7

UWHAD7 responded well to NIR imaging. As seen in Figure 8.27, the visibility of the tree rings has increased considerably. Now, each ring can be easily counted without the risk of missing one due to the dirt staining present on the surface. In addition, other features such as small holes and medullary rays are clearly visible against the lighter background of the interior wood. The outer bark surface remains darker and easily differentiated from the inner wood of the artifact.

Figure 8.27: Infrared image of UWHAD7

When flipped to the reverse side (Figures 8.28 and 8.29), the results are nearly identical. The pattern of tree rings can be traced to the core of the tree, which rests just to the right of the groove cut for the missing treenail. Also seen, on the left, are a series of small gouges of unknown origin. The lightening of the wood color and the ability of the

NIR waves to penetrate dirt and light staining give researchers a much clearer picture of the tree rings and other surface features.

Figure 8.28: Unmodified image of the reverse of UWHAD7

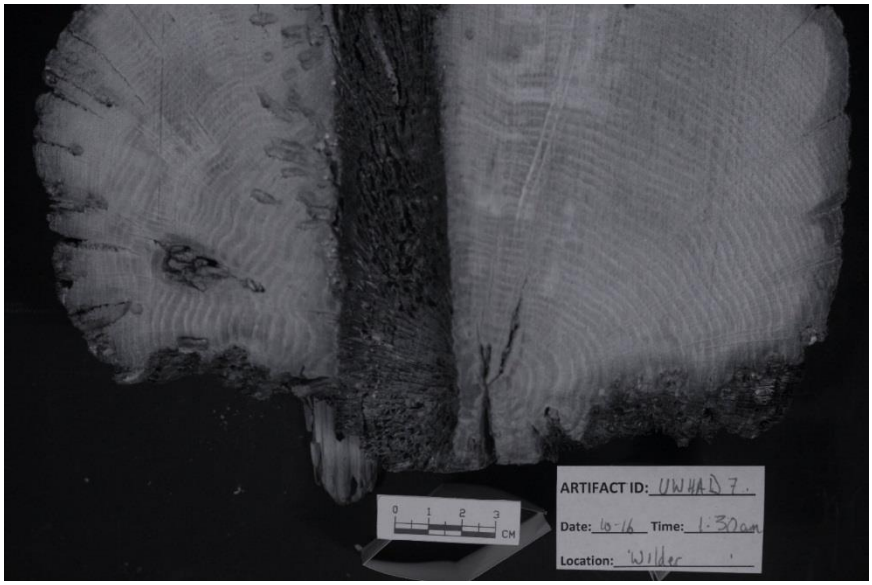

Figure 8.29: Infrared image of the reverse of UWHAD7

Conclusions for UWHAD7

As seen in previous examples within this chapter, the modified NIR camera has the ability to see through surface dirt and staining to clarify the details underneath, particularly tree rings. This trend continues with UWHAD7. While tree rings are visible in the conventional photographs, the addition of the grey and black spots of grime make some of them difficult to see, a problem for researchers attempting to accurately count their number. Under NIR, however, the rings become clear and easily countable on both sides. Also becoming clearer are other features that mark the surface, including light scratches, medullary grooves and gouges near the treenail groove. There is no doubt that the use of a NIR dSLR enhanced the visibility and clarity of tree rings and other details in UWHAD7. The visualization of these traits allows researchers to better understand the artifact and obtain additional information from it. Near-infrared imaging is recommended for UWHAD7.

Conclusions for Wood

Overall, the converted 20D proved to be a useful tool in the analysis of the seven archaeological wood samples selected for this chapter. Of these seven, five were recommended through their ability to reveal additional traits of the wood that were unclear or not visible through conventional photographic means. The two that were not recommended UWSAD1 and CWSP6, were no worse under NIR imaging than conventional photography.

The use of near-infrared in analyzing wood for stain patterns, tree rings, and wood grain was effective in the majority of artifacts. While this thesis does not cover the scientific explanations for these changes in visibility, the consistency among the results for wood demonstrates that a modified dSLR is worthwhile to a researcher when examining similar artifacts. Figure 8.30 summarizes final recommendations.

ARTIFACT ID	ARTIFACT TYPE	SPECIFIC TYPE	ID EXPLANATION	RATING: IR vs VISIBLE
WOOD				
UWSAD1	Wood	Soft Wood	Unconserved Wood Soft Air Dry	No Change
CWSPF2	Wood	Soft Wood	Conserved Wood Soft PEG Freeze	Recommended
CWHP3	Wood	Hard Wood	Conserved Wood Hard PEG	Recommended
CWHSO4	Wood	Hard Wood	Conserved Wood Hard Silicone Oil	Recommended
CWHSO5	Wood	Hard Wood	Conserve Wood Hard Silicone Oil	Recommended
CWSP6	Wood	Soft Wood	Conserved Wood Soft PEG	No Change
UWHAD7	Wood	Hard Wood	Unconserved Wood Hard Air Dry	Recommended

Figure 8.30: Final recommendations for wooden artifacts

CHAPTER IX

CONCLUSIONS

The use of NIR by archaeologists has historically been sparsely practiced, particularly in regards to artifacts. With the advent of the digital age of photography, digital dSLRs with an increased sensitivity to NIR wavelengths have become increasingly easy to use and available for archaeologists and researchers alike. However, even with this technology becoming increasingly affordable and accessible, the effects of its use on a large variety of artifacts was unknown.

Twenty nine artifacts in five groups were analyzed to determine whether a Canon 20D dSLR converted to capture NIR waves between 830nm and approximately 1120 nm provided any benefit in the study of artifacts. This study did not seek to explain how or why visual changes in the artifacts may occur, but rather create a baseline of what types of artifacts may change and to what degree. Each of the artifacts studied was photographed by both conventionally and with NIR, and afterwards given a rating of "Not Recommended", "No Change" or "Recommended" by the author depending on the degree of change seen.

"Not Recommended"

Of the twenty nine artifacts, five were "Not Recommended" for use with NIR due to the loss of diagnostic features, poor imaging, or a response that in some way made the resulting NIR photograph worse in comparison to the unmodified photograph

in visible light. Four of these six were ceramics, particularly ones that had printed designs. With the exception of UCPW1, the infrared waves completely penetrated the printed designs of the ceramics, heavily fading them or causing them to completely disappear from view in NIR.

The remaining artifact, UMC5, was a composite artifact consisting of cupreous metal and heavily waterlogged wood. When examined with the NIR camera, parts of the corrosion of the cupreous metal stood out well, however, the waterlogged wood appeared to absorb large amounts of NIR waves, causing it to image darkly. The high IR absorption coefficient of water was hypothesized to be a possible cause.

"*No Change"*

Eleven artifacts were determined to show no significant change between visible light and NIR photography. These included three ceramic, six metal, and two wooden artifacts. Surprisingly, of the five groups, metals had the largest proportion of artifacts that did not change. It was expected that metal corrosion products, particularly iron oxides, would be easier to map. However, little change was noticed. The natural desaturation of NIR often caused metal surfaces to become slightly more uniform in color, making enhanced identification of corrosion products no easier than with normal photography. A photography technique that enhanced color rather than removed it, such as Expended Spectrum Photography examined by Smith (2005) would likely produce more conclusive results.

Ceramics that did not undergo any visual change were devoid of printed designs and, with the exception of slipware, had an earthy body. It is likely no subsurface features were present in these ceramics for infrared waves to identify.

The two wooden pieces that appeared similar in both photographic methods di so despite radically different conservation procedures. UWSAD1, of the same piece of timber as CWSPF2, which imaged well with NIR, was air dried and allowed to shrink considerably. It is believed this shrinkage obliterated any remnants of tree rings or other diagnostic data of the wood grain. CWSP6, a softwood conserved using a PEG treatment, showed evidence of coloration change common with such treatments. The degree to which this affected the ability of NIR to derive hidden details similar to other woods is unknown.

"Recommended"

Thirteen artifacts of the collection were recommended for use with NIR imaging. They included two bone, two ceramic, two metal, two textile and paper, and five wood. For bone, use of the infrared camera was able to better image bone and skin characteristics that were present, including folds, cracks, and stains.

The two ceramics responded to NIR photography in different ways. UCPW1, a pearlware ceramic, had a printed 'blue willow' design of cobalt blue that was penetrated by infrared waves enough to help clarify the image that had bled during the glazing and firing process. It is not known why this printed design imaged well and others using

similar cobalt blue materials did not, but the author hypothesizes it is due to the depth and thickness of the print.

UCWC9, a used clay pipe for Port Royal, revealed areas within the pipe bowl where the burning of tobacco was most intense. NIR waves penetrated and obscured areas of light charring, leaving behind only the spots that were heavy enough to fully absorb the infrared radiation. These findings could allow researchers to determine patterns in how the people of Port Royal, Jamaica smoked their white clay pipes.

Of the two metals recommended for infrared imaging, both were non-iron. The first, a brass buckle, exposed the difference of original versus corroded surfaces through infrared. The second, a small lead ball, highlighted areas where the surface had cracked, revealing the remaining lead surface underneath.

The paper and textile samples responded well to NIR imaging. UTPGI1, a historic mid-18th century bible, featured several pages of handwritten passages in a variety of different inks. Through NIR photography, inks that appeared similar to the naked eye were proved to be different chemically due to their varying responses and visibility in the infrared photograph. In addition, numerous stains, which made reading areas of the text more difficult, were able to be imaged away by using the modified camera. CTRSO2, a silicone oil treated piece of rope, showed enhanced staining patterns throughout its fibers. The author was unable to identify the type of staining, however, it may prove useful to archaeologists and conservators alike.

Wood, on the whole, responded favorably to infrared photography. Five of its seven artifacts showed significant change in the visibility of diagnostic features,

particularly in the imaging of stains and tree rings, both important to archaeologists. The NIR camera was able to enhance both characteristics, seeing through surface layers of dirt and grime to give a better image of the underlying surface.

Overall Conclusions and Final Thoughts

A variety of artifacts responded well to the modified NIR dSLR, though many in different ways. It proved strong in its ability to penetrate thin surfaces and image the underlying characteristics, whether it be inks, tree rings, or staining and corrosion patterns. When faces with dense or wet objects, however, the effectiveness of NIR imaging decreased substantially.

Organic artifacts appear to have imaged the best consistently, with only two of eleven not being recommended by the author. Of these, none imaged poorly enough to be placed in the "not recommended" category. However, despite this consistency, it is important to interpret these results conservatively. Artifacts often vary wildly depending on their deposition environment and conservation. The fact that an artifact images well in this study does not preclude that it will photograph well with NIR after a variety of conservation treatments or from different areas of deposition. Each artifact should be examined independently and at the researcher's discretion for its suitability to be imaged by a modified NIR digital camera.

The study of this thesis sought to gauge baseline responses of a wide variety of archaeological artifacts of varying conditions to a NIR dSLR. It did not seek to explain how or why artifacts respond in the fashion they did, but rather test the capabilities of

easy to use, affordable NIR cameras that can painlessly be added to an existing photographic system. Given the results listed above, it is apparent that these cameras provide an analytical benefit to researchers analyzing a substantial number of these artifacts. Future research needs to seek to better understand why different artifact types image in infrared and how it may change from pre-conservation to post conservation.

REFERENCES

Agache, R.
1968. "Essai d'utilisation ae´ rienne et au sol d'e´mulsions spectrozonales, dites infrarouges couleurs," *Bulletin de la Socie´ te´ Pre´ historique Française,* Vol. 65, pp. 198–200.

Alvrus, Annalisa, Merbs, Charles F., and Wright, David.
2001. "Examination of Tattoos on Mummified Tissue using Infra-red Reflectography," *Journal of Archaeological Science,* Vol. 28, pp. 395-400.

Aqdus, Syed Ali, Hanson, William S., and Drummond, Jane
2012. "The Potential of Hyperspectral and Milt-spectral Imagrery to Enhance Archaeological Cropmark Detection: A Comparative Study," *Journal of Archaeological Science,* Vol. 39 (2012), pp. 1915-1924.

Baldia, Christel M. and Jakes, Kathryn A.
2007. "Photographic Methods to Detect Colourants in Archaeological Textiles," *Journal of Archaeological Science,* Vol. 34 (2007), pp. 519-525.

Barnett, Shawn and Etchells, Dave
2006. "Canon EOS 30D". *Imaging Resource Digital Camera Reviews – Canon Digital Cameras.* Web. Accessed 09 27 2014. <http://www.imaging-resource.com/PRODS/E30D/E30DA2.HTM>.

Barr, E. Scott.
1961. "The Infrared Pioneers –I. Sir William Herschel," *Infrared Physics,* Volume 1, Issue I, March 1961.

Braasch, O.
2007. "Gallipoli Ahead – Air Survey Between the Baltic and Mediterranean," In*: Kuzma, I. Publika´ cia vznikla v ramci Centra excelentnosti SAV Vy´skumne´ centrum Najstarsıch dejı´n Podunajska pri Archeologickom ustave SAV v Nitre. Archeologickom ustave SAV, Nitra,* pp. 84–96.

Buti, D. *et al.*
2014. "Non-invasive Investigation of a Pre-Hispanic Maya Screengold Book: The Maya Codex," *Journal of Archaeological Science,* vol. 42, pp. 166-178.

Beuttner-Janusch, John.
1954. "Use of Infrared Photography In Archaeological Fieldwork," *American Antiquity,* Vol. 20, No. 1 (July 1954), pp. 84-87.

Canon, 2014. Canon USA.
"EOS 20D," Canon USA. Web. Accessed on 2014.09.15. <http://www.usa.canon.com/cusa/support/consumer/eos_slr_camera_systems/eos_digital_slr_cameras/eos_20d#Overview.>.

Conlon, Vera M.
1973. *Camera Techniques in Archaeology,* John Baker Publishing, London.

Coremans, P.
1938. "Les rayons infra-rouges. Leur nature. Leurs applications dans les Musées," *Bulletin des musées royaux d'art et d'histoire,* Vol. 10, pp. 87–91.

Cox, Starr.
2008. *Enfield Rifles: The Composite Conservation of Our American Civil War Heritage.* Master's Thesis. Texas A&M University, College Station, Texas, 2010.

Curcio, Joseph A., and Petty, Charles C.
1951. "The near Infrared Absorption Spectrum of Liquid Water," *Journal of the Optical Society of America,* Vol. 43, Number 5. pp. 302-304.

Daniel, Shanna.
2007. *A Mammoth of a Project: The Conservation of a Columbian Mammoth.* Master's Thesis. Texas A&M University, College Station, Texas, 2010.

Darmont, Arnaud.
2009. "Spectral Response of Silicon Image Sensors," White Paper, Aphesa. Web. Accessed 07 March 2015. < http://www.aphesa.com/documents.php?class=wp>.

Davidhazy, Andrew
1993. "Infrared photography," The *Focal Encyclopedia of Photography, 3rd ed.* Leslie Stroebel and Richard Zakia (*eds.)* Focal Press, Boston. pp. 389 - 395.

Dorrell, Peter G.
1994. *Photography in Archaeology and Conservation, 2nd ed.* Cambridge Manuals in Archaeology. Cambridge University Press. Cambridge, NY.

Duncan, Christopher and Klingle, Curtis.
2011. "Using Reflected Infrared Photography to Enhance the Visibility of Tattoos," *Journal of Forensic Identification,* Vol. 61, No. 5, pp. 495-519.

Edeine, B.
1956. “Une me´thode pratique pour la de´ tection ae´ rienne des sites archeologiques, en particulier par la photographie sur films en couleurs et sur film infra-rouges*,” Bulletin de la Societe´ Prehistorique Française,* Vol. 53, pp. 540–546.

Encyclopedia Britannica Online.
2015. “Robert Williams Wood,” *Encyclopedia Britannica Online.* Web. Retrieved 10 February 2015. <http://www.britannica.com/EBchecked/topic/647385/Robert-Williams-Wood >

Falcone,L., Bloisi,F., Califano,V., Pagano,M., Vicari,L.
2008. “An Old Notice Board at Ancient Herculaneum Studied Using Near Infrared Reflectography,” *Journal of Archaeological Science,* Vol. 35, Iss. 6. pp. 1708-1716.

Fisher, Lisa Jayne
2009. “BAJR Practical Guide Series: Photography For Archaeologists Part I: Site Specific Record,” *BAJR Practical Guide Series*, Guide 25 (June 2009). Web. Accessed 09 25 2014. <http://www.bajr.org/BAJRGuides/25.%20Site%20Specific%20Photography/25PhotographyforArchaeologists.pdf>

Freedman, Roger, A., and Kaufmann, William .J.
2005. *Universe, 7th ed*. W.H. Freeman and Company, New York.

Gotelipe-Miller, Shirley.
1990 “Pewter and Pewterers from Port Royal, Jamaica: Flatware Before 1692,” Thesis. Texas A&M University, College Station, TX. August 1990.

Gumerman, George J. and Neely, James A.
1972. “An Archaeological Survey of the Tehuacan Valley, Mexico: A Test of Color Infrared Photography,” *American Antiquity,* Vol. 37, No. 4 (Oct. 1972), pp. 520-527.

Hamilton, Donny L.
2010. *Methods for Conserving Archaeological Material from Underwater Sites.* Revision II. Conservation Reasearch Laboratory, Center for Maritime Archaeology and Conservation, Texas A&M University. <http://nautarch.tamu.edu/CRL/conservationmanual/ConservationManual.pdf>

Hamilton, Donny L.
2015. "Historical Archaeology, ANTH 313," Class notes portal. Ceramics: Period II. Web. Accessed 21 February 2015.< http://nautarch.tamu.edu/class/313/ceramics/period-2.htm>.

Hamilton, Donny L.
2015. "Historical Archaeology, ANTH 313," Class notes portal. Ceramics: Period IV. Web. Accessed 21 February 2015.< http://nautarch.tamu.edu/class/313/ceramics/period-4.htm>.

Hampton, J. N.
1974. "An Experiment in Multispectral Air Photography for Archaeological Research," *The Photogrammetric Record*, Vol. 8, pp 37-64.

Herschel, William, LL. D. F. R. S.
1800. "Investigation of the Powers of the Prismatic Colours to Heath and Illuminate Objects; With Remarks, That Prove the Different Refrangibility of Radiant Heat. To which is Added, an Inquiry into the Method of Viewing the Sun Advantageously, with Telescopes of Large Apertures and High Magnifying Powers," *Philosophical Transactions, Royal Society of London* 1800, Volume 90, pp. 285-283.

Hirsch, Ethel S. and Hurtgen, Thomas P.
1975. "Infrared Photography and Archaeology: Painted Floors at Goiurnia," *Archaeology*, Vol. 28, No. 4 (October 1975), pp. 260-266.

Hornsby, Peter R. G.
1983. *Pewter of the Western World, 1600-1850.* Schiffer Publishing, Ltd. Exton, Pennsylvania.

Lamore, Lewis.
1959. "Infrared Photography," *Proceedings of the Institute of Radio Engineers (IRE).* Volume 47, Issue 9. pp. 1487-1888.

LifePixel.
2015. "Chapter 1- Introduction to infrared photography – Development of infrared film," *Digital Infrared Photography Primer,* Web. Retrieved 09 February 2015 < http://www.lifepixel.com/infrared-photography-primer/ch1-development-of-infrared-film>.

LifePixel
2015. “Chapter 2- Basic Theory – How Filters Work,” *Digital Infrared Photography Primer.* Web. Retrieved 09 February 2015. < http://www.lifepixel.com/infrared-photography-primer/ch-basic-theory-how-filters-work>.

LifePixel
2014. “Digital Infrared Photography Primer: Chapter 2 – Basic Theory – Light Sources,” *Digital Infrared Photography Primer* Web. Accessed 09 24 2014. <http://www.lifepixel.com/infrared-photography-primer/ch2-basic-theory-light-sources>

LifePixel
2014. “Digital Infrared Photography Primer: Chapter 4 –Digital Photography Infrared Advantages– Focus,” *Digital Infrared Photography Primer*. Web. Accessed 09 24 2014 <http://www.lifepixel.com/infrared-photography-primer/ch4-digital-infrared-photography-advantages-focus>.

Pizzo, Bendetto, *et. Al*
2008. “Characterization of Waterlogged Wood by Infrared Spectroscopy,” Web. Retrieved 18 February 2015 < http://www.woodculther.com/wp-content/uploads/2008/10/macchioni.pdf>.

Milanesi, Q.
1963.:Proposta di una facile metodica ausiliaria per lo studio della ceramiche di epoca preistorica e protostorica*,” Rivista di Scienze Preistoriche* Vol. 18, pp. 287–293.

Nielsen, Harald H.
1951. “Infrared Spectroscopy,” *Science,* Vol. 113, No 2940 (May 4, 1951), p. 3a

Orlandini, Valeria.
2005. “A Study of Examination and Photo-Documentation of Iron-Gall Ink and Other Inks,” *The Book and Paper Group Annual*, Vol. 24, pp. 45-46. Presented at the Book and Paper Group Session, AIC, 33rd Meeting, June 8-13, 2005, Minneapolis, Minnesota.

Peal, Christopher A.
1983. *Pewter of Great Britain.* John Gifford, London.

Photozone.
2005. “Canon EF-S 60mm f/2.8 USM macro - Review / Test Report,” Photozone. Web. Accessed 09 21 2014.< http://www.photozone.de/reviews/162-canon-ef-s-60mm-f28-usm-macro-test-report--review.>

Picollo, Marcello, *et al.*
2011. "Spectral Characterization of Ancient Wooden Artefacts with the Use of Traditional AR Techniques and ATR Device: A Methodological Approach," *e-Preservation Science.* Vol. 8, pp. 23-28.

Powlesland, Dominic, Lyall, James, and Donoghue, Daniel.
1997. "Enhancing the record through remote sensing: The application and integration of multi-sensor, non-invasive remote sensing techniques for the enhancement of the Sites and Monuments Record. Heslerton Parish Project, N. Yorkshire, England," *Internet Archaeology,* Iss. 2, 1997. Web. Retrieved 18 Feb 2015 < http://intarch.ac.uk.lib-ezproxy.tamu.edu:2048/journal/issue2/pld_index.html>.

Precision Camera.
2014. "Information About Precision Camera Infrared Conversion Services," Precision Camera. Web. Accessed on 2014.09.17 <http://www.precisioncamera.com/infrared-conversion-services_sub2.html>.

Rand, Glenn, Davis, Robert G., and Litschel, David.
2005. *Digital Photographic Capture.* Taylor and Francis, New York.

Rawling, S.O.
1933. *Infra-red Photography.* Blackie & Son, Ltd, London & Glascow.

Reichstein, J.
1974. Schwarz-Weiß-Infrarotphotographie als Hilfsmittel für die Analyse schwer beobachtbarer Befunde. Offa 31, pp. 108–125.

Rigaud, P., and Bouyer, P.
1986. "Archeologie aerienne: teledection infrarouge par photographies verticales a` partir d'un ballon captif et d'un avion,". *Travaux d'archeologie limousine,* Vol. 7, pp. 7–12.

Roberge, Pierre, R.
2006. *Corrosion Basics: An Introduction, 2nd ed.* NACE Press Book.

Sager, Rebecca.
2008. *Hair Today, Gone Tomorrow: The Degradation and Conservation of Archaeological Hair Fibers.* Master's Thesis. Texas A&M University, College Station, Texas, 2010.

Smith, C. Wayne.
1998. “Silicone Oil: A New Technique for Preserving Waterlogged Rope,” Archaeological Preservation Research Laboratory (APRL), Report 5, Nautical Archaeology Program, Texas A&M University. <http://nautarch.tamu.edu/APRL/report05.htm>.

Smith, C. Wayne.
2010. “Expanded Spectrum Photography and Archaeological Conservation,” *Technical Briefs in Archaeology*, Vol. 5, pp. 16-19.

Smith, George S. and Zimmerman, Michael R., M.D.
1975. “Tattooing Found On a 1600 Year-Old Frozen, Mummified Body from St. Lawrence Island, Alaska,” *American Antiquity*, Vol. 40, No. 4 (1975). pp. 433-437.

Strandberg, C.H.
1967. “Photoarchaeology,” *Photogrammetric Engineering*, Vol. 33, pp. 1152-1157.

Tsuchikawa, Satoru, and Schwanniger, Mandred.
2013. “A review of Recent Near-Infrared Research for Wood and Paper (Part 2),” *Applied Spectroscopy Reviews*, Vol. 48, Iss. 7, pp. 560-587.

Verhoeven, Geert.
2007. “Becoming a NIR-sensitive aerial archaeologist,” In: Neale, C., Owe, M., D’Urso, G. (Eds.*), Remote Sensing for Agriculture, Ecosystems, and Hydrology IX*, Florence, Italy, 17–19 September 2007. SPIE, Bellingham, pp. 333–345.

Verhoeven, Geert.
2008. “Imaging the Invisible Using Modified Digital Still Cameras for Straightforward and Low-cost Archaeological Near-Infrared Photography,” *Journal of Archaeological Science*, Vol. 35, pp. 3087-3100.

Via, Brian K., *et al.*
2014. “Near Infrared Spectroscopy Calibration for Wood Chemistry: Which Chemometric Technique is Best for Prediction and Interpretation?,” *Sensors*, Vol. 14. pp. 13532-13547.

Wood, Robert Williams.
1910. “Photography of Invisible Rays,” *Photogr. J., Volume* 50 (Oct.), pp. 329-338.

Zhang, Michael.
2010. “The World’s First Digital Camera by Kodak and Steve Sasson,” *Petapixel*. Web. Retrieved 03 01 2015. < http://petapixel.com/2010/08/05/the-worlds-first-digital-camera-by-kodak-and-steve-sasson/>.

APPENDIX I

FINAL TABLE OF ARTIFACTS

ARTIFACT ID	ARTIFACT TYPE	SPECIFIC TYPE	CONSERVATION METHOD	ID EXPLANATION	IMAGING LOCATION	RATING: IR vs VISIBLE
BONE						
CBPS1	Bone	Pig Bone and Fat	Silicone Oil	Conserved Bone Pig Skin	Riverside	Recommended
UBS2	Bone	Stained Pig Bone	Unconserved	Unconserved Bone Stained	Wilder	Recommended
CERAMICS						
UCPW1	Ceramic	Pearlware	Unconserved/fresh water bath	Unconserved Ceramic Pearl Ware	Wilder	Recommended
UCP2	Ceramic	Porcelain	Unconserved/fresh water bath	Unconserved Ceramic Porcelain	Wilder	Not Recommended
UCWW3	Ceramic	Whiteware	Unconserved/fresh water bath	Unconserved Ceramic White Ware	Wilder	Not Recommended
UCCW4	Ceramic	Creamware	Unconserved/fresh water bath	Unconserved Ceramic Cream Ware	Wilder	Not Recommended
UCSW5	Ceramic	Slipware	Unconserved/fresh water bath	Unconserved Ceramic Slip Ware	Wilder	No Change
UCTE6	Ceramic	Tin Enamel	Unconserved/ fresh water bath	Unconserved Ceramic Tin Enamel	Wilder	Not Recommended
UCStW7	Ceramic	Stoneware	Unconserved/fresh water bath	Unconserved Ceramic Stone Ware	Wilder	No Change
UCCE8	Ceramic	Coarse Earthenware	Unconserved/fresh water bath	Unconserved Ceramic Coarse Earthenware	Wilder	No Change
UCWC9	Ceramic	White Clay	Unconserved/fresh water bath	Unconserved Ceramic White Clay	Wilder	Recommended
METALS						
CMPER1	Metal	Pewter	Electrolydic Reduction	Conserved Metal Pewter Electrolydic Reduction	Wilder	No Change
UMSC2	Metal	Silver	Unconserved	Unconserved Metal Silver Coin	Riverside	No Change
UMBB3	Metal	Cupreous (Brass)	Unconserved	Unconserved Metal Brass Buckle	Riverside	Recommended
UMWM4	Metal	White Metal	Unconserved	Unconserved Metal White Metal	Riverside	No Change
UMC5	Metal	Cupreous and Wood	Unconserved	Unconserved Metal Cupreous	Riverside	Not Recommended
UMLB6	Metal	Lead	Unconserved	Unconserved Metal Lead Ball	Riverside	Recommended
UMIC7	Metal	Iron Concretion	Unconserved	Unconserved Metal Iron Concretion	Riverside	No Change
UMISD8	Metal	Iron with wood	Unconserved	Unconserved Metal Iron Spike Dry	Riverside	No Change
CMIERT9	OMITTED					
CMLBER10	Metal	Lead	Electrolydic Reduction, Tannic Acid, and Microcrystalline wax	Conserved Metal Lead Bar Electrolydic Reduction	Wilder	No Change
TEXTILE						
UTPGI1	Paper	Paper	Unconserved	Unconserved Textile Paper Gall Ink	Wilder	Recommended
CTRSO2	Textile	Rope	Silicone Oil	Conserved Textile Rope Silicone Oil	Riverside	Recommended
WOOD						
UWSAD1	Wood	Soft Wood	Unconserved/ Air Dry	Unconserved Wood Soft Air Dry	Wilder	No Change
CWSPF2	Wood	Soft Wood	Polyethylene Glycol and Freeze Dried	Conserved Wood Soft PEG Freeze	Wilder	Recommended
CWHP3	Wood	Hard Wood	Polyethylene Glycol	Conserved Wood Hard PEG	Wilder	Recommended
CWHSO4	Wood	Hard Wood	Silicone Oil	Conserved Wood Hard Silicone Oil	Riverside	Recommended
CWHSO5	Wood	Hard Wood	Silicone Oil	Conserve Wood Hard Silicone Oil	Riverside	Recommended
CWSP6	Wood	Soft Wood	Polyethylene Glycol	Conserved Wood Soft PEG	Riverside	No Change
UWHAD7	Wood	Hard Wood	Unconserved/ Air Dry	Unconserved Wood Hard Air Dry	Wilder	Recommended

APPENDIX II

ARTIFACT IMAGES

Appendix II contains all photographs used for the research conducted in this thesis. Images are organized by type and then by artifact name. Shown first are the unmodified photographs taken by the 30D, followed by the NIR images taken with the modified 20D camera.

Bone

CBPS1

UBS2


ARTIFACT ID: UBS 2
Date: 10-15 Time: 11:16 am
Location: Wilder
ABFO No. 2


ABFO No. 2
ARTIFACT ID: UBS 2
Date: 10-15 Time: 11:16 am
Location: Wilder


ABFO No. 2
ARTIFACT ID: UBS 2
Date: 10-15 Time: 12:49 pm
Location: Wilder

Ceramics

UCPW1

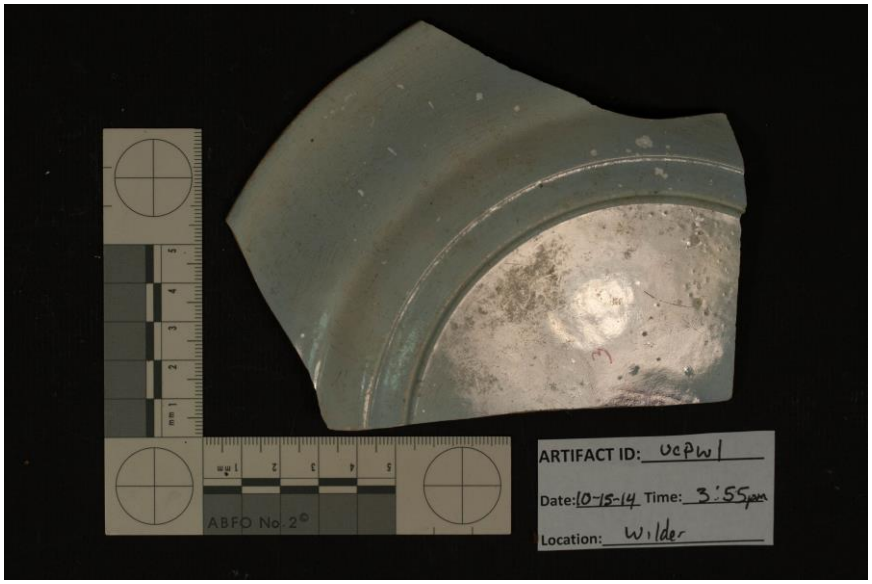
ABFO No. 2©
ARTIFACT ID: UCPW1
Date: 10-15-14 Time: 3:55pm
Location: Wilder

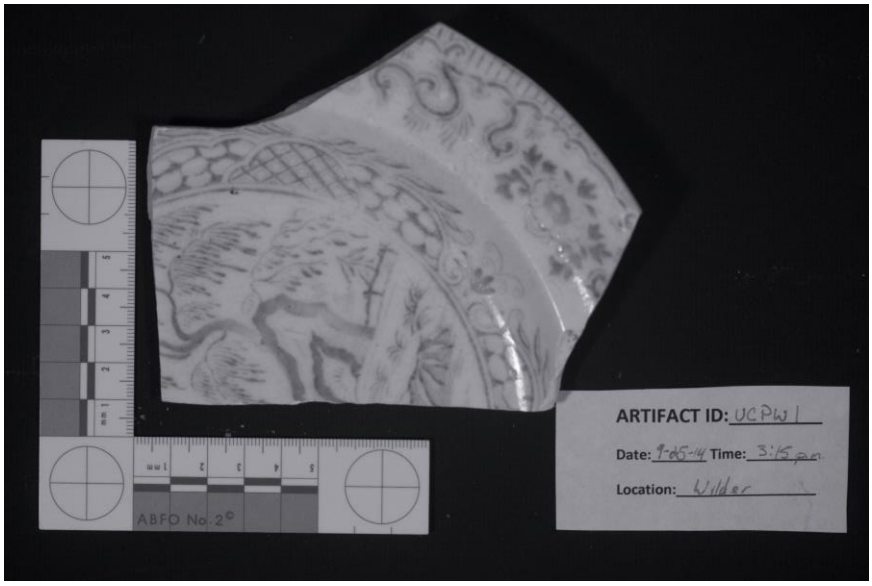
ABFO No. 2©
ARTIFACT ID: UCPW1
Date: 9-05-14 Time: 3:15 pm
Location: Wilder

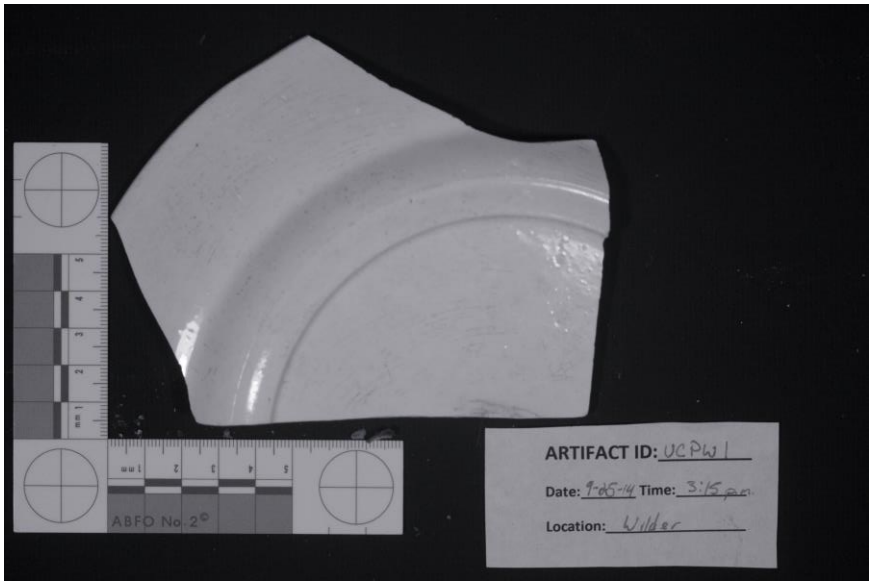
ABFO No. 2
ARTIFACT ID: UCPW1
Date: 1-05-14 Time: 3:15 p.m.
Location: Wilder

UCP2


ABFO No. 2
ARTIFACT ID: UCP2
Date: 10-15 Time: 4:08 pm
Location: Wilder

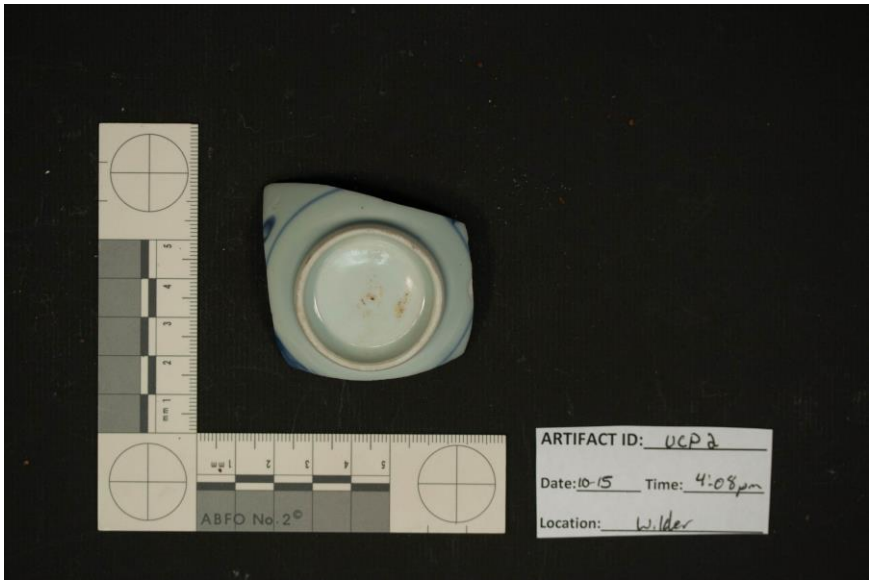
ABFO No. 2©
ARTIFACT ID: UCP 2
Date: 10-15 Time: 4:08 pm
Location: Wilder

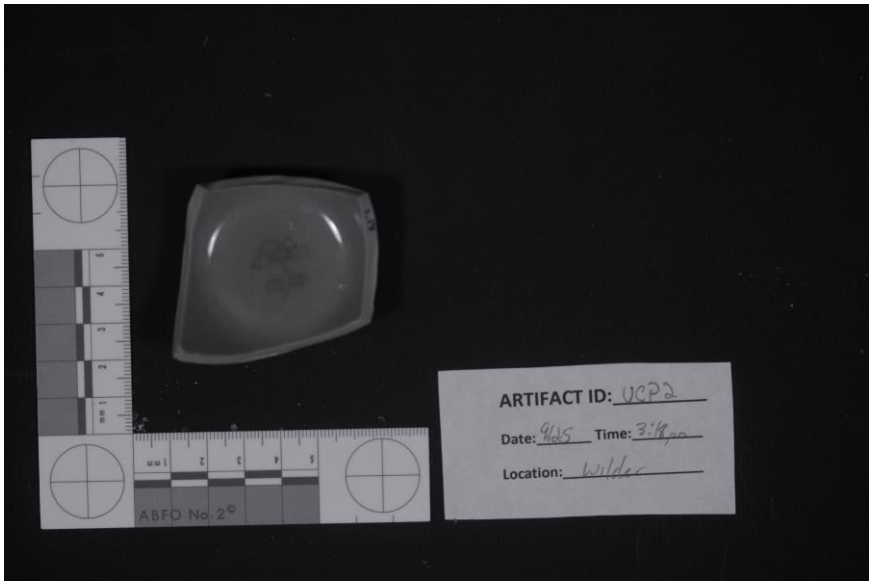
ABFO No. 2©
ARTIFACT ID: UCP2
Date: 9/25 Time: 3:19 pm
Location: Wilder


ARTIFACT ID: UCP2
Date: 9/25 Time: 3:19pm
Location: Wilder
ABFO No. 2©

UCWW3

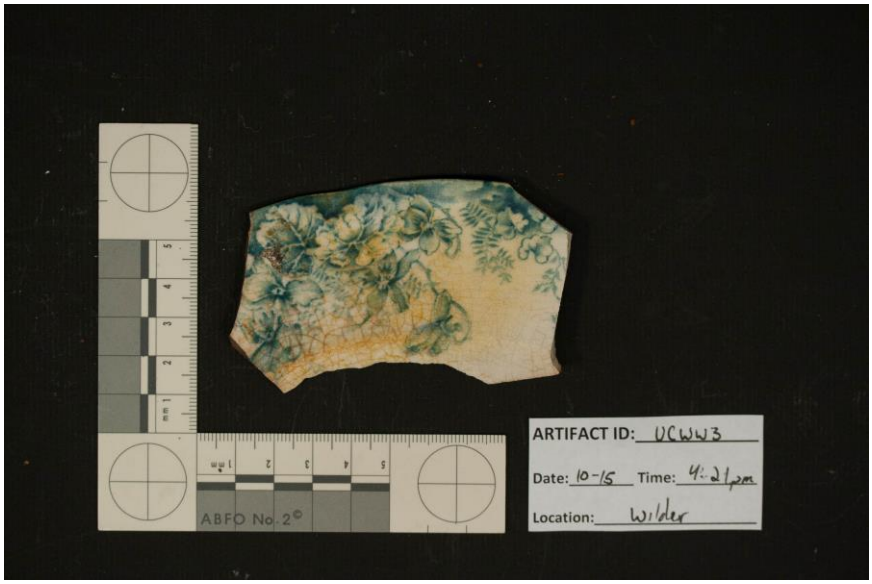
ARTIFACT ID: UCWW3
Date: 10-15 Time: 4:21pm
Location: Wilder
ABFO No. 2©


ABFO No. 2
ARTIFACT ID: UCWW3
Date: 10-15 Time: 4:21pm
Location: Wilder

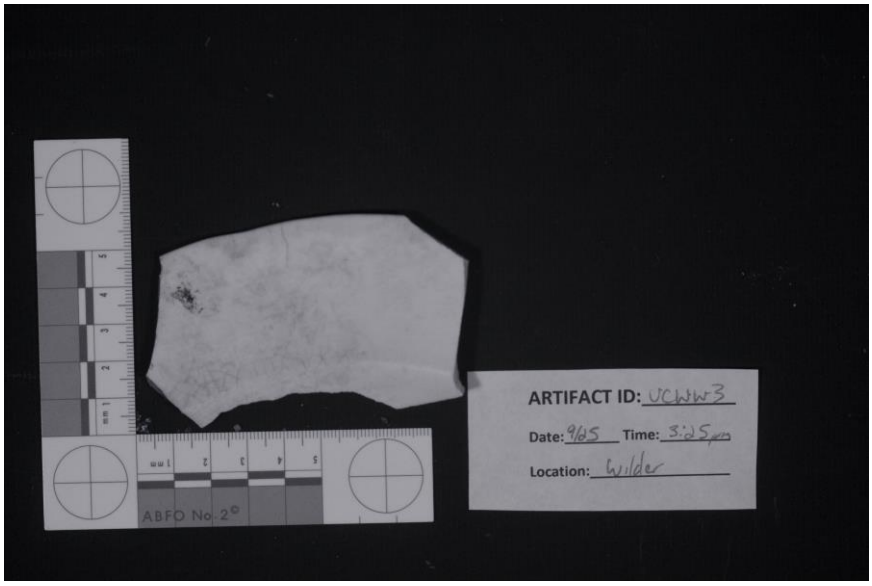
ABFO No. 2
ARTIFACT ID: UCWW3
Date: 9/05 Time: 3:25pm
Location: Wilder

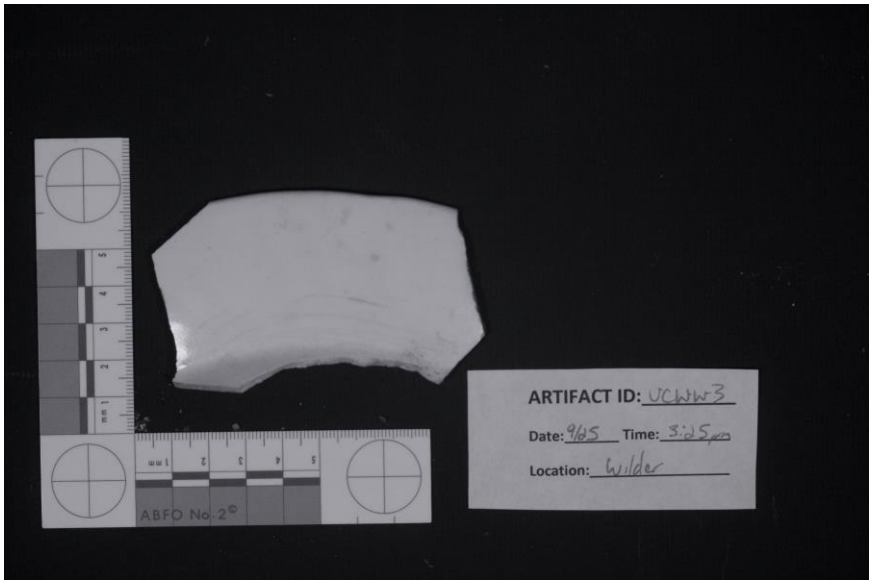
ARTIFACT ID: UCWW3
Date: 9/15 Time: 3:25pm
Location: Wilder
ABFO No. 2

UCCW4

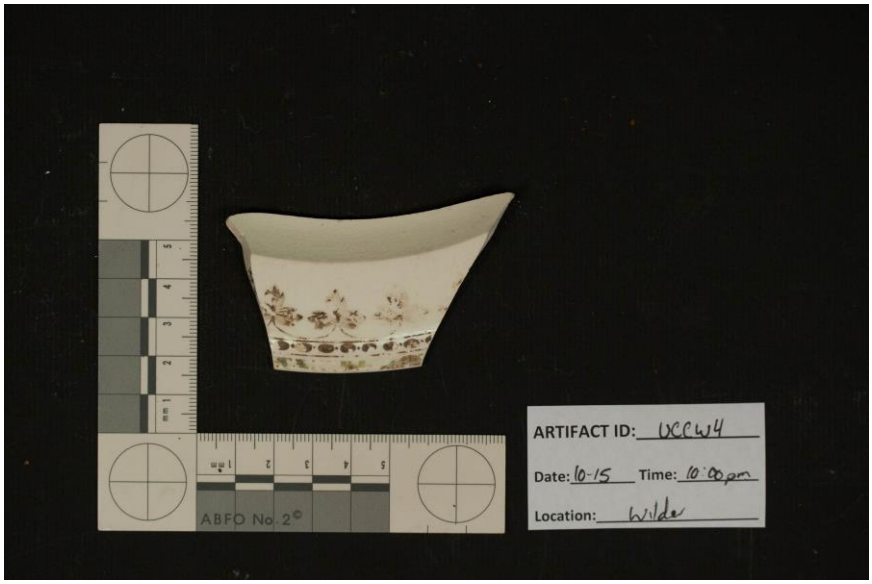
ARTIFACT ID: UCCW4
Date: 10-15 Time: 10:00pm
Location: Wilder
ABFO No. 2

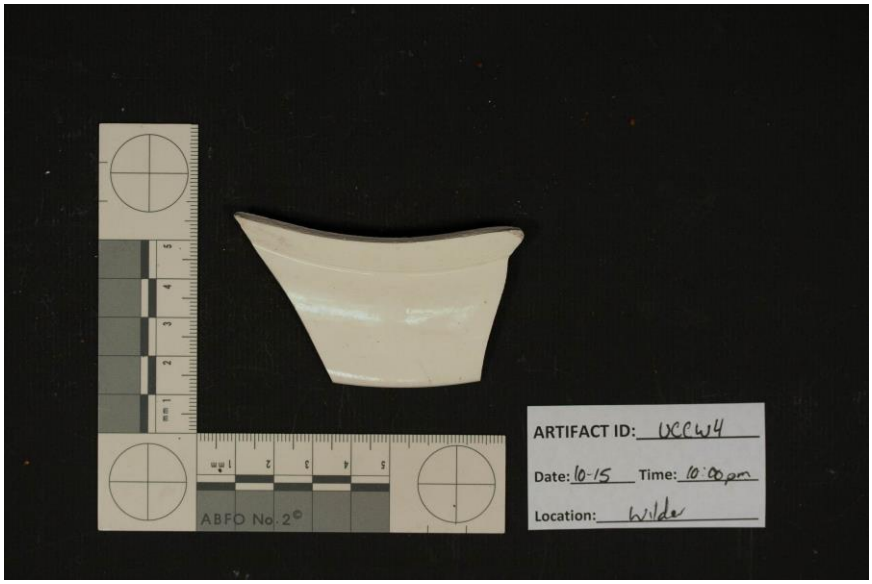
ABFO No. 2©
ARTIFACT ID: UCC4W4
Date: 10-15 Time: 10:00pm
Location: Wilder

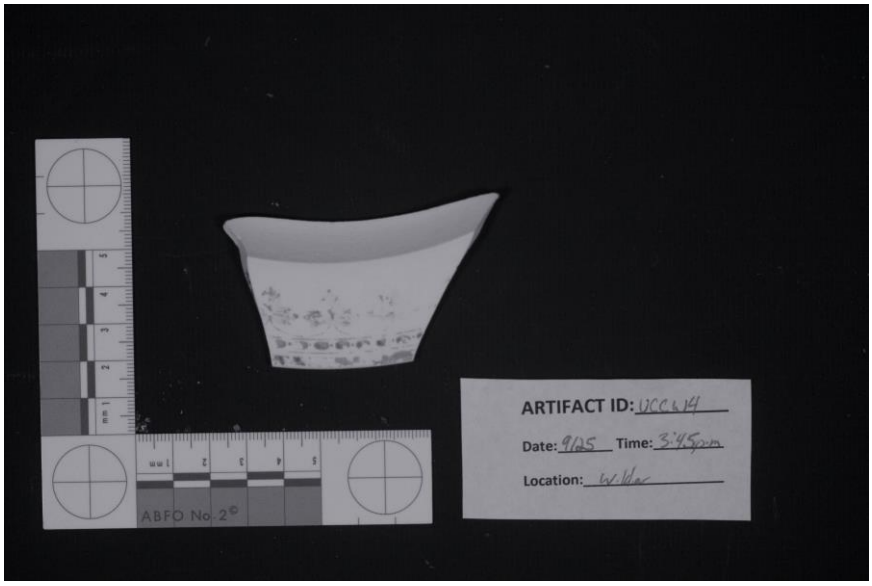
ABFO No. 2©
ARTIFACT ID: UCC4W4
Date: 9/25 Time: 3:45pm
Location: Wilder

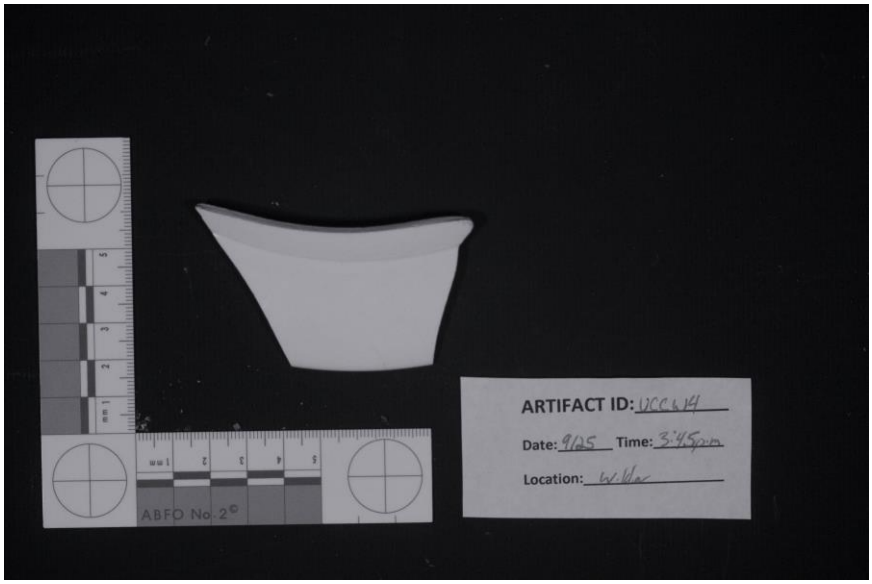
ARTIFACT ID: UCSW4
Date: 9/25 Time: 3:45pm
Location: Wilder
ABFO No. 2©

UCSW5

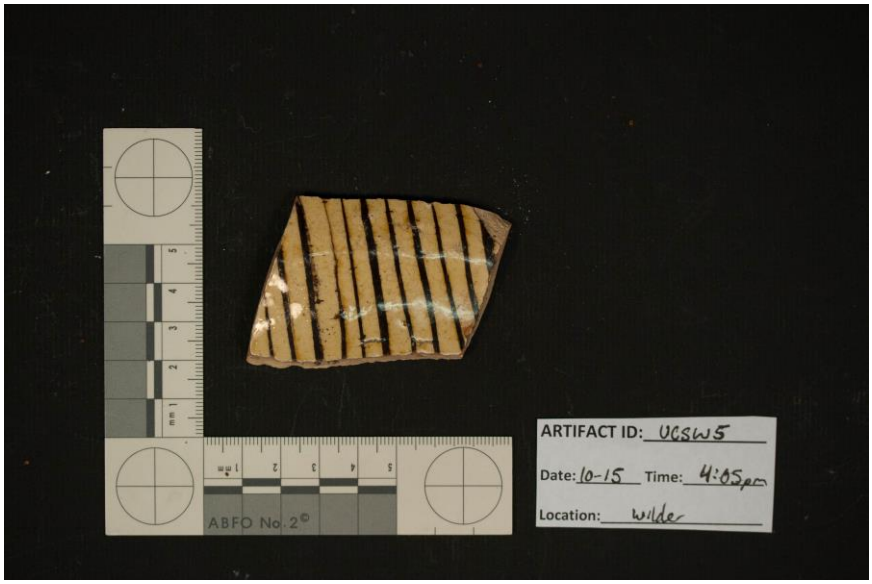
ARTIFACT ID: UCSW5
Date: 10-15 Time: 4:05pm
Location: Wilder
ABFO No. 2©

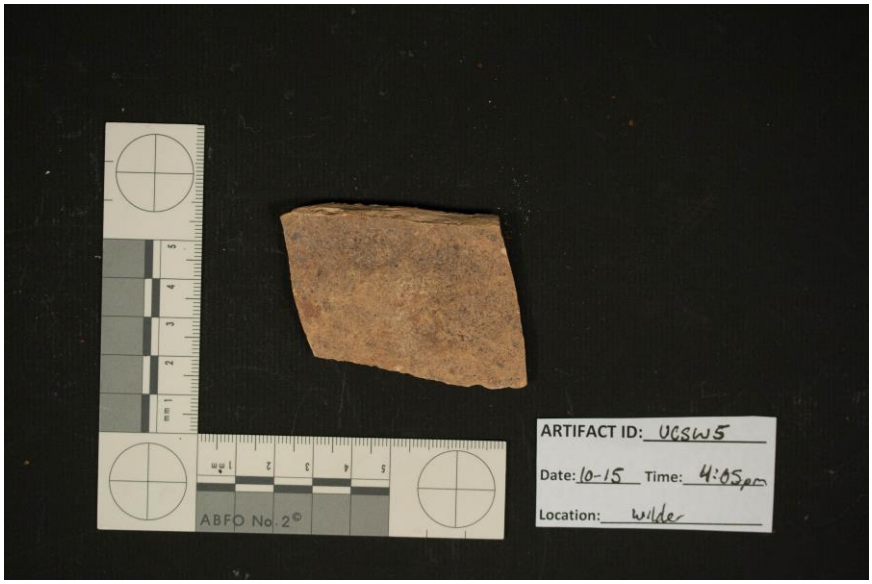
ABFO No. 2©
ARTIFACT ID: UCSW5
Date: 10-15 Time: 4:05pm
Location: Wilder

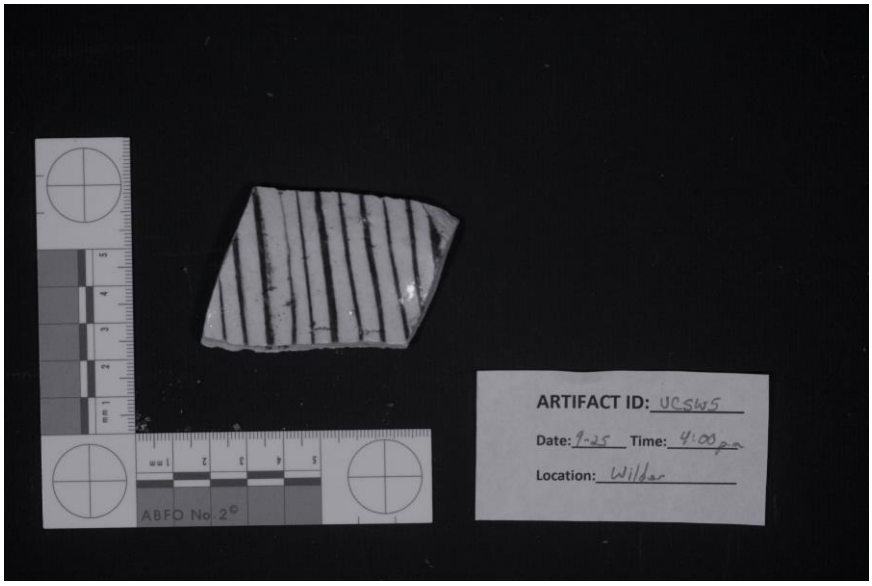
ABFO No. 2©
ARTIFACT ID: UCSW5
Date: 9-25 Time: 4:00pm
Location: Wilder

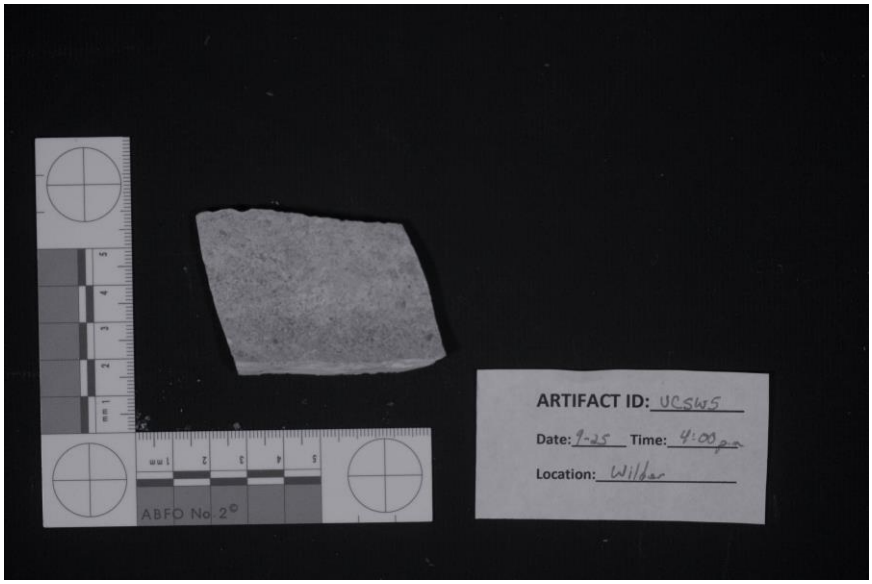
ARTIFACT ID: UCSW5
Date: 9-25 Time: 4:00 pm
Location: Wilder
ABFO No. 2

UCTE6

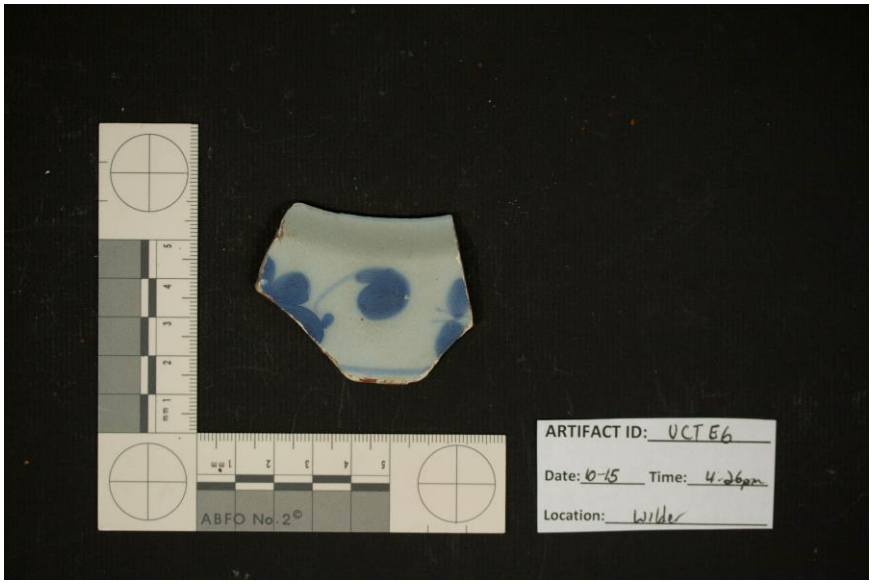
ARTIFACT ID: UCTE6
Date: 10-15 Time: 4:26pm
Location: Wilder
ABFO No. 2

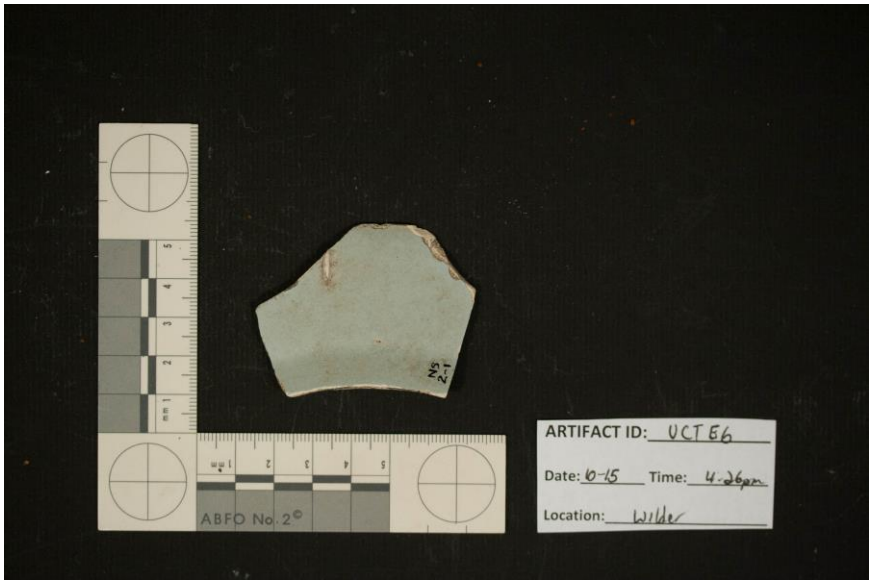
ABFO No. 2
ARTIFACT ID: UCT 66
Date: 6-15 Time: 4:26pm
Location: Wilder

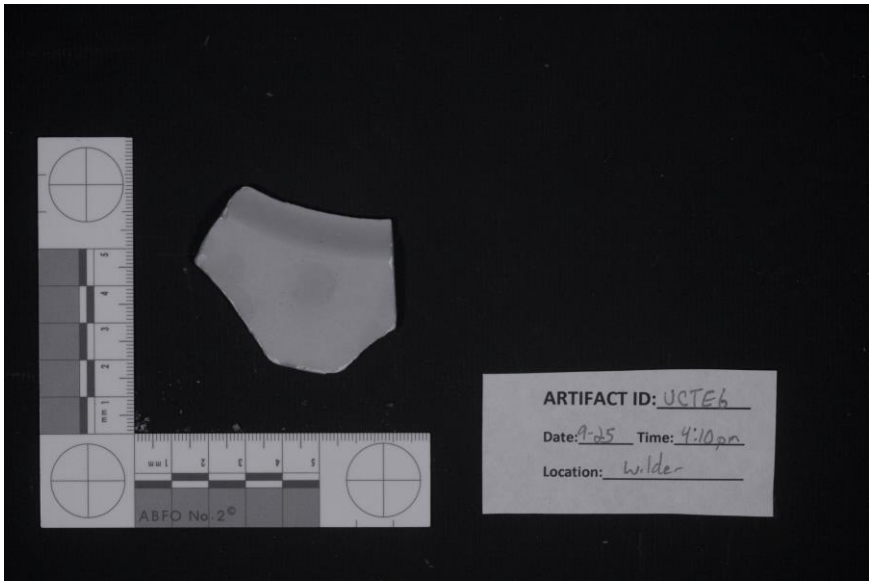
ABFO No. 2
ARTIFACT ID: UCT66
Date: 7-25 Time: 4:10pm
Location: Wilder

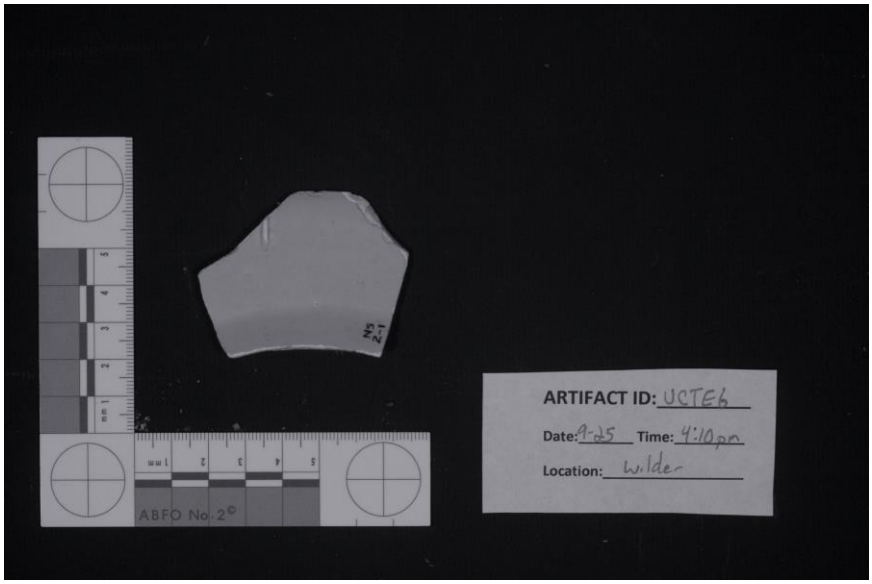
ARTIFACT ID: UCTE6
Date: 9-25 Time: 4:10pm
Location: Wilder
ABFO No. 2

UCStW7

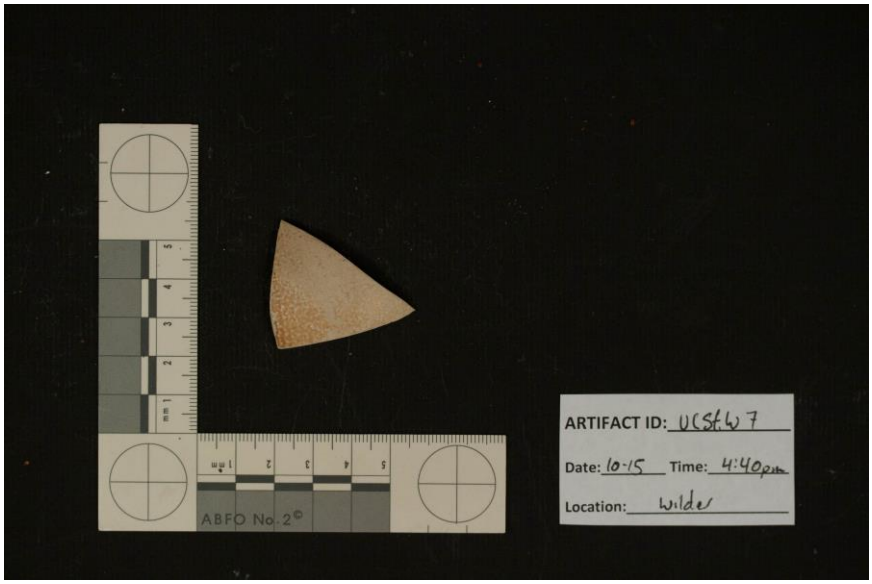
ARTIFACT ID: UCStW7
Date: 10-15 Time: 4:40pm
Location: Wilder
ABFO No. 2

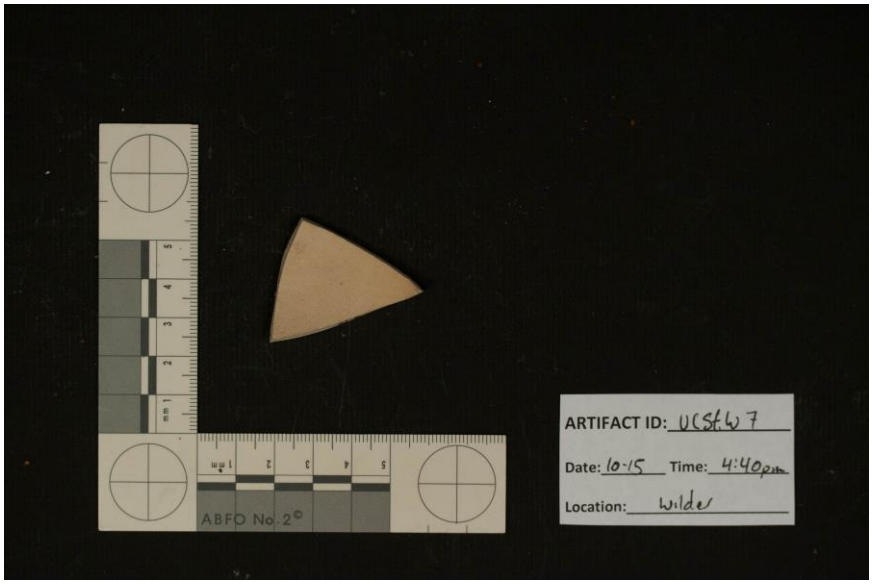
ABFO No. 2©
ARTIFACT ID: UCStW7
Date: 10-15 Time: 4:40pm
Location: Wilder

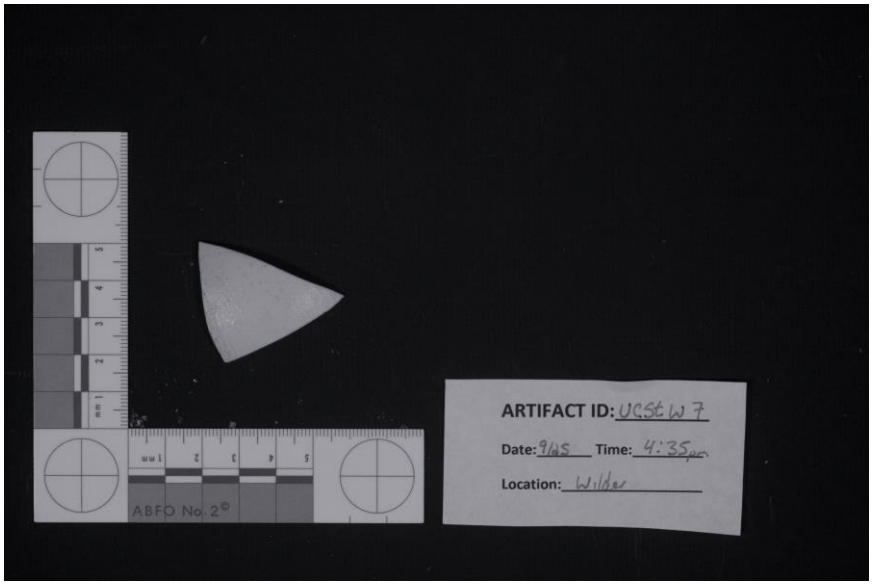
ABFO No. 2©
ARTIFACT ID: UCStW7
Date: 9/25 Time: 4:35pm
Location: Wilder

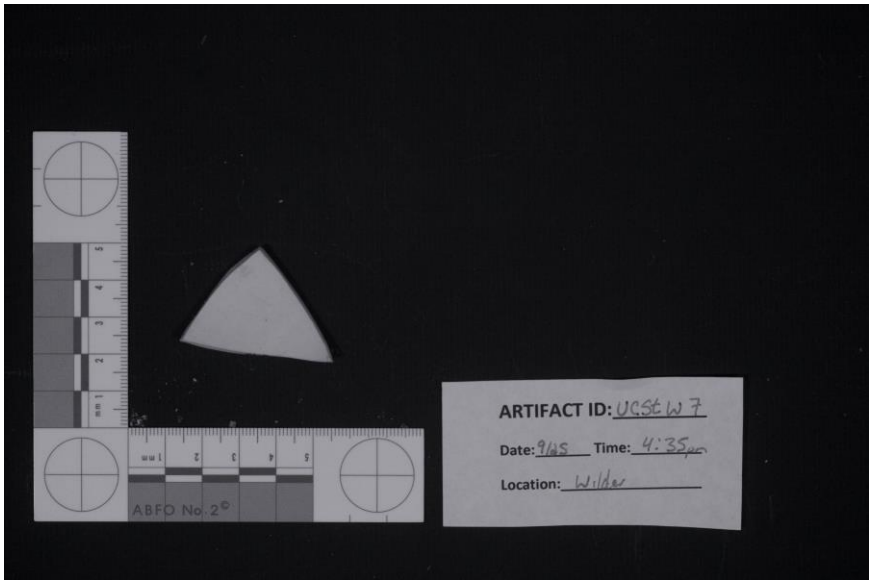
ARTIFACT ID: UCSt W 7
Date: 9/25 Time: 4:35pm
Location: Wilder
ABFO No. 2

UCCE8


ARTIFACT ID: UCCE8
Date: 10-15 Time: 10:007pm
Location: Wilder
ABFO No. 2


ABFO No. 2
ARTIFACT ID: UCCE8
Date: 10-15 Time: 10:00 am
Location: Wilder

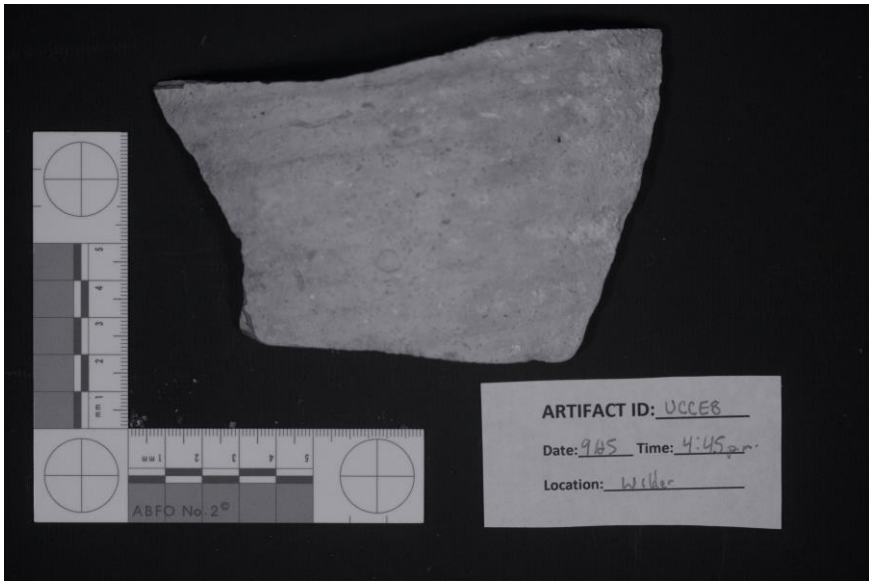
ABFO No. 2
ARTIFACT ID: UCCE8
Date: 9/25 Time: 4:45 pm
Location: Wilder

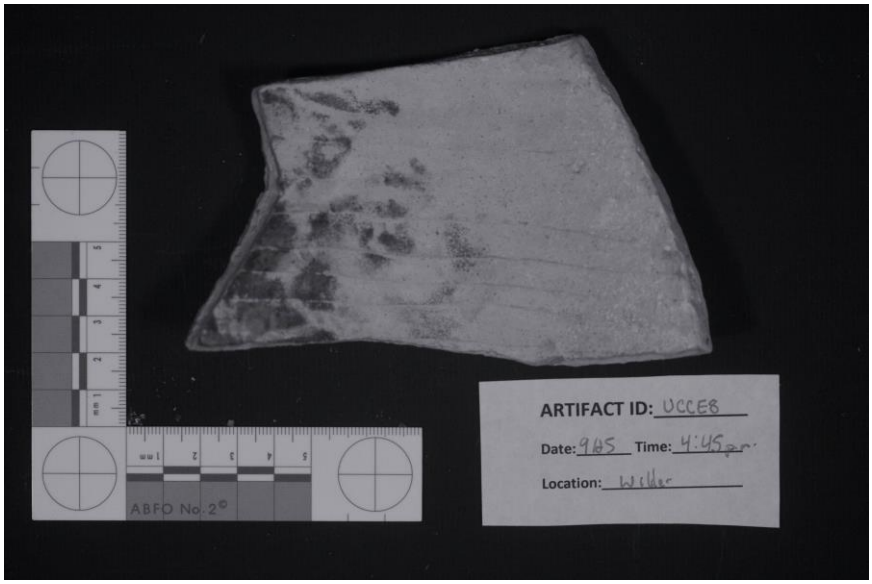
ABFO No. 2
ARTIFACT ID: UCCE8
Date: 9/25 Time: 4:45pm
Location: Wilder

UCWC9


ABFO No. 2
ARTIFACT ID: UCWC9
Date: 10-15 Time: 4:15pm
Location: Wilder


ABFO No. 2©
ARTIFACT ID: UCWC9
Date: 10-5 Time: 4:15pm
Location: Wilder

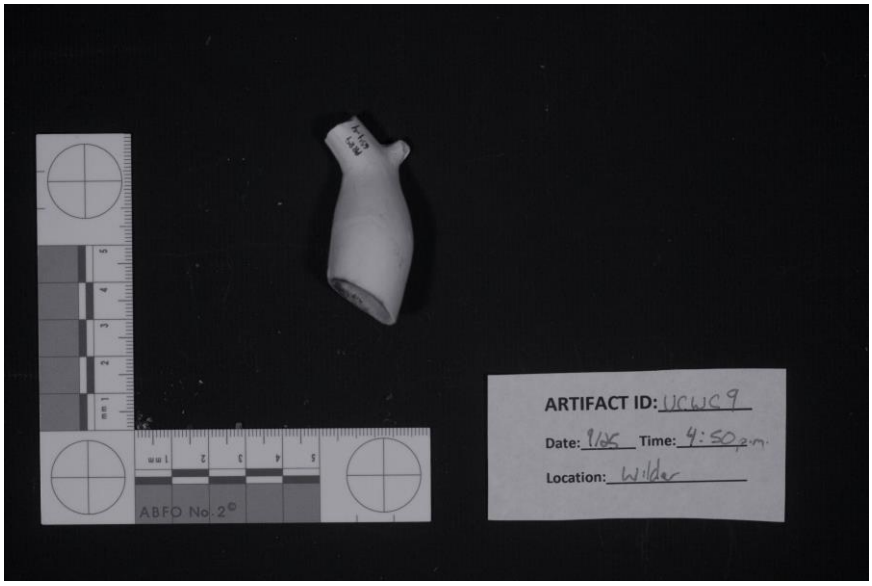
ABFO No. 2©
ARTIFACT ID: UCWC9
Date: 9/05 Time: 4:50 p.m.
Location: Wilder

Metals

CMPER1

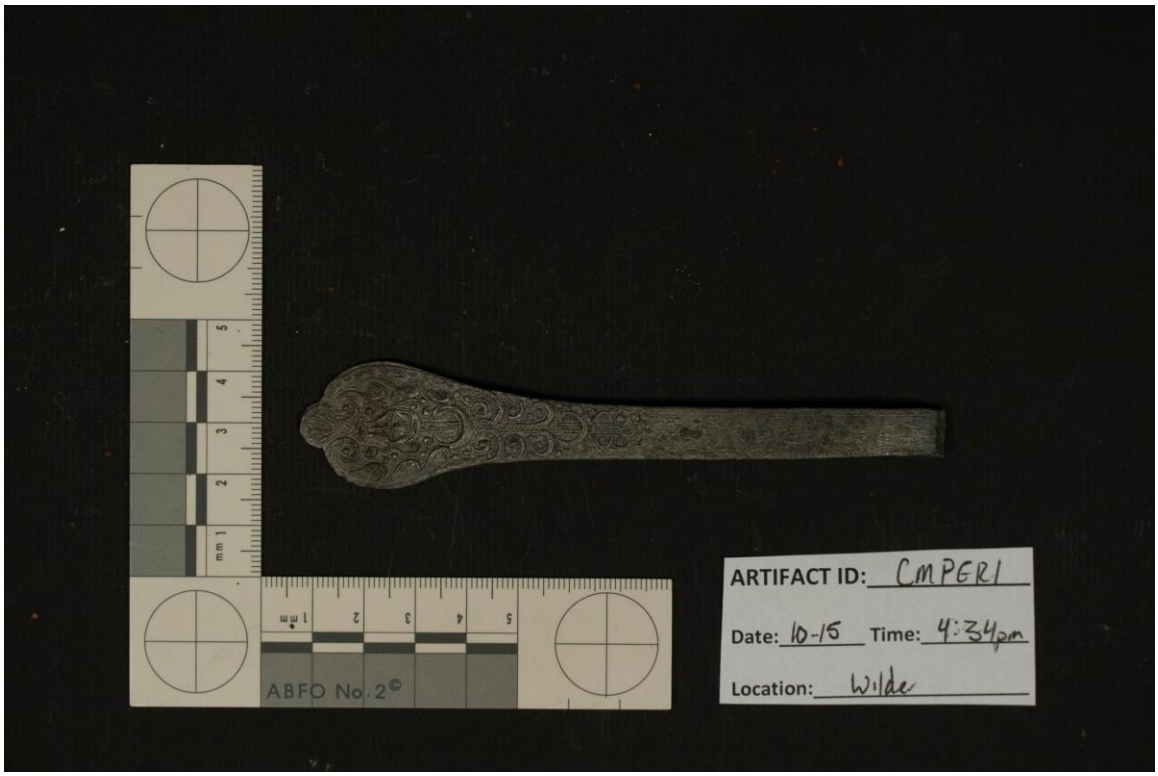

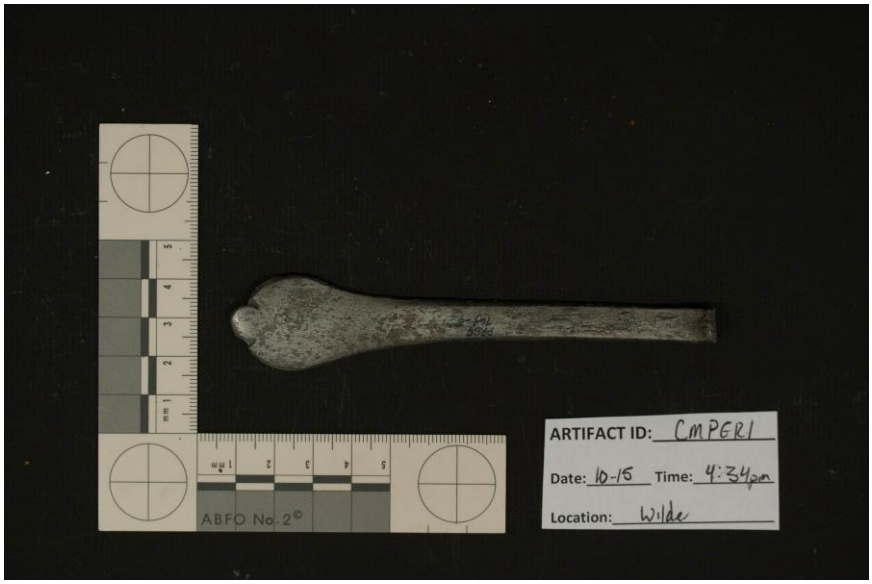
ABFO No. 2©
ARTIFACT ID: CMPER1
Date: 10-15 Time: 4:34pm
Location: Wilder

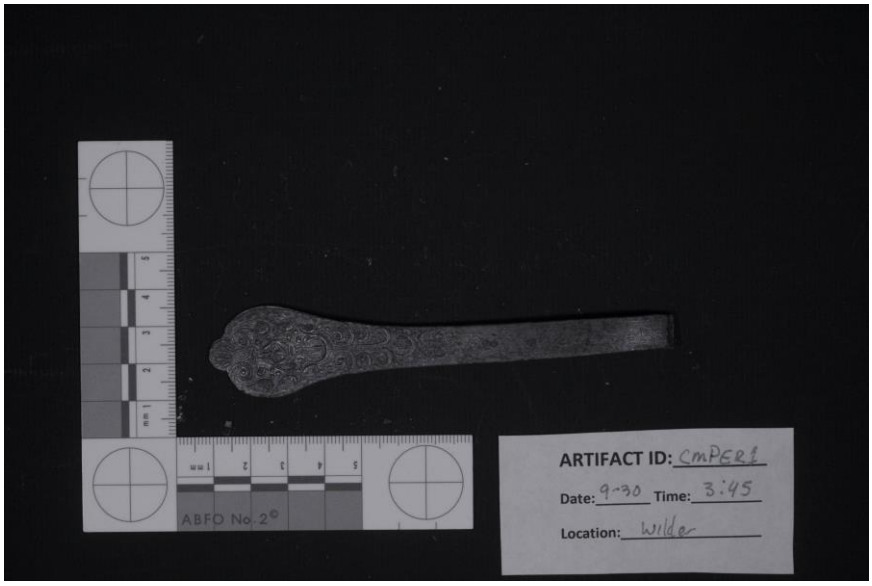
ABFO No. 2©
ARTIFACT ID: CMPER1
Date: 9-30 Time: 3:45
Location: Wilder

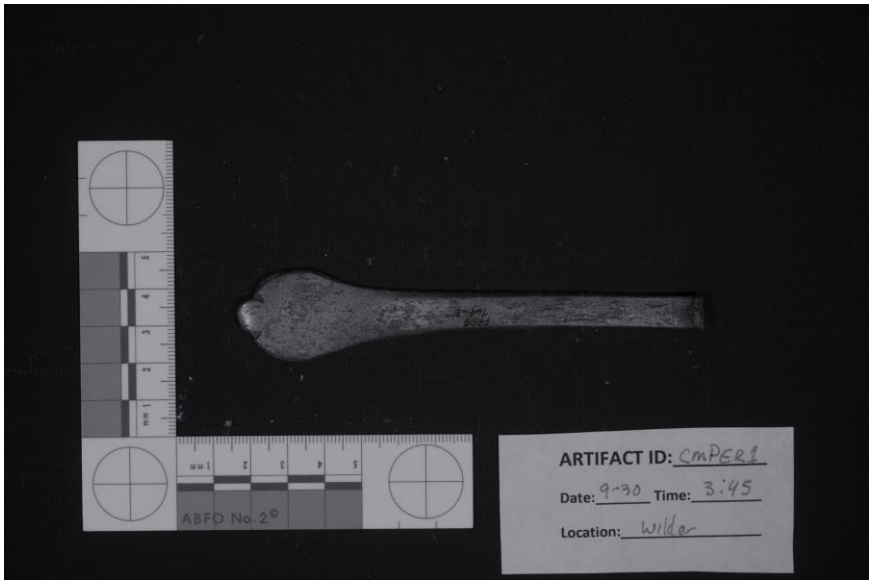
ABFO No. 2©
ARTIFACT ID: CMPER1
Date: 9-30 Time: 3:45
Location: Wilder

UMSC2

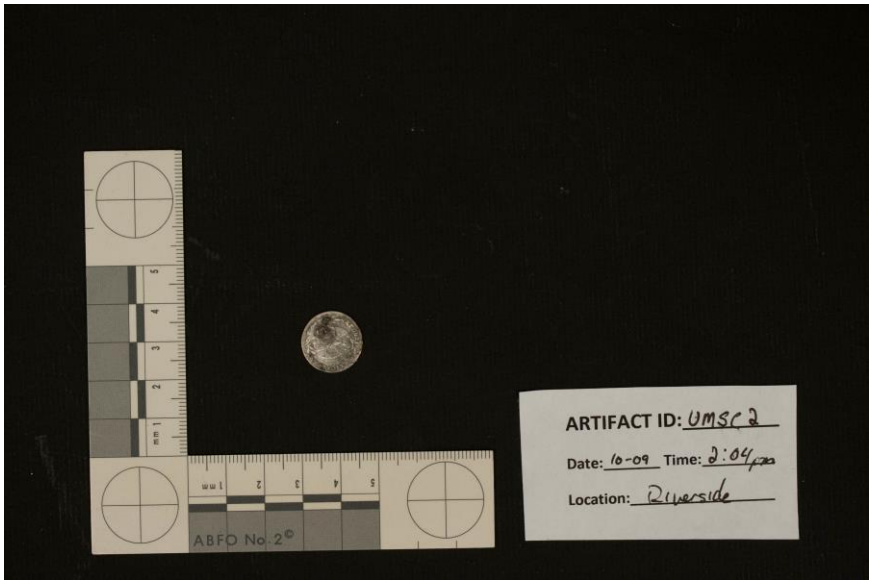
ABFO No. 2©
ARTIFACT ID: UMSC2
Date: 10-09 Time: 2:04pm
Location: Riverside


ABFO No. 2©
ARTIFACT ID: UMSC2
Date: 10-09 Time: 2:04pm
Location: Riverside

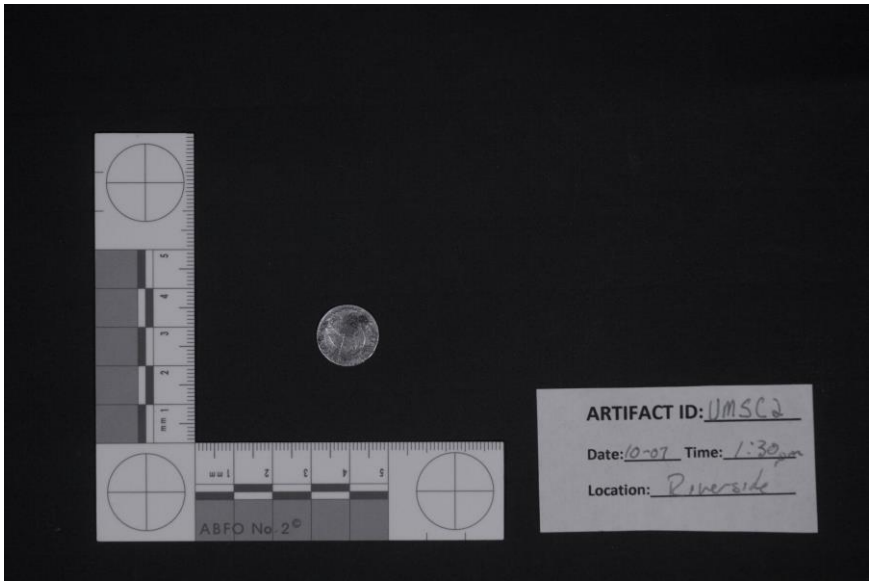
ABFO No. 2©
ARTIFACT ID: UMSC2
Date: 10-07 Time: 1:30pm
Location: Riverside

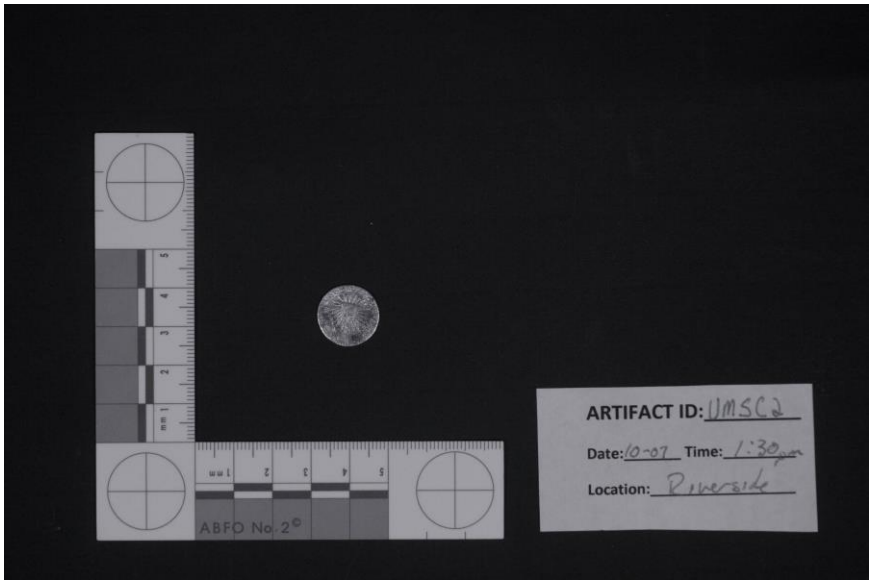
ARTIFACT ID: UMSC2
Date: 10-07 Time: 1:30pm
Location: Riverside
ABFO No. 2©

UMBB3

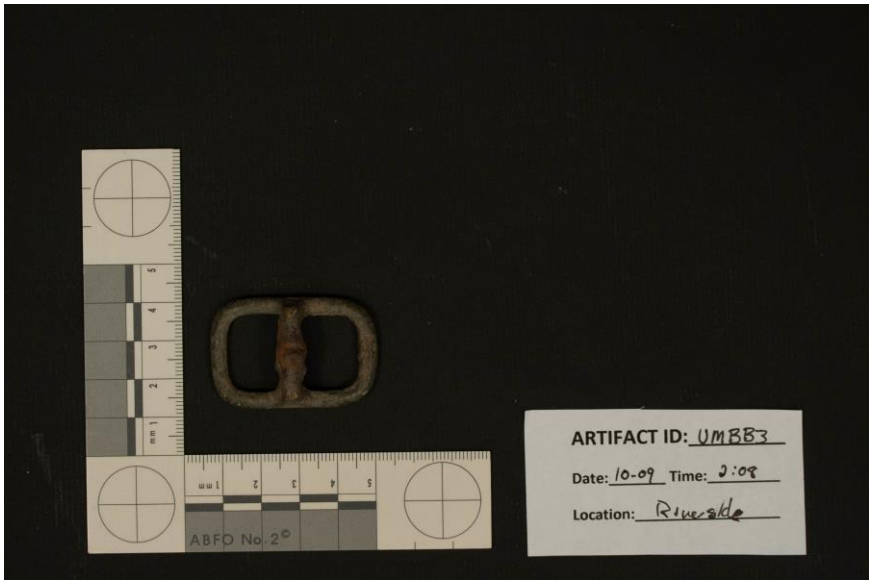
ARTIFACT ID: UMBB3
Date: 10-09 Time: 2:08
Location: Riverside
ABFO No. 2©


ABFO No. 2©
ARTIFACT ID: UMBB3
Date: 10-09 Time: 2:08
Location: Riverside


ABFO No. 2©
ARTIFACT ID: UMBB3
Date: 10-09 Time: 2:08
Location: Riverside

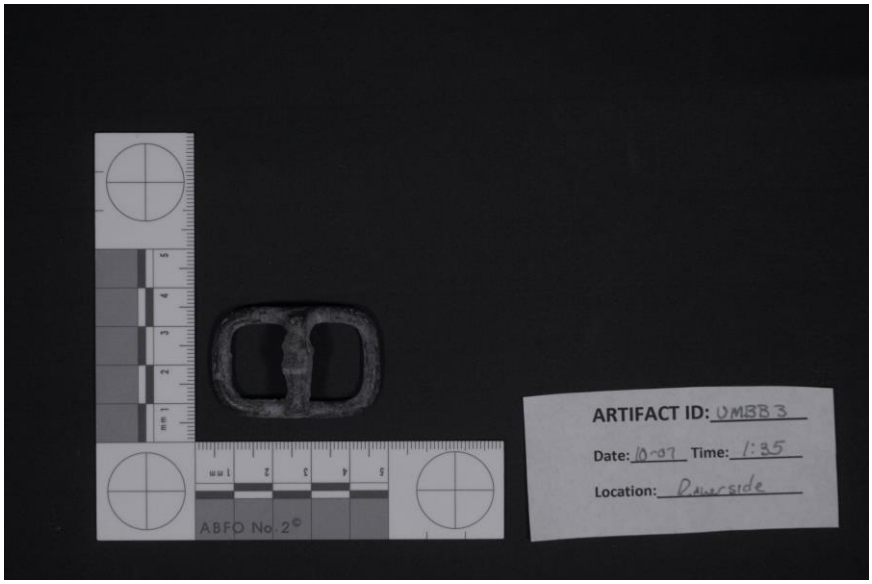
ABFO No. 2©
ARTIFACT ID: UMBB3
Date: 10-07 Time: 1:35
Location: Powerside

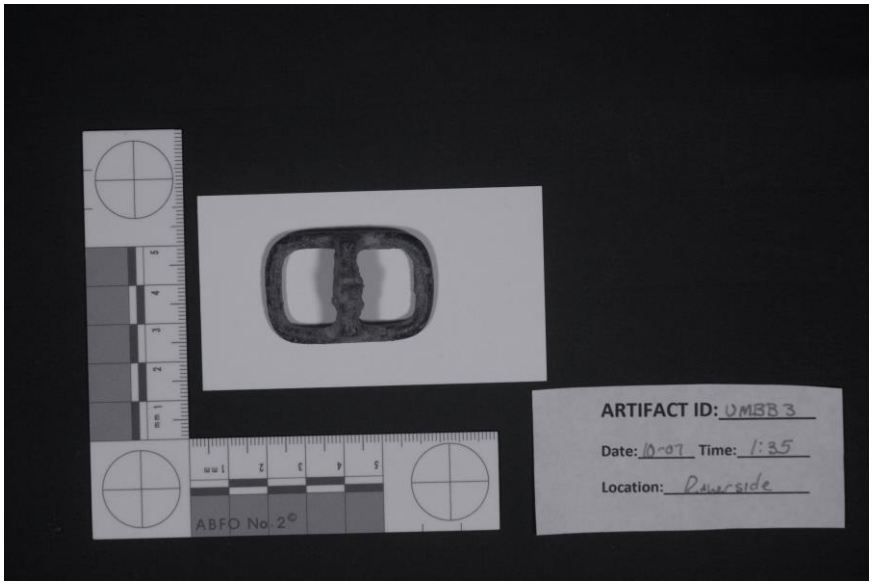
ABFO No. 2©
ARTIFACT ID: UMBB3
Date: 10-07 Time: 1:35
Location: Powerside

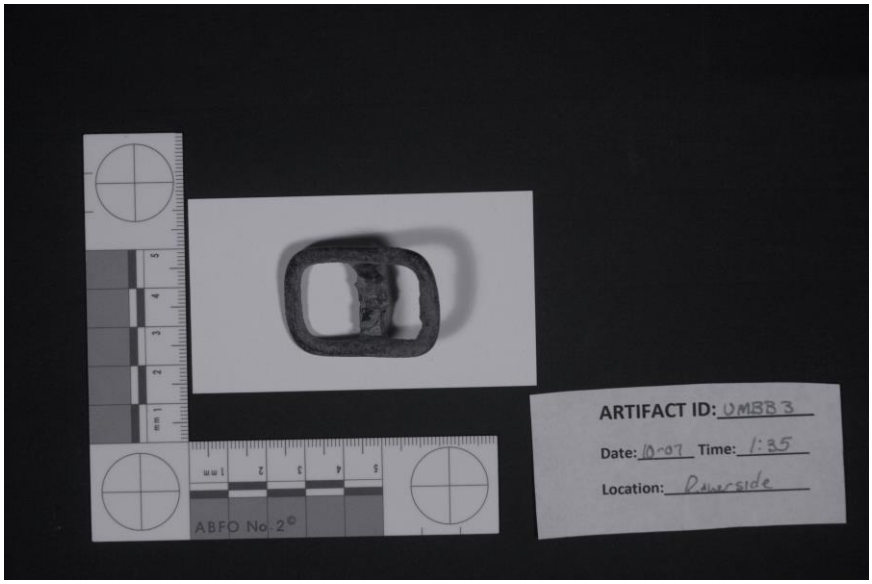
ABFO No. 2©
ARTIFACT ID: UMBB3
Date: 10-07 Time: 1:35
Location: Riverside

UMWM4

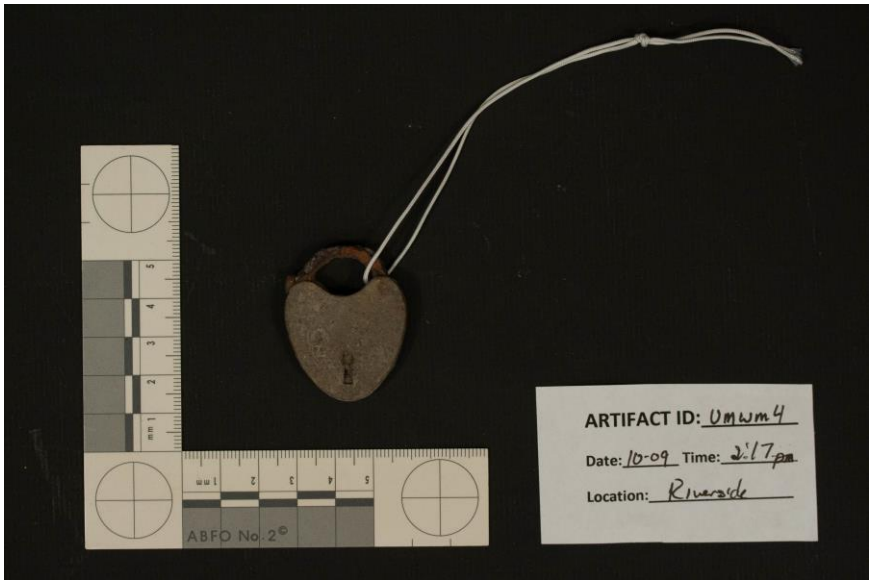
ABFO No. 2©
ARTIFACT ID: UMWM4
Date: 10-09 Time: 2:17pm
Location: Riverside

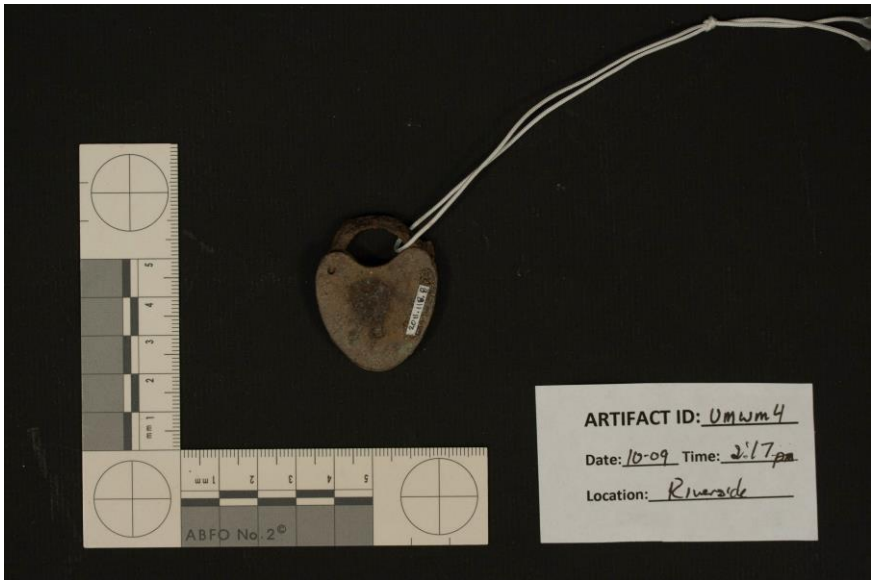
ABFO No. 2©
ARTIFACT ID: UMWM4
Date: 10-09 Time: 2:17 pm
Location: Riverside

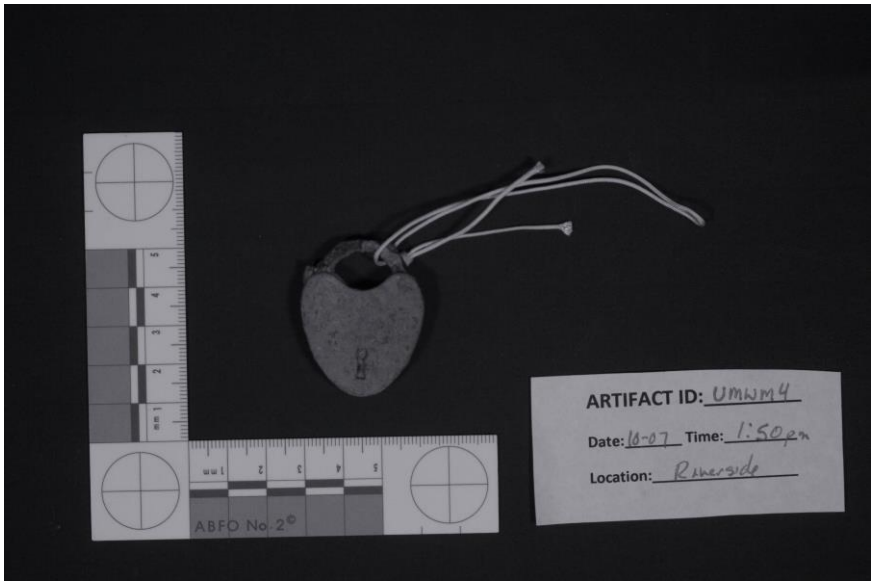
ABFO No. 2©
ARTIFACT ID: UMWM4
Date: 10-07 Time: 1:50 pm
Location: Riverside

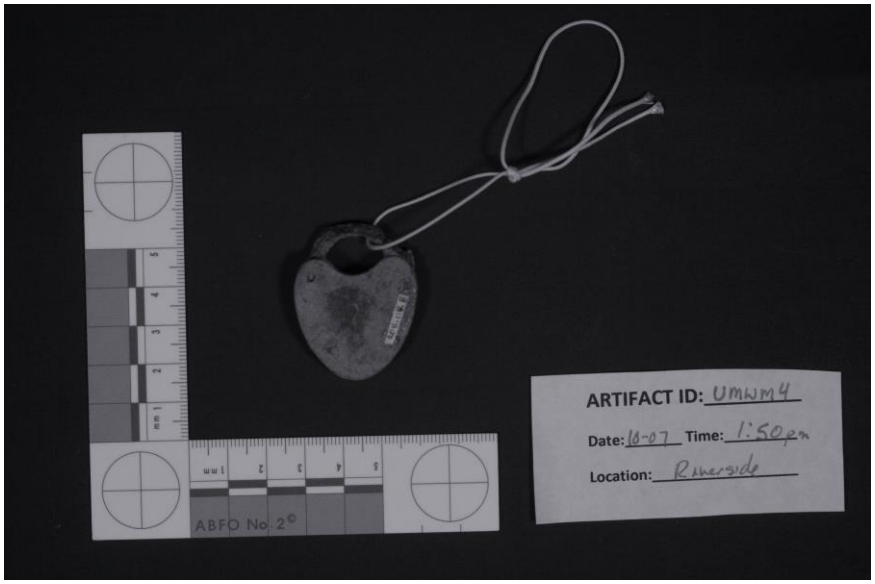
ARTIFACT ID: UMWM4
Date: 10-07 Time: 1:50pm
Location: Riverside
ABFO No. 2

UMC5


ARTIFACT ID: UMC5
Date: 10-09 Time: 4:15pm
Location: Riverside
ABFO No. 2


ABFO No. 2
ARTIFACT ID: UMCS
Date: 10-09 Time: 4:15pm
Location: Riverside


ABFO No. 2
ARTIFACT ID: UMCS
Date: 10-07 Time: 3:09pm
Location: Riverside


ARTIFACT ID: UMLB5
Date: 10-07 Time: 3:09
Location: Riverside
ABFO No. 2

UMLB6

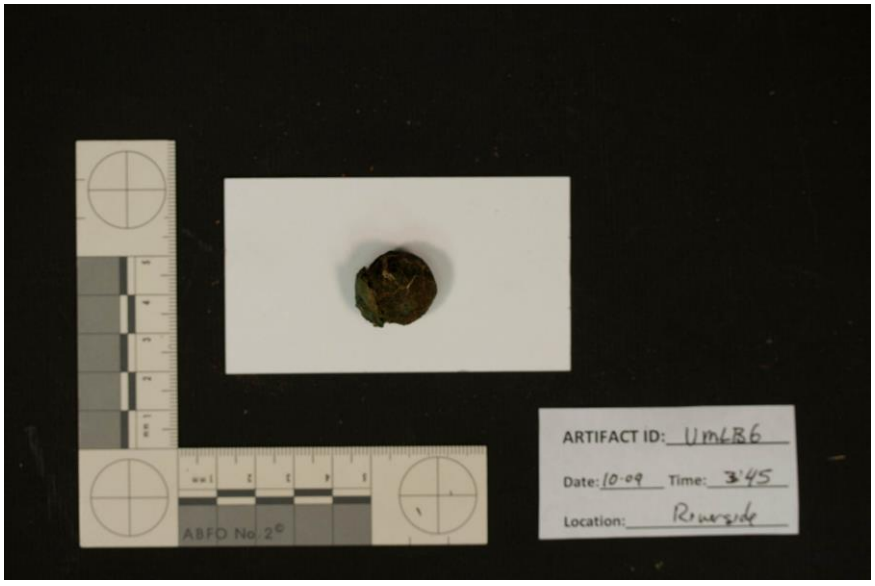
ARTIFACT ID: UMLB6
Date: 10-09 Time: 3:45
Location: Riverside
ABFO No. 2

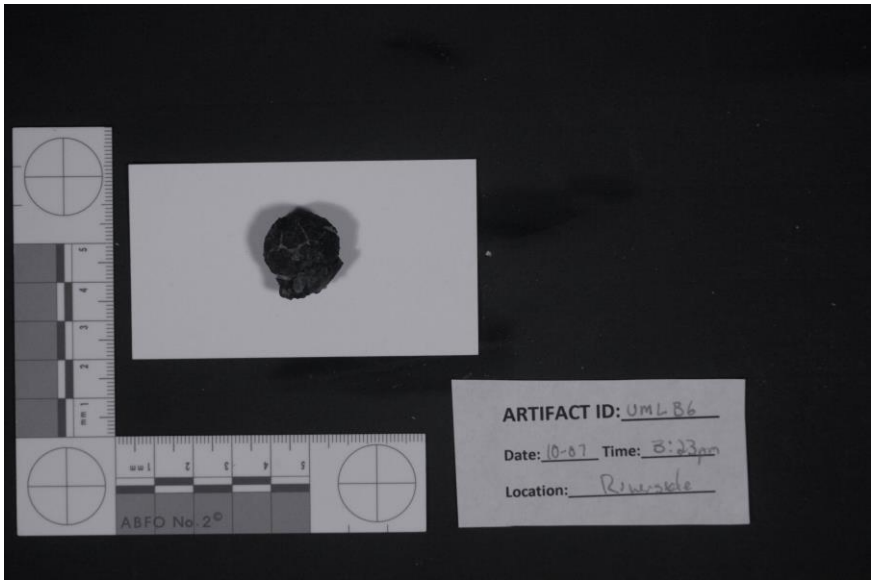
ARTIFACT ID: UMLB6
Date: 10-07 Time: 8:23pm
Location: Riverside
ABFO No. 2

UMIC7

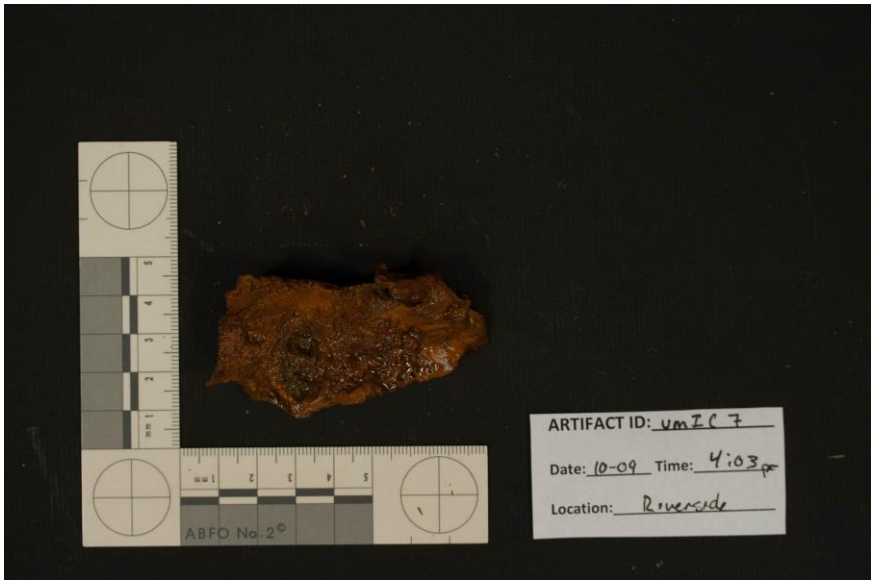
ARTIFACT ID: umIC7
Date: 10-09 Time: 4:03pm
Location: Riverside
ABFO No. 2


ABFO No. 2
ARTIFACT ID: umIC 7
Date: 10-09 Time: 4:03
Location: Riverside


ABFO No. 2
ARTIFACT ID: umPC 7
Date: 10-07 Time: 4:05
Location: Riverside

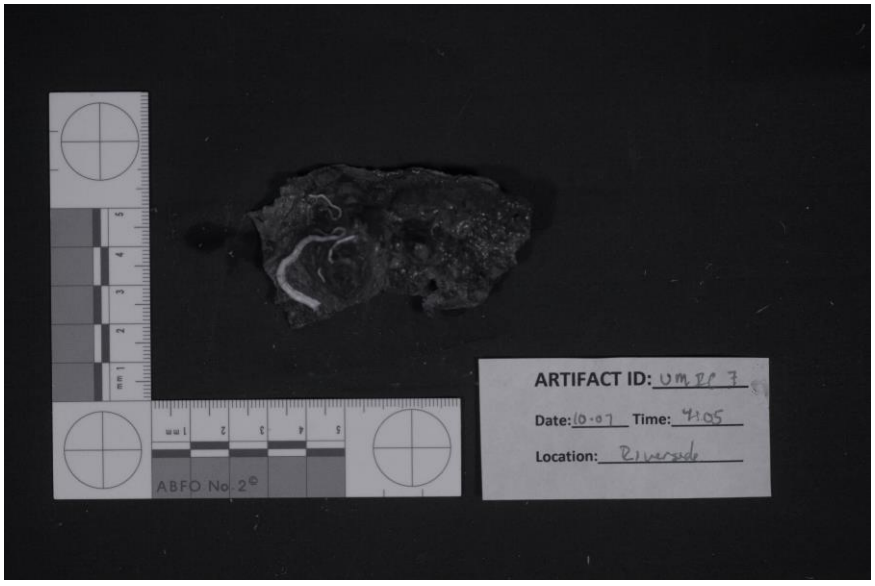
ARTIFACT ID: UMISD 7
Date: 10-07 Time: 4:05
Location: Riverside
ABFO No. 2

UMISD8


ARTIFACT ID: UMISD 8
Date: 10-09 Time: 3:30pm
Location: Riverside
ABFO No. 2


ABFO No. 2
ARTIFACT ID: UMISD 8
Date: 10-09 Time: 5:30pm
Location: Riverside


ABFO No. 2
ARTIFACT ID: UMISD 8
Date: 10-07 Time: 4:20
Location: Riverside

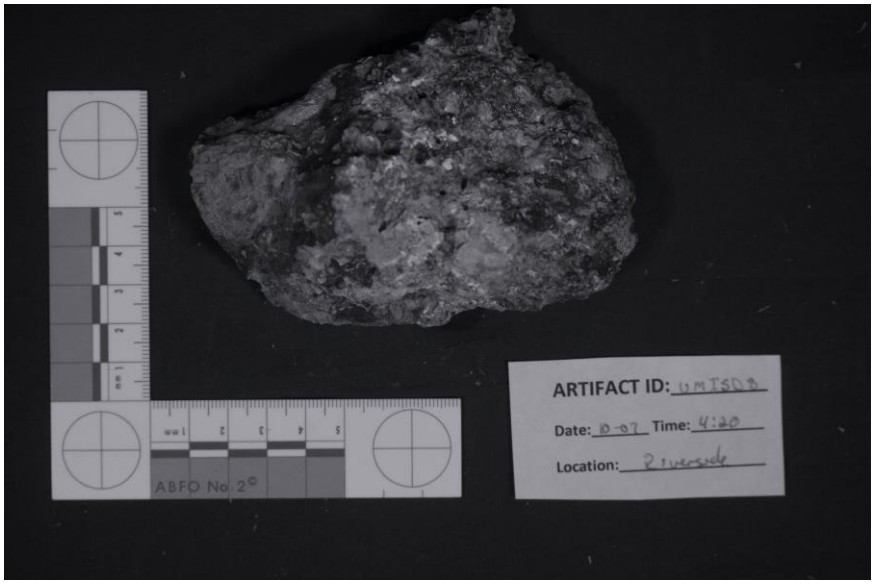
ARTIFACT ID: UMTSD2
Date: 10-07 Time: 4:20
Location: Riverside
ABFO No. 2©

CMIERT9


ARTIFACT ID: CMIERT 9
Date: 10-15 Time: 1147pm
Location: Wilder
ABFO No. 2©


ABFO No. 2©
ARTIFACT ID: CMIERT9
Date: 10-15 Time: 1147pm
Location: Wilder


ABFO No. 2©
ARTIFACT ID: CMIERT9
Date: 10-16 Time: 1:15pm
Location: Wilder


ARTIFACT ID: CMIGRI9
Date: 10-16 Time: 12:15pm
Location: Wilder
ABFO No. 2

CMLBER10

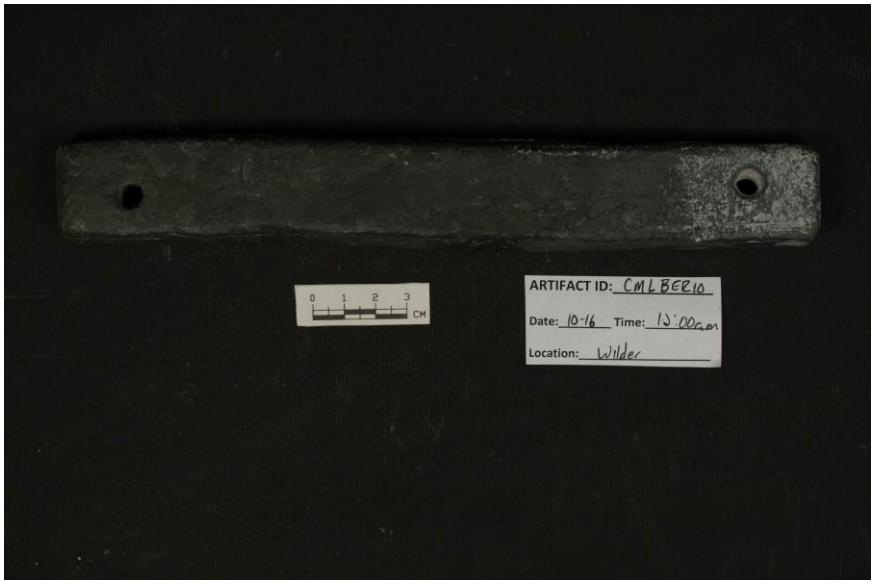
ARTIFACT ID: CMLBER10
Date: 10-16 Time: 12:00pm
Location: Wilder
0 1 2 3
CM

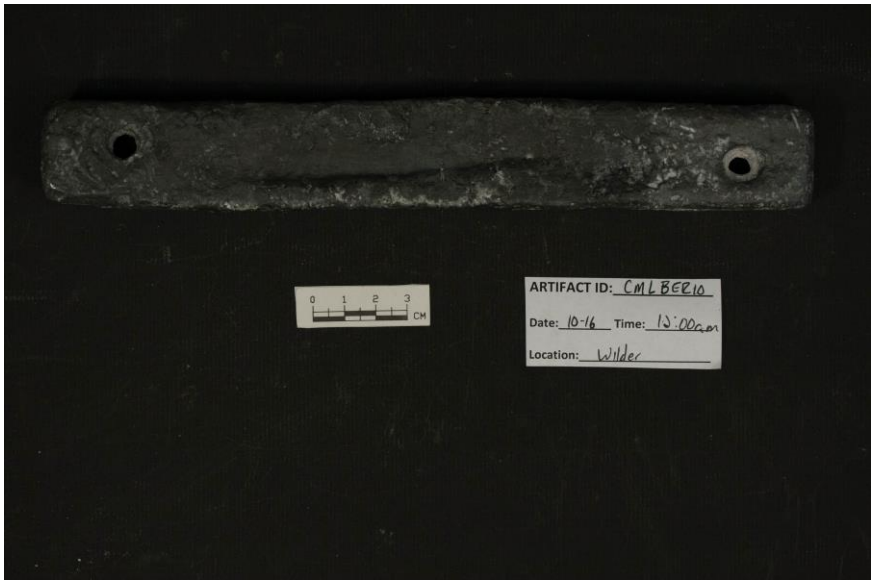
0 1 2 3
CM
ARTIFACT ID: CMLBER10
Date: 10-16 Time: 12:00am
Location: Wilder

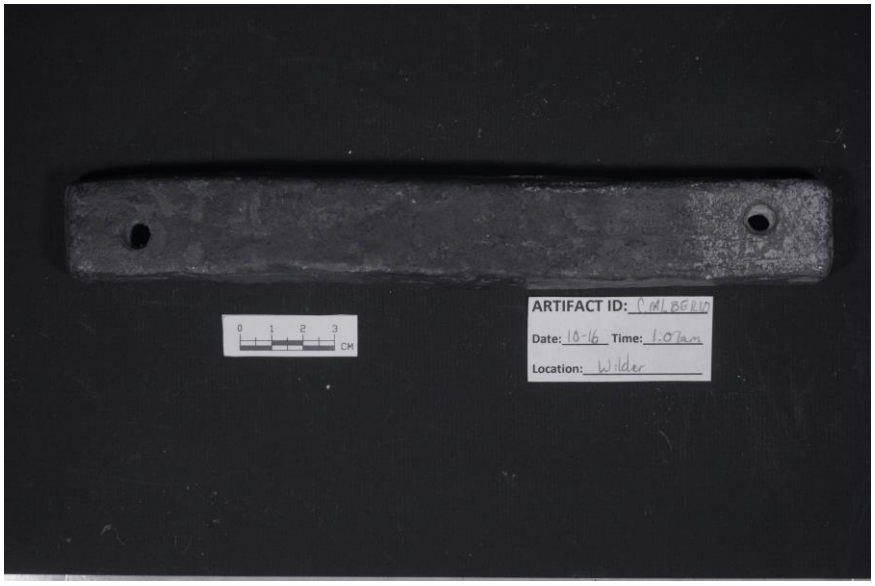
0 1 2 3
CM
ARTIFACT ID: CMLBER10
Date: 10-16 Time: 1:07am
Location: Wilder

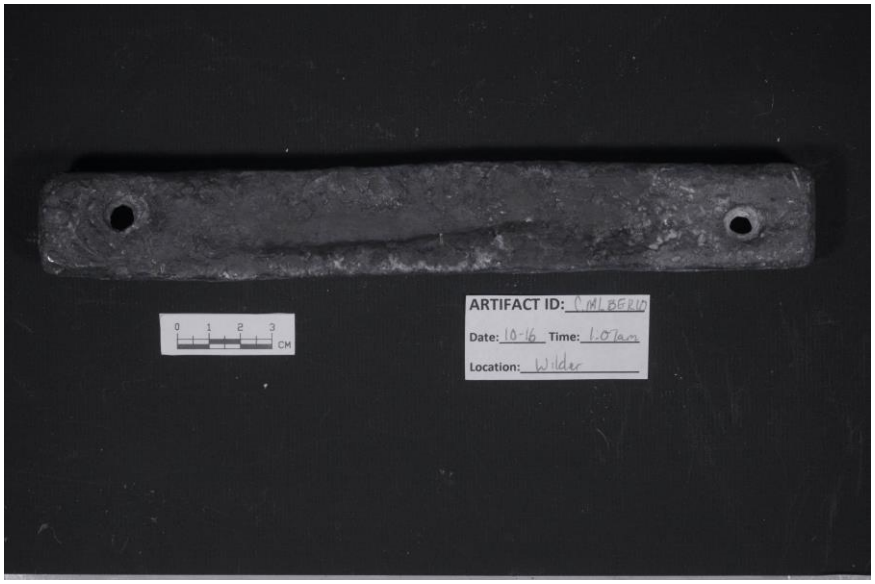

Textile

UTPGI1

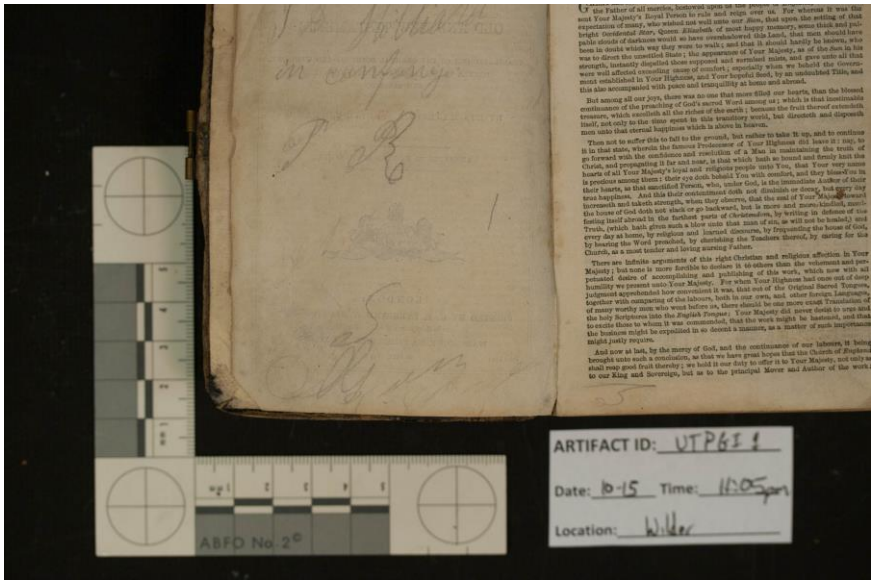
ARTIFACT ID: UTPGI 1
Date: 10-15 Time: 11:05am
Location: Miller
ABFO No. 2


ARTIFACT ID: UTPGI 1
Date: 10-15 Time: 11:05am
Location: Miller
ABFO No. 2

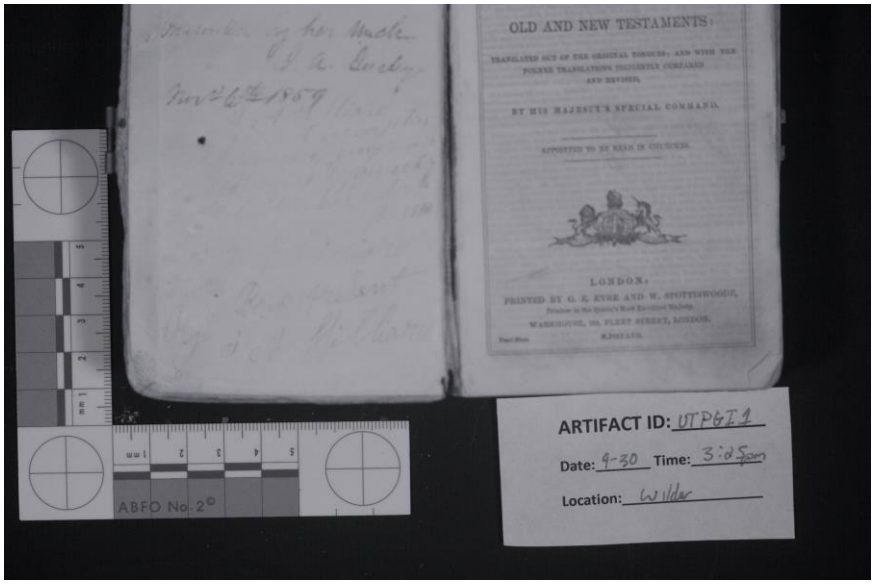
OLD AND NEW TESTAMENTS:
LONDON:
ABFO No. 2
ARTIFACT ID: UTPGT1
Date: 9-30 Time: 3:05pm
Location: Wilder

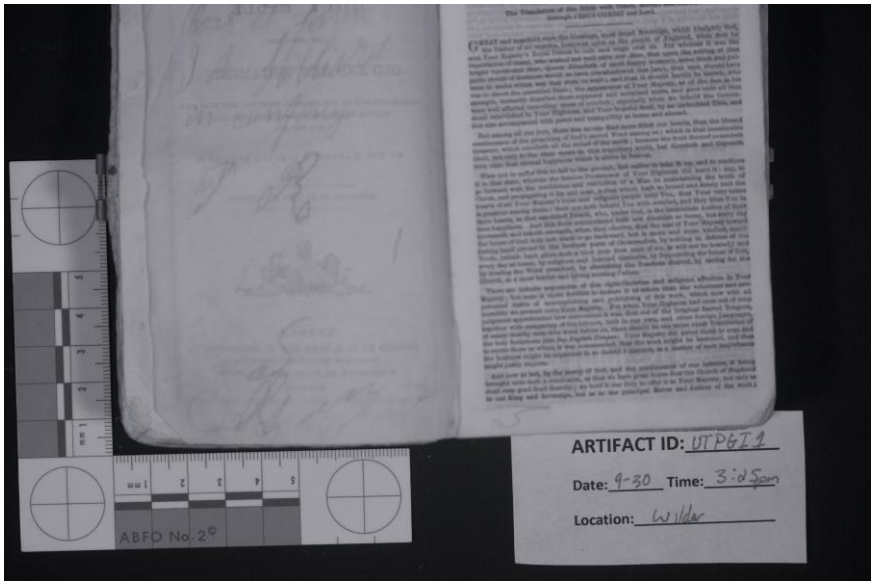
ABFO No. 2
ARTIFACT ID: UTPGT1
Date: 9-30 Time: 3:05pm
Location: Wilder

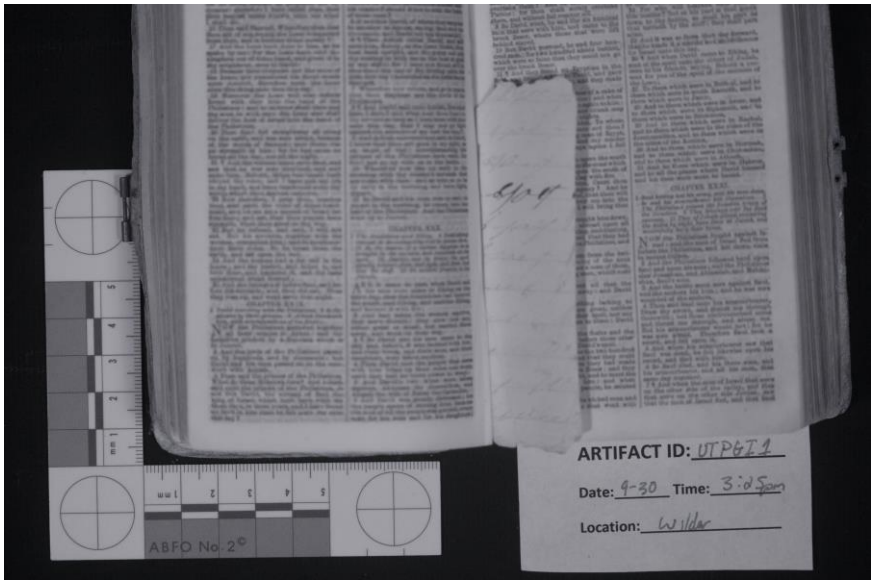
ABFO No. 2
ARTIFACT ID: UTPGI1
Date: 9-30 Time: 3:25pm
Location: Wilder

CTRSO2


ABFO No. 2
ARTIFACT ID: CTRSO2
Date: 10-09 Time: 3:08
Location: Riverside


ABFO No. 2©
ARTIFACT ID: CTRS02
Date: 10-09 Time: 3:08
Location: Riverside

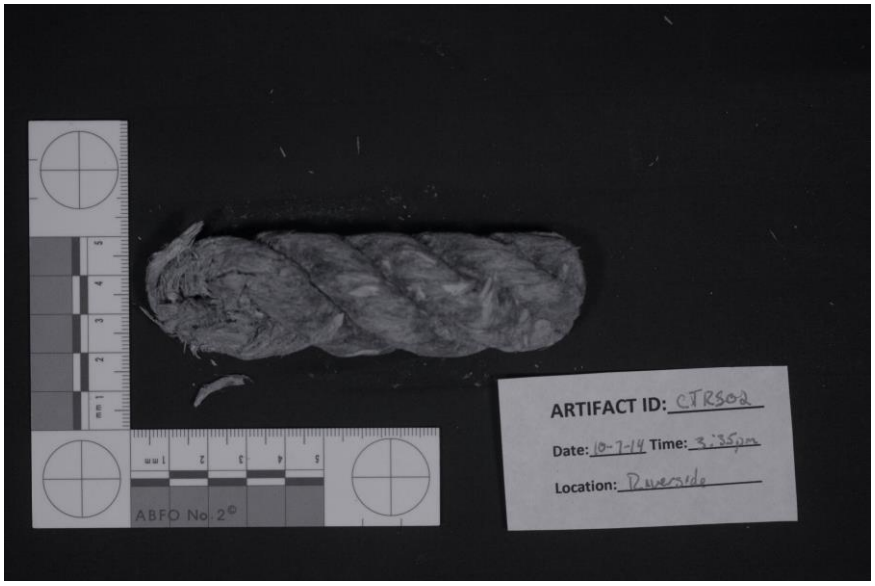
ABFO No. 2©
ARTIFACT ID: CTRS02
Date: 10-7-14 Time: 3:35pm
Location: Riverside

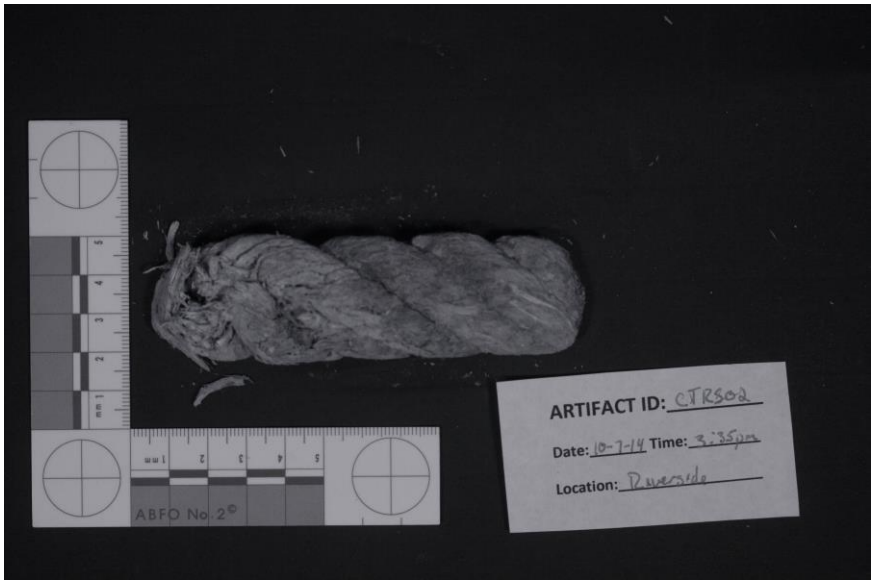
ARTIFACT ID: CTRS02
Date: 10-7-14 Time: 3:35pm
Location: Riverside
ABFO No. 2©

Wood

UWSAD1


ARTIFACT ID: UWSAD1
Date: 10-15 Time: 10:33pm
Location: Wilder
ABFO No. 2©


ABFO No. 2©
ARTIFACT ID: UWSA01
Date: 10-15 Time: 10:33pm
Location: Wilder


ABFO No. 2©
ARTIFACT ID: UWSA01
Date: 10-15 Time: 10:33pm
Location: Wilder


ABFO No. 2©
ARTIFACT ID: UWSA21
Date: 10-15 Time: 10:33pm
Location: Wilder

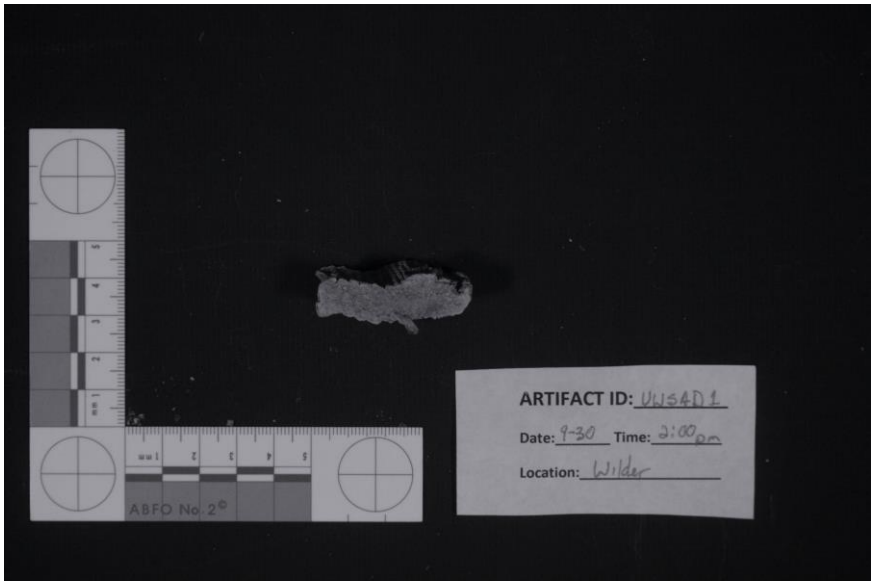
ABFO No. 2©
ARTIFACT ID: UWSAD1
Date: 9-30 Time: 2:00pm
Location: Wilder

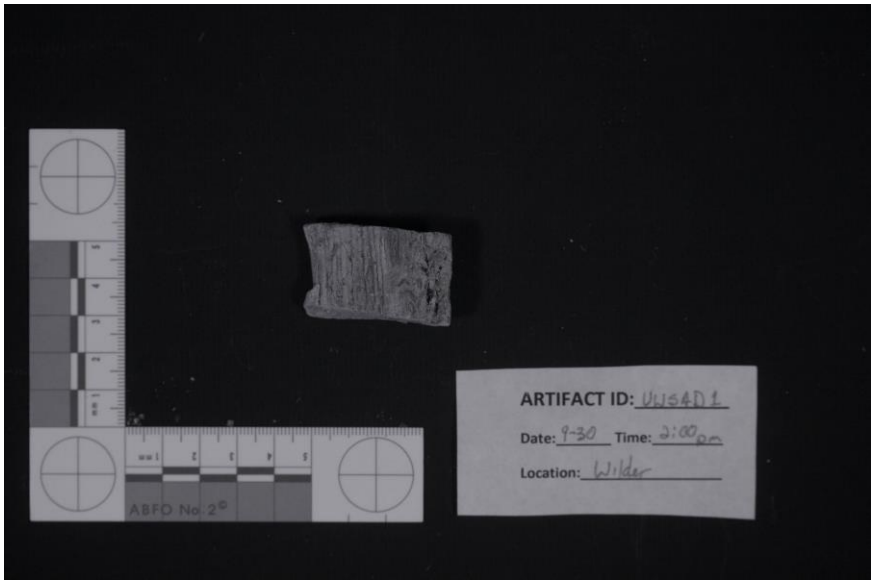
ABFO No. 2
ARTIFACT ID: UWS4D1
Date: 9-30 Time: 2:00pm
Location: Wilder

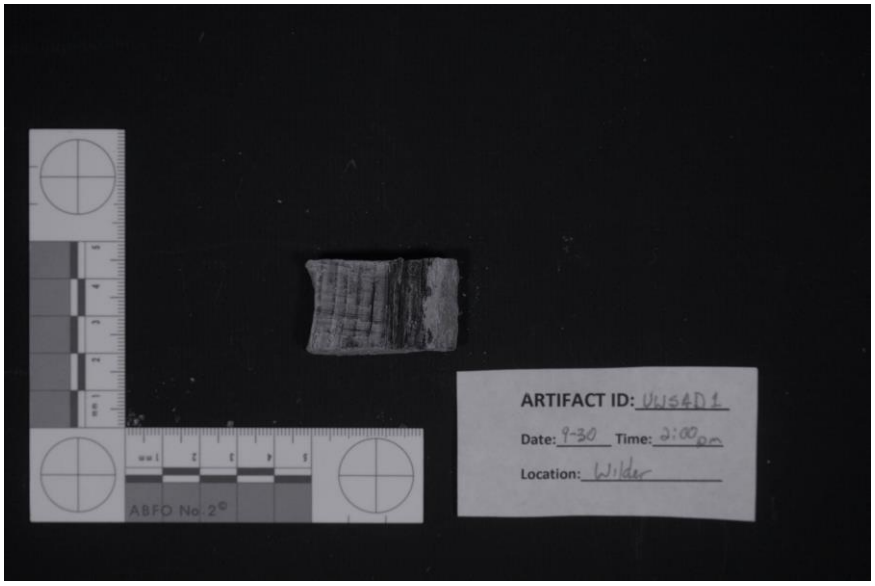
ABFO No. 2
ARTIFACT ID: UWS4D1
Date: 9-30 Time: 2:00pm
Location: Wilder

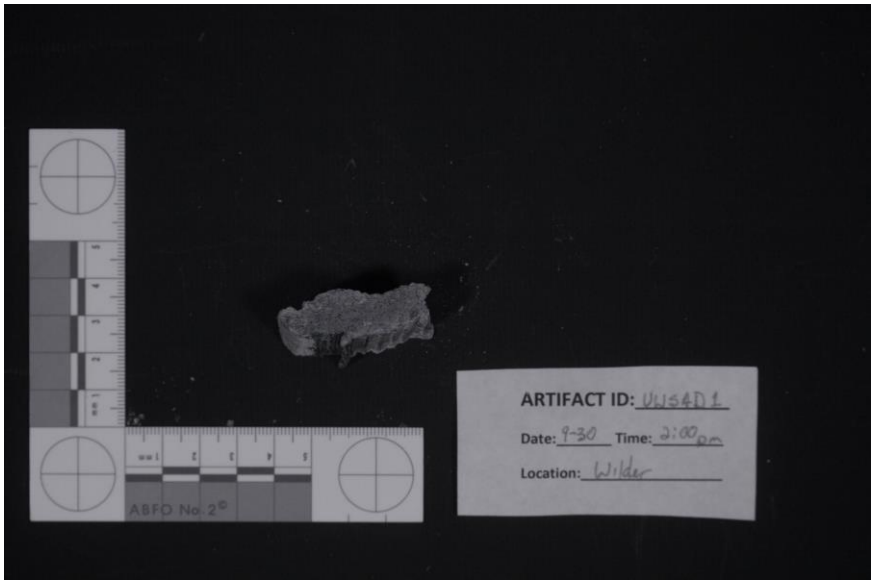
ABFO No. 2
ARTIFACT ID: UWS4D1
Date: 9-30 Time: 2:00pm
Location: Wilder

CWSPF2


ABFO No. 2
ARTIFACT ID: CWSPF2
Date: 10-15 Time: 3:45pm
Location: Wilder


ABFO No. 2
ARTIFACT ID: CWSPF 2
Date: 10-15 Time: 3:45pm
Location: Wild


ABFO No. 2

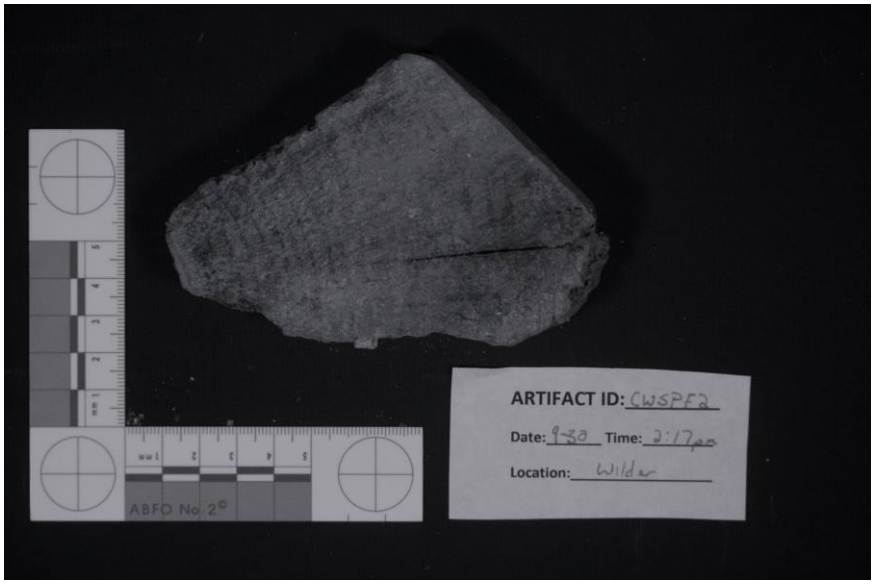
ABFO No. 2
ARTIFACT ID: CWSPF2
Date: 9-30 Time: 2:17pm
Location: Wilder

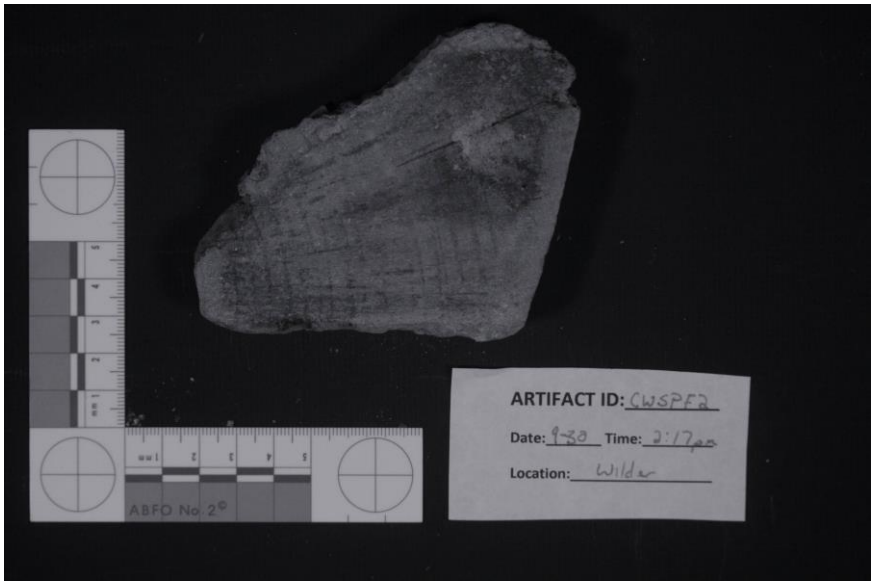
ABFO No. 2
ARTIFACT ID: CWSPF2
Date: 9-30 Time: 2:17pm
Location: Wilder

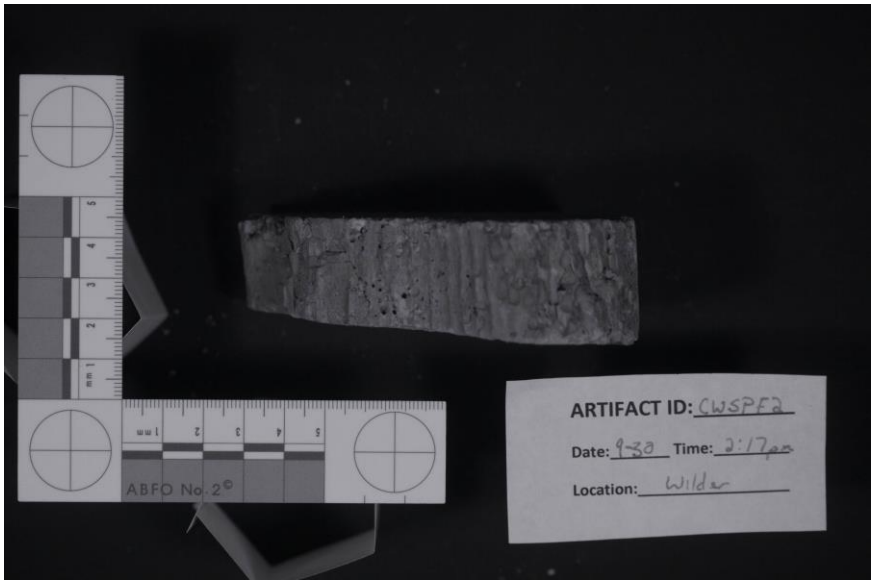
ABFO No. 2
ARTIFACT ID: CWSPF2
Date: 9-30 Time: 2:17pm
Location: Wilder

CWHP3


ABFO No. 2
ARTIFACT ID: CWHP3
Date: 10-15 Time: 4:15pm
Location: Wilder

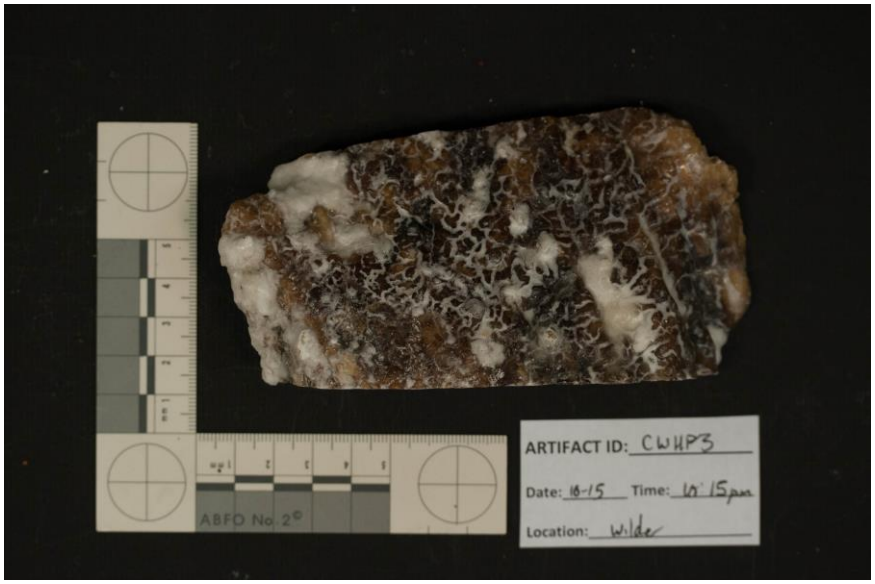
ABFO No. 2©
ARTIFACT ID: CWHP3
Date: 10-15 Time: 10:15pm
Location: Wilder


ABFO No. 2©
ARTIFACT ID: CWHP3
Date: 10-15 Time: 10:15pm
Location: Wilder

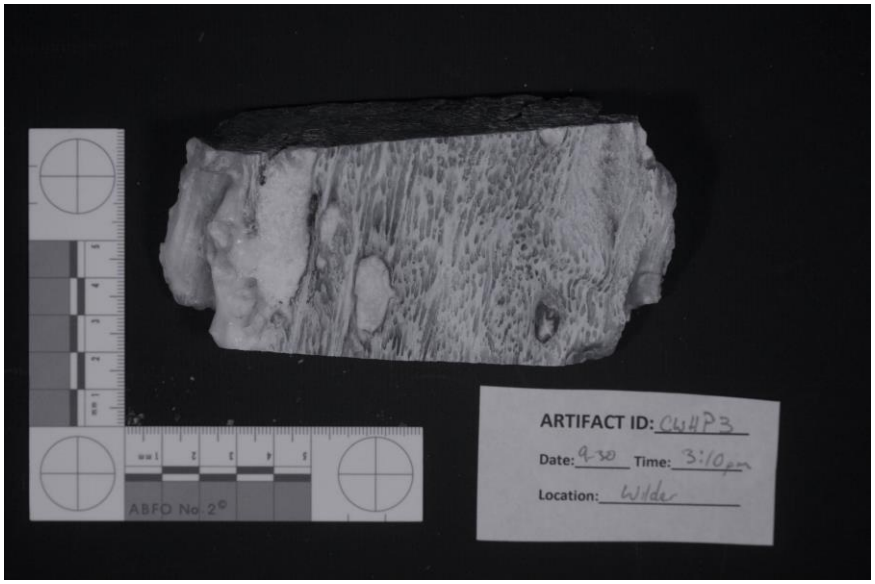
ABFO No. 2
ARTIFACT ID: CWHP3
Date: 9-30 Time: 3:10pm
Location: Wilder

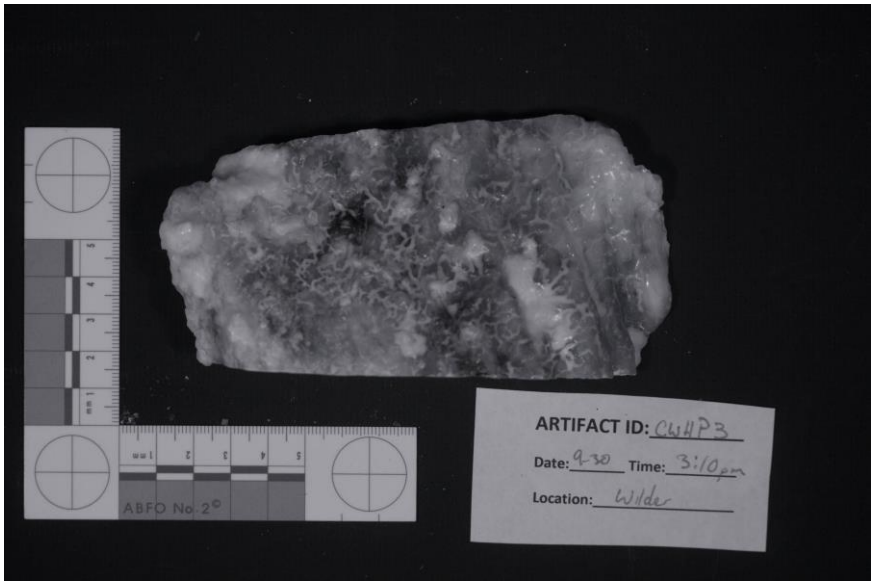
ABFO No. 2
ARTIFACT ID: CWHP3
Date: 9-30 Time: 3:10pm
Location: Wilder


ARTIFACT ID: CWHP3
Date: 9-30 Time: 3:10pm
Location: Wilder
ABFO No. 2©

CWHSO4


ARTIFACT ID: CWHSO4
Date: 10-09 Time: 1:48
Location: Riverside
ABFO No. 2©


ARTIFACT ID: CW4504
Date: 10-09 Time: 1:48
Location: Riverside
ABFO No. 2©

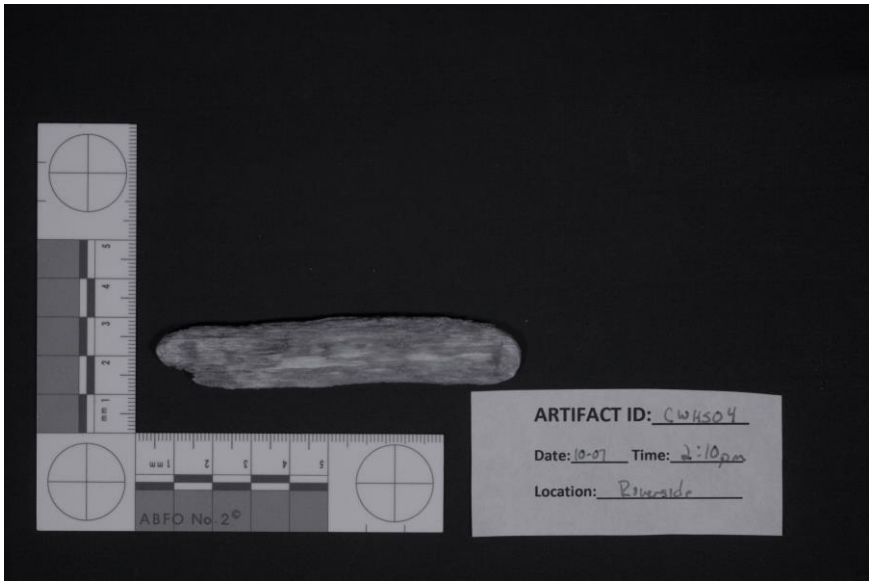
ARTIFACT ID: CW4504
Date: 10-07 Time: 2:10pm
Location: Riverside
ABFO No. 2©

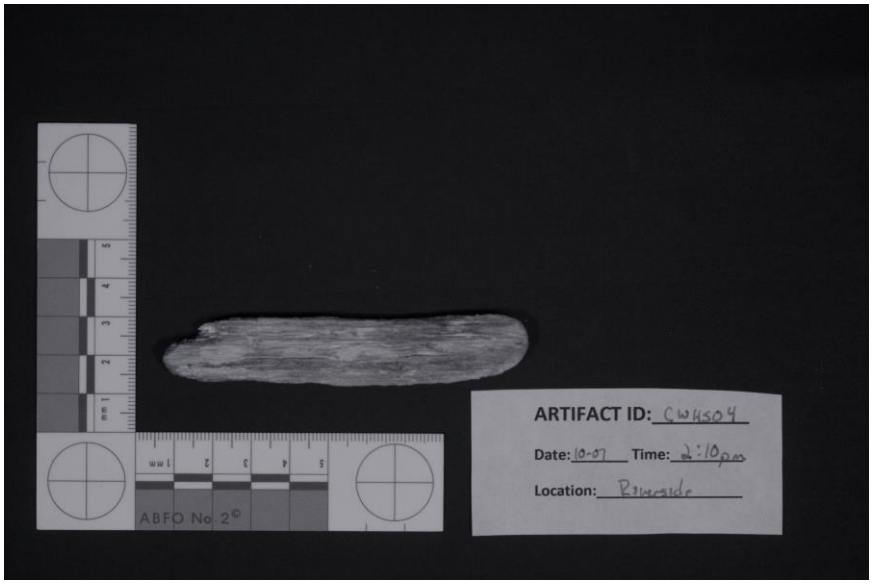
ABFO No. 2
ARTIFACT ID: CWHSO4
Date: 10-07 Time: 2:10pm
Location: Riverside

CWHSO5


IN
ARTIFACT ID: CWHSO5
Date: 10-09 Time: 4:30
Location: Riverside


IN
ARTIFACT ID: CWH505
Date: 10-09 Time: 4:30
Location: Riverside

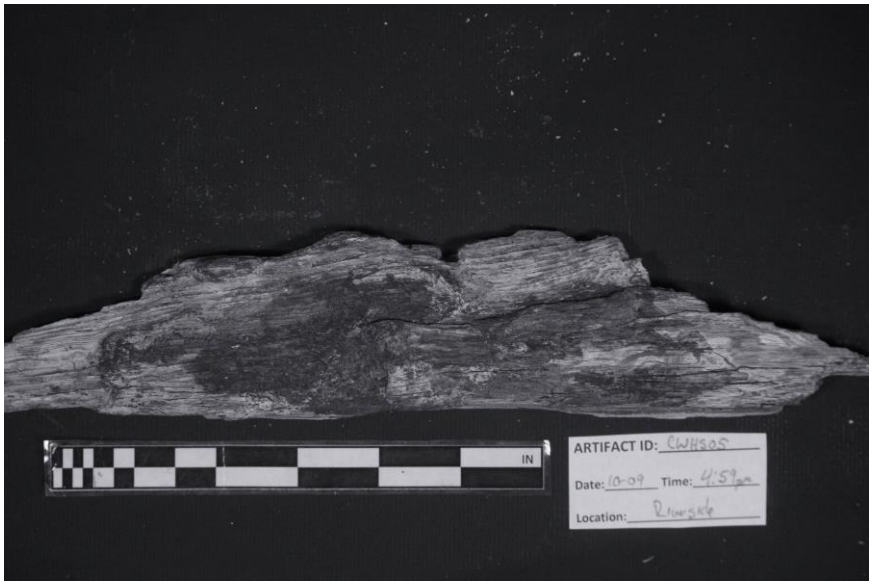
IN
ARTIFACT ID: CWH505
Date: 10-09 Time: 4:59pm
Location: Riverside


IN
ARTIFACT ID: CWHS05
Date: 10-09 Time: 4:59pm
Location: Riverside

CWSP6

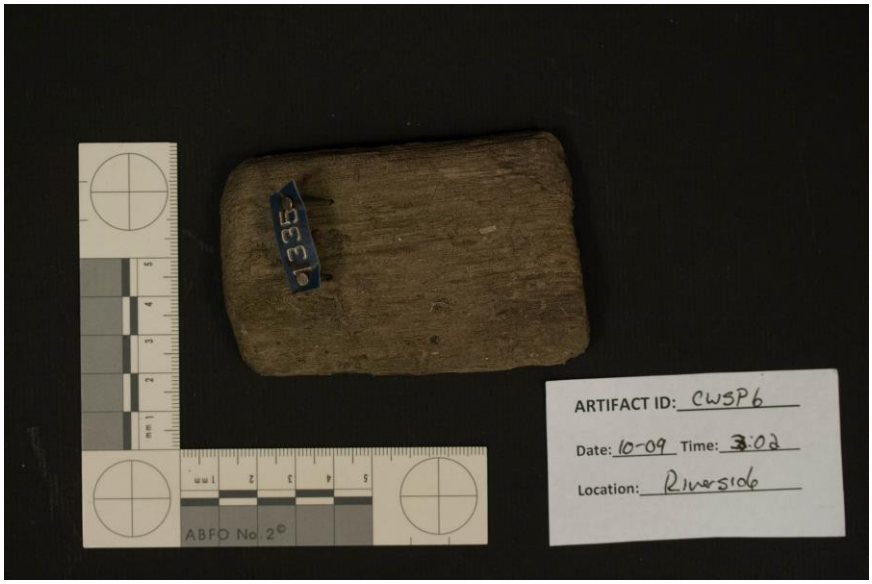
ABFO No. 2
ARTIFACT ID: CWSP6
Date: 10-09 Time: 3:02
Location: Riverside

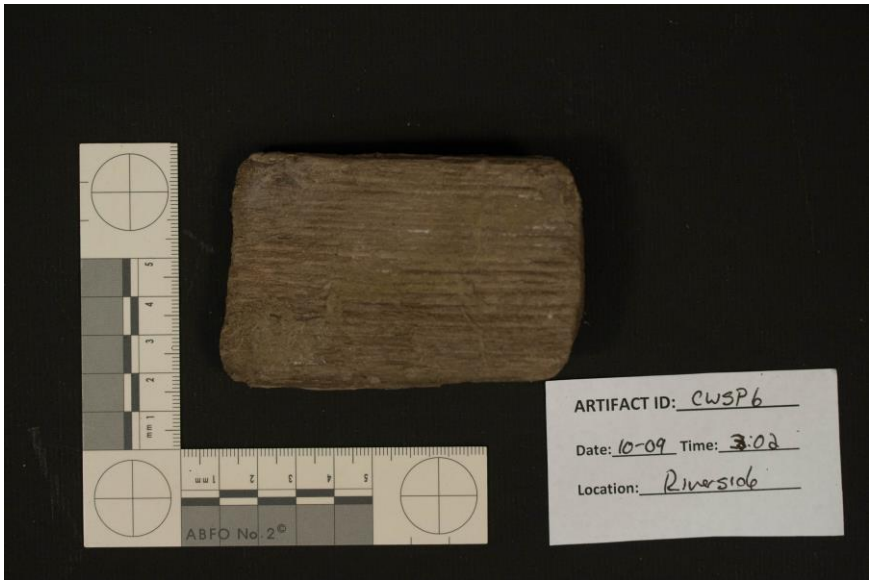
ABFO No. 2©
ARTIFACT ID: CWSP6
Date: 10-09 Time: 3:02
Location: Riverside

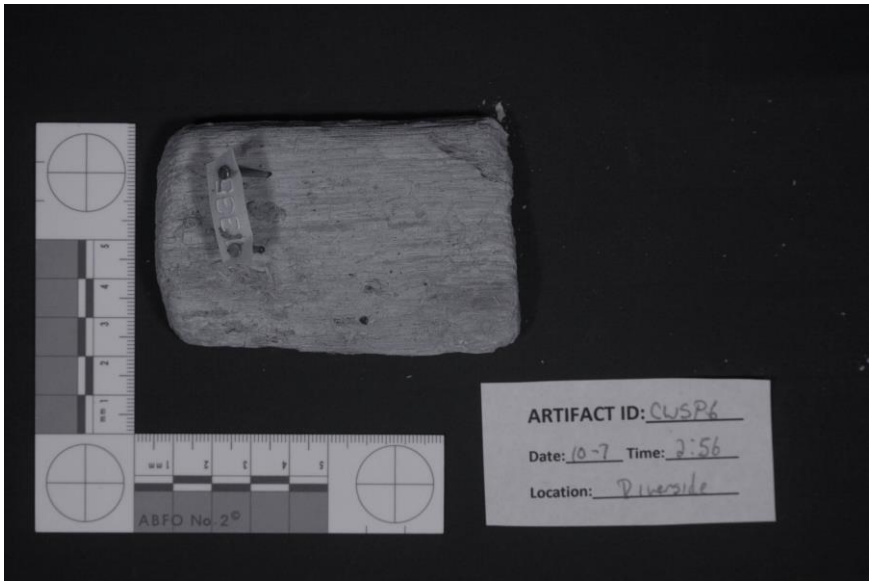
ABFO No. 2©
ARTIFACT ID: CWSP6
Date: 10-7 Time: 2:56
Location: Riverside

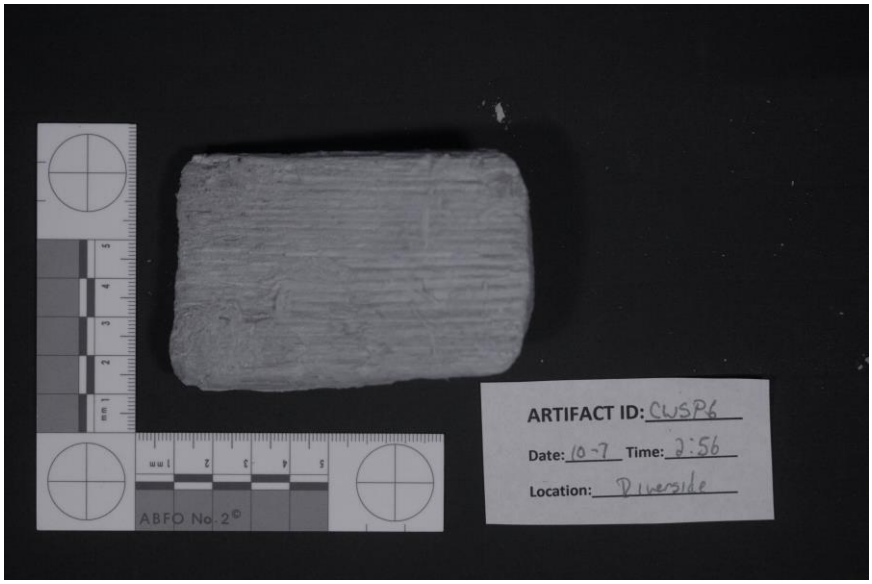
ABFO No. 2©
ARTIFACT ID: CWSP6
Date: 10-7 Time: 2:56
Location: Riverside

UWHAD7

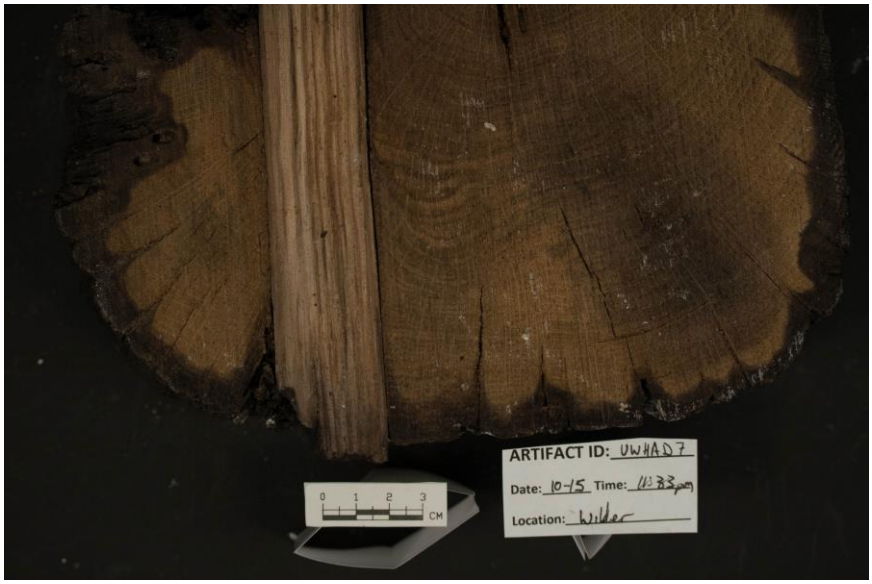
0 1 2 3
CM
ARTIFACT ID: UWHAD7
Date: 10-15 Time: 11:33am
Location: Wilder


ARTIFACT ID: UWHAD7
Date: 10-15 Time: 11:33pm
Location: Wilder
0 1 2 3
CM


ARTIFACT ID: UWHAD7
Date: 10-16 Time: 1:30am
Location: Wilder
0 1 2 3
CM

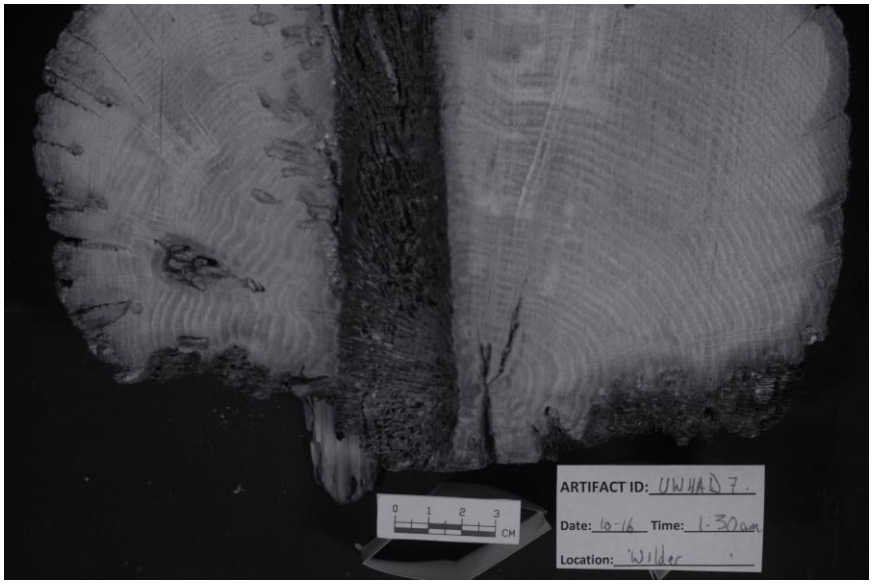
0 1 2 3
CM
ARTIFACT ID: UWHAD 7.
Date: 10-16 Time: 1:30am
Location: Wilder